AD-A278 556

CALCULATION OF PHASE STABILITY IN ZR-NB-RU USING LMTO

AND THE CLUSTER VARIATION METHOD

by

JOHN DAVID BECKER

DISSERTATION

Presented to the Faculty of the Graduate School of

The University of Texas at Austin

in Partial Fulfillment

of the Requirements

for the Degree of

DOCTOR OF PHILOSOPHY

THE UNIVERSITY OF TEXAS AT AUSTIN

December, 1993

DTIC
ELECTE
APR 26 1994
S F D

154P0 94-12696

94 4 25 108

DTIC QUALITY INSPECTED 3

CALCULATION OF PHASE STABILITY IN ZR-NB-RU USING LMTO AND THE CLUSTER VARIATION METHOD

by

JOHN DAVID BECKER

DISSERTATION

Presented to the Faculty of the Graduate School of

The University of Texas at Austin

in Partial Fulfillment

of the Requirements

for the Degree of

DOCTOR OF PHILOSOPHY

THE UNIVERSITY OF TEXAS AT AUSTIN

December, 1993

Accesion For	
NTIS CRA&I	☑
DTIC TAB	☐
Unannounced	☐
Justification	
By	
Distribution /	
Availability Codes	
Dist	Avail and / or Special
A-1	

ACKNOWLEDGEMENTS:

CALCULATION OF PHASE STABILITY IN ZR-NB-RU USING LMTO AND THE CLUSTER VARIATION METHOD

Publication No. _____

John David Becker, Ph.D.

The University of Texas at Austin, 1993

Supervisor: Juan M. Sanchez

The ground-state structural energies of several binary compounds in the systems zirconium-niobium, niobium-ruthenium, and zirconium-ruthenium were calculated using first-principles total-energy electronic-structure calculations with the linearized muffin-tin orbital (LMTO) approximation. These energies were used in a cluster expansion to determine the ground-state configurations of each of the three binary systems. Notably, the calculations imply that the stable equilibrium structure of the compound $NbRu_3$ is DO_{19}. The calculated excess structural energies are in good agreement with reported measurements. The long-term objective of this approach is the calculation of equilibrium thermomechanical properties of alloys without resort to experimental measurements, for example, phase diagrams. Finite temperature phase stability calculations are implemented using a generalized Ising model and the cluster variation method (CVM). Vibrational free energy is included using the Debye-

Grüneisen approximation. Predicted phase equilibria are in excellent agreement with measurements.

TABLE OF CONTENTS

LIST OF TABLES

LIST OF FIGURES

xiii

INTRODUCTION

Progress in a long-standing objective in computational materials science, the calculation of alloy phase diagrams from first-principles, has been paced by the associated problems of accurate yet efficient total-energy calculations and statistical approximations of the alloy partition function. The former is well understood, and the evolution of Density-Functional Theory (DFT) [1] to computationally suitable methods using the Local-Density Approximation (LDA) [2] is a renowned (though, arguably, a qualified) success. The high precision required of the total-energy band-structure methods for phase-equilibrium calculations is attainable for most chemical systems. The connection between the total-energy calculations and a general solution to the Ising problem is provided by a **cluster expansion** in a series of multi-atom interaction energies [3]. This rigorous expansion may be inverted to calculate the total energy of any lattice configuration using the multi-atom interactions. Two main aspects of the cluster expansion method remain unresolved: the convergence of the expansion and the effect of strain energy on the convergence. These two issues are central to this thesis, and a major portion of this study is devoted toward a resolution.

First-principles phase diagrams have been computed with partial success for noble metals [3-5], semiconductors [6], metal-oxide

1

superconductors [7], ordering systems [8-17], and systems dominated by the effects of coherency [18] or surfaces [19]. Yet important aspects are missing from each of these studies. For example, vibrational free energy is rarely included, except using strictly empirical means. Incorporation of elastic relaxation, critical in some cases, is far from satisfactory resolution. Local-volume relaxation has been included by somewhat different methods, as have distortional modes, but as yet even this seemingly simple problem has no rigorous treatment. For even the simplest systems, successful phase-diagram calculation requires much experience to complement the impressive set of computational tools now available.

In this study phase stability in the systems zirconium-niobium, niobium-ruthenium, and zirconium-ruthenium are investigated via the cluster expansion using total energies obtained with the **Linear-Muffin-Tin-Orbital** method [20] in the **Atomic-Sphere Approximation (LMTO-ASA)**. The systems are well chosen to test at different levels the method for calculating phase equilibrium and for comparison with experimental data (though few data have been reported for Nb-Ru). The Zr-Ru system is simple with only one intermediate ground-state ordered compound -- ZrRu with the B2 structure. Zr-Nb is also a simple system, with a broad miscibility gap, and is a good test for the accuracy of the method. The phase transition of Zr from hcp to bcc requires some treatment of vibrational free energy. The Nb-Ru system is complex, and several subtle aspects of phase equilibrium have eluded experimental

investigators. The cluster expansion of the formation energy of alloys in this system are used to resolve some of these controversial aspects.

The Ising Hamiltonian for a given lattice configuration can be expressed through a series expansion in the cluster correlation functions (variables describing the geometry in an average sense) of each type of cluster of lattice sites comprising the lattice (crystal). This expansion is rigorous and exact in the thermodynamical limit [21, 22]. The coefficients of the cluster expansion, known as the effective chemical interactions provide the connection between the first-principles total-energy calculations and the approximate expansion solutions to the Ising model. These interaction energies can be obtained through inversion of the cluster expansions of the total energies of several perfectly ordered structures. The application of the cluster expansion using *ab initio* total-energy calculations was first made by Connolly and Williams [23], and is now a standard method in first-principles phase-equilibrium calculations. For a perfectly ordered structure the correlations may be ascertained *a priori.* Thus, using the interaction energies, the cluster expansion may be used to ascertain the formation energy of any ordered structure. This obviates total-energy calculations of every likely lattice configuration in the process of determining the stable-equilibrium ground-state structures.

The cluster-expansion method as used by Connolly and Williams includes no implicit prescription for the volume dependence of the formation energy of the partially ordered alloy. Sever...

techniques for including elastic relaxation into the minimization of the configurational energy have been studied. The so-called "G-ε" method [6, 10] is based upon the stringent presupposition that th volume and bulk modulus of an alloy are independent of the chemic... order. This assumption allows a simple calculation of the elastic part of the energy, G, dependent solely upon the concentration and the volume-independent chemical part, ε, dependent upon the configuration. Sluiter *et al* [13] proposed a slightly more realistic model that is rigorously correct if the atoms in the alloy were jellium soft spheres. The model uses a relaxation energy that is quadratic in the volume. This energy is subtracted from the formation energy leaving the unrelaxed energy. This unrelaxed energy is used in calculation of the configurational free energy using the **Cluster-Variation Method (CVM)**. In contrast to the two preceding techniques, which account solely for volumetric relaxation, Zunger *et al* [24] included some structural-relaxation modes in the total-energy calculations, thereby including more realistic relaxation energies in the configurational free energy.

Except in the thermodynamic limit of the expansion, the interaction energies obtained from the inversion method are not necessarily invariant irrespective of the choice of the ordered structures used in the expansion. Nor is there an *a priori* knowledge of the range (both length and complexity) beyond which interactions become insignificant. These are the two principal aspects of convergence of the cluster expansion and as such are examined

closely in this (and other) first-principles phase-stability studies. However, for a well converged cluster expansion the interaction energies are sufficiently precise to reproduce formation energies within 5% of the total-energy calculations.

At finite temperatures, disorder and, commensurately, configurational entropy become significant. The Ising model lends itself to two solution methods: Monte Carlo techniques [25-28] and the CVM. Several studies have gauged the accuracy of the CVM by comparison with Monte Carlo calculations (see, for example, [28]). The CVM was proposed by Kikuchi [29], simplified by Barker [30], and reformulated by Morita [31] in the context of a variational statement of statistical mechanics. Sanchez and de Fontaine [22, 32] developed the method into a formulation suitable for the study of alloys. The method, which reduces to the well known Bragg-Williams or Bethe approximations in a single-site or pair approximation, prescribes a series of increasingly higher order approximations of the free-energy functional to an arbitrary level. The functional may then be minimized with respect to the configurational variables, i.e., the cluster probabilities or, alternatively, the correlation functions. This minimization of the configurational free energy requires calculation of the values of the correlation function of all sub-clusters of the maximum cluster. A small increase in the maximum cluster size from, say, the joint tetrahedron-octahedron cluster in the fcc lattice results in a large increase in the number of sub-clusters, thus increasing significantly the number of operations. As with the cluster

expansion of the formation energy, the convergence of this statistical approximation must be assured. In order to include longer-range interactions in the Ising Hamiltonian without increasing the maximum cluster size, many studies (for example [6, 10, 12, 16, and 33]) have employed the so-called **renormalization** method in which long-range interactions are included using a Bragg-Williams type approximation.

Vibrational free energy is a critical driving force behind some phase transformations. As noted in Reference 15 the leading effect of vibrational entropy is responsible for the curvature of the fcc-bcc phase boundary in the Cu-Zn phase diagram. However, *ab initio* treatments of vibrational effects are rarely included in first-principles phase-stability studies. Instead, either alloy systems are chosen so that the vibrational free energy is **expected** to be insignificant (e.g., all structures having same parent Bravais lattice), or atomic vibrations are included empirically. Since *ab initio* calculations of phonon spectra of compounds are common [e.g. 34], a state-of-the-art first-principles study should incorporate vibrational effects without resort to measurements. Moruzzi *et al* [35] calculated Debye temperatures of several cubic transition metals using a very simple model with good results. Their model, based on an effective speed of sound derived from the bulk modulus, incorporates quasi-harmonic dependence of the vibrational free energy through the Debye-Grüneisen approximation. This technique is well suited to the CVM and is employed in this study.

The first chapter of this thesis summarizes the reported thermodynamic measurements of the three binary systems (Zr-Nb, Nb-Ru, and Zr-Ru), and the results of the total-energy calculations using the Linear Muffin-Tin-Orbital Method in the Atomic-Sphere Approximation (LMTO-ASA) are presented. Reported experimental data for the systems range in abundance for the three systems. For Zr-Nb, phase diagram features and calorimetry data have been well documented. The phase diagram for Zr-Ru has been established, but few measurements have been reported for the equilibrium phases other than solubility limits. The phase diagram for Nb-Ru is by no means determinate. Studies of the crystallography have pointed to the phase diagram compiled by Massalski [36] (see Figure 1.5), but results from the present study and those of Raub and Fritzsche [37] and Das et al [38] show that diagram to be incomplete.

Formation energies are extracted from the total-energy calculations and are approximated using a volume-dependent Morse potential. Several ground-state properties such as bulk moduli and lattice constants are then available from these fit potentials which are compared with reported measurements. The, as yet, undetermined crystal structure of the $NbRu_3$ phase is posited to be hexagonal DO_{19}., and a "newly discovered" stable ground-state phase, Nb_3Ru with bcc DO_3 structure is predicted.

Chapter 2 contains a concise description of the cluster expansion method and an in-depth analysis of its implementation in this study. Several optimization schemes are examined, with no one

method emerging as definitive -- though they prove to be invaluable. The convergence of the cluster expansion is gauged according to how precisely the formation energy of an ordered configuration can be estimated using the derived cluster interactions. Through this energy expansion the ground-state crystal structures of the phases Nb_3Ru and $NbRu_3$ are determined to be the most stable.

Finite-temperature free-energy calculations are presented in Chapter 3. The CVM expression for the configurational free energy is set forth, and the solution method developed by Sanchez and de Fontaine [32] is outlined. Included is the treatment of vibrational free energy after Moruzzi [35]. This allows calculation of thermal expansion, and the coefficients of thermal expansion of the pure elements as a function of temperature are calculated and compared with measurements. The calculated miscibility gap in Zr-Nb is in excellent agreement with measurements.

CHAPTER 1. REPORTED MEASUREMENTS AND TOTAL ENERGY CALCULATIONS

In this chapter a review of reported measurements of thermochemical properties of the three binary systems Zirconium-Niobium, Niobium-Ruthenium, and Zirconium-Ruthenium is provided. In Section 1.5 the results of the total-energy calculations are presented, and some of the calculated properties are compared with measurements.

1.1 Elemental properties

Table 1.1 includes several basic properties of the constituent elements of the system. Notably, the bulk modulus and density increase with atomic number, but the melting temperature does not. The hcp → bcc transition of zirconium at 866 °C is driven primarily by vibration modes [39].

1.2 Zirconium-Niobium

Zirconium-Niobium is a simple system with small, positive formation enthalpies. Figure 1.1 shows the phase diagram as

9

Table 1.1. Measured properties of Zr, Nb, and Ru.

Element	Atomic no.	Atomic wt.	Electron configuration	Crystal structure	[4] Lattice parameters (@ 25°C) [Å]	Density [g/cm³]	[4] Bulk modulus [Mbar]	[4] Melting temperature [°C]
Zr	40	91.22	$4d^2 5s^2$	hcp [bcc @ temp below 866 °C]	3.23 5.15	6.51	0.83	1855
Nb	41	92.91	$4d^4 5s^1$	bcc	3.30	8.58	1.70	2477
Ru	44	101.07	$4d^7 5s^1$	hcp	2.71 4.28	12.36	3.21	2254
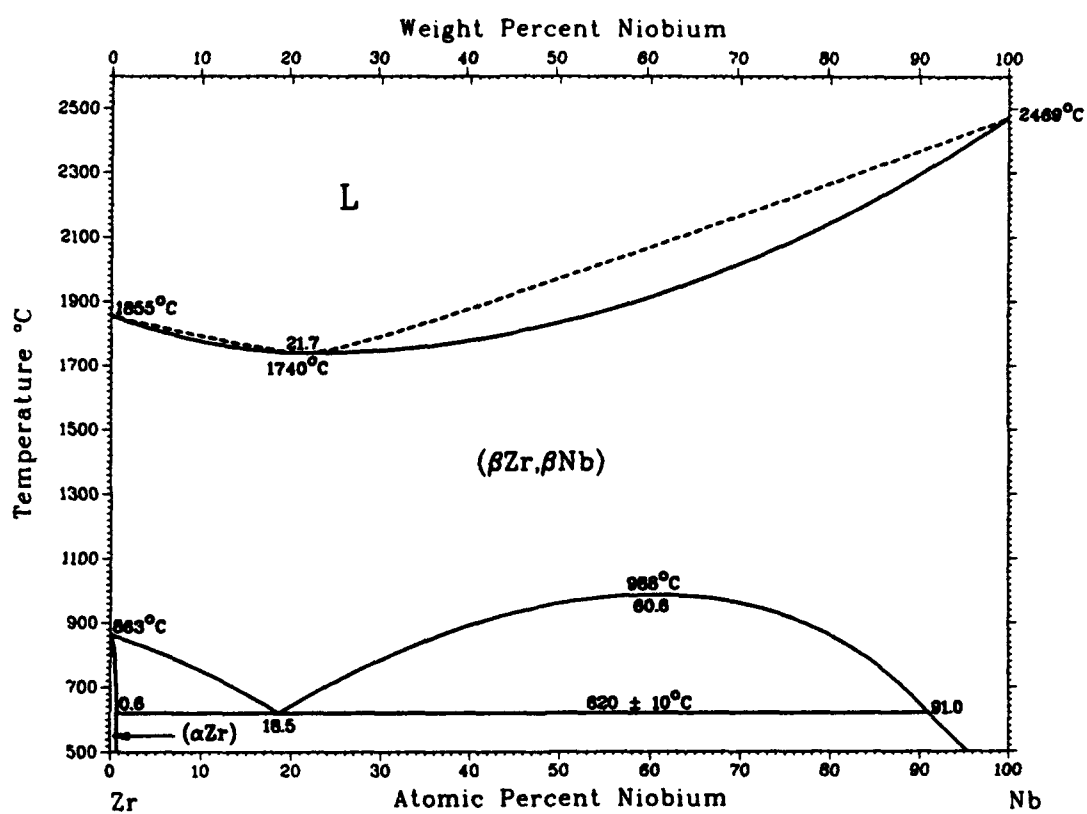
Figure 1.1. Zr-Nb phase diagram as compiled by Gullermet [41].

compiled by Guillermet [41]. The high-temperature miscibility gap in the bcc phase field has a critical temperature reportedly at 988 °C at an approximate concentration of 60.6 % Nb [42]. The monotectoid equilibrium temperature is reported as 610-620 °C with (Zr) concentration between 0.6 and 1 weight percent Zr, Zr-rich bcc concentration between 15 and 20.3 weight percent Zr, and Nb-rich bcc concentration of 85 - 93 weight percent Zr [42].

1.3 Zirconium-Ruthenium

Zirconium-Ruthenium is also a relatively simple system. Figure 1.2 shows the assessed phase diagram of Raub and Röschel [43]. The salient feature of the system is the compound ZrRu with B2 (CsCl) structure. The ordered phase is stable until melting at approximately 2100 °C. A high-temperature (above 1300 °C) Laves phase (C14) at $ZrRu_2$ is destabilized at temperatures below 1285 °C.
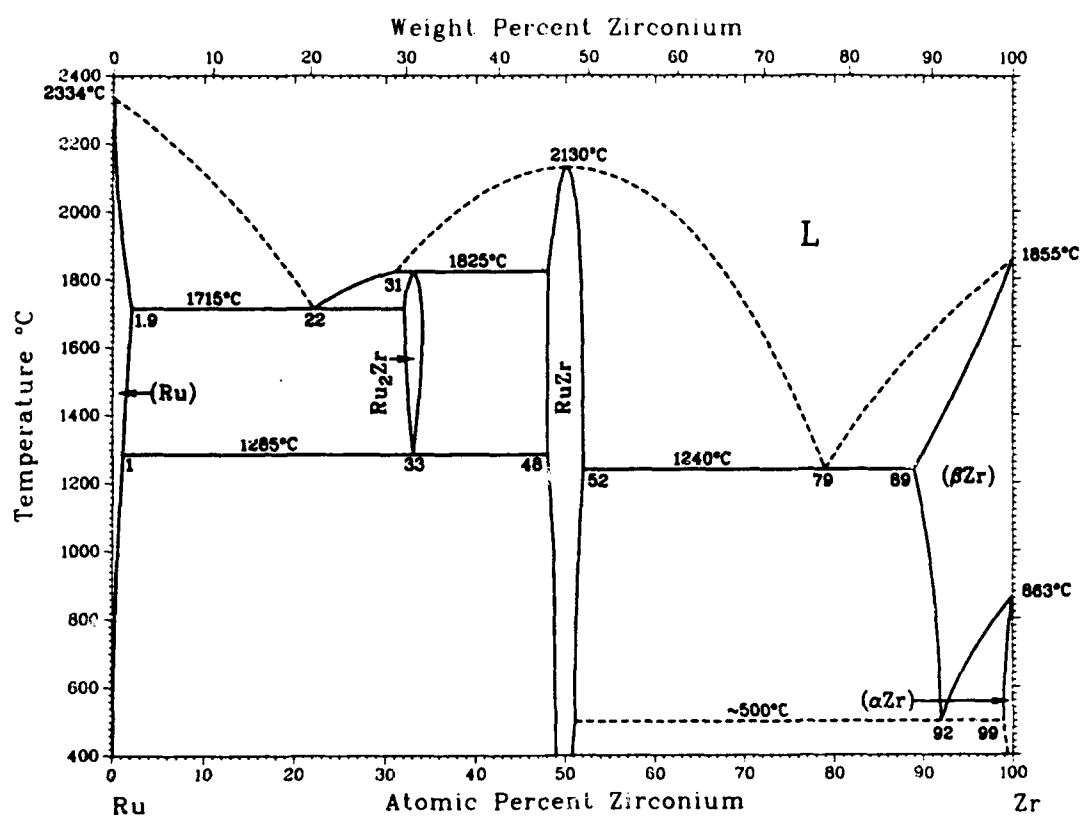
Figure 1.2. Zr-Ru phase diagram from Reference 43.

1.4 Niobium-Ruthenium

The niobium-ruthenium phase diagram is, as yet, incomplete. In fact, some controversy exists among authors concerning the pure ruthenium phase. Jaeger and Rosenboom [44] reported studies suggesting five allotropic transformations in ruthenium. However, Hall and Crangle [45] performed high-temperature x-ray measurements showing a continuous phase with the Mg structure. Their conclusion is that the anamolous calorimetry data are due to non-structural second-order transitions of unspecified nature. Nevertheless, Panteleemenov et al [46] proposed a phase diagram for Nb-Ru assuming the existence of the high-temperature polymorph δ.

Greenfield and Beck [47] made diffraction measurements of several alloys in the system. They postulated a B2-type ordering of the near equi-atomic alloys based on the report of Dwight [48], but the scattering power of Nb and Ru are nearly indistinguishable for Chromium-K X-rays, and no superlattice peaks could be distinguished. However, vanadium and tantalum which are in the same group as zirconium, form B2 phases with ruthenium.

Raub and Fritzsche [37] and Hurley and Brophy [49] reported a tetragonal distortion at a concentration of approximately 40% Ru. Raub and Fritzsche postulated narrow two-phase regions of bcc + bct near 40 atomic-percent Ru and bct + rhombohedral near 46

atomic-percent Ru. Hurley and Brophy mistakenly concluded that a single (Nb) phase field spans concentrations up to 55 atomic-percent Ru, and that the equi-atomic alloy is a "distorted bcc phase." Das *et al* [38] also reported the tetragonal phase at concentrations up to 46 % Ru where an orthorhombic distortion occurs. Figure 1.3 shows the lattice-parameter measurements of Das *et al* and Raub and Fritzsche of Nb-Ru alloys as a function of Ru concentration. It is clear that both studies are in close agreement concerning the tetragonal distortion, but they differ as to the lattice type of the equi-atomic alloy. Das *et al* determined the transition temperature of the tetragonal phase to the parent cubic phase at three concentrations (45.8%, 51.1%, and 55.8% Ru) using resistance measurements. Based on their measurements and the reports of Raub and Fritzsche and of Greenfield and Beck they posited a low-temperature ordered face-centered orthorhombic phase, a higher-temperature face-centered tetragonal phase with $L1_0$ ordering, and the high-temperature parent cubic phase with B2 type ordering. However, no direct evidence of ordering is reported due to the difficulty of detecting superlattice lines for the system. Tsukamoto *et al* [50] also measured the temperature of the tetragonal to cubic transition. Figure 1.4 shows the phase boundary between the cubic and tetragonal phases for $Nb_{50+x}Ru_{50-x}$ proposed by Tsukamoto *et al.*

Hurley and Brophy reported a hexagonal compound of unknown structure at $NbRu_3$. Popova [51] synthesized a high-pressure, high-temperature compound with the $L1_2$ (Cu_3Au) structure
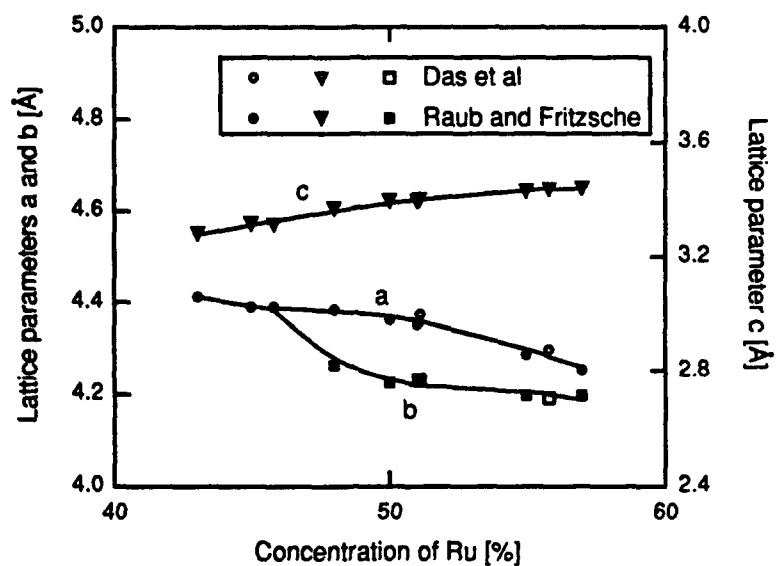
Figure 1.3. Measured lattice parameters of near equi-atomic alloys in Nb-Ru. From Das *et al* [38] and Raub and Fritzsche [37].
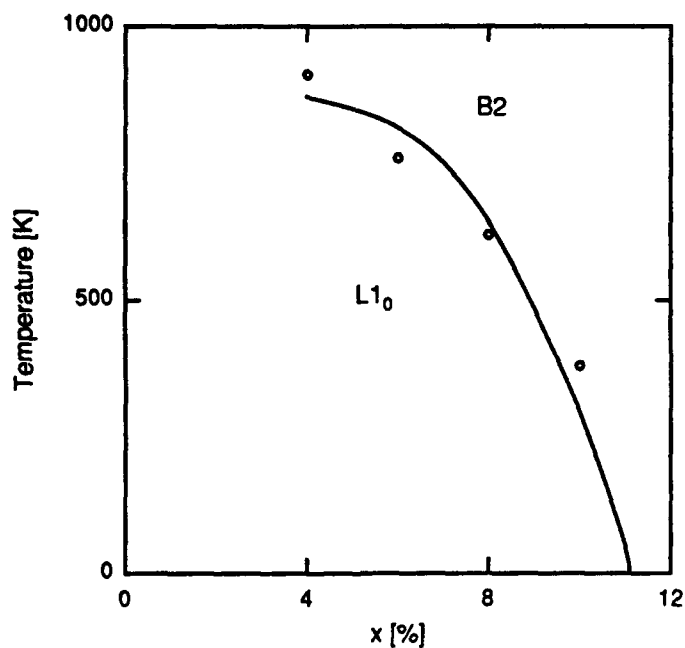
Figure 1.4. Transition temperature of $L1_0$ phase, $Nb_{50+x}Ru_{50-x}$. . . . . as a function of x. (From Tsukamoto *et al* [50]).

at $NbRu_3$ (which, incidentally, is superconducting at 15 K); however no details were included in the abstract [51]. Raub and Fritzsche detected no distinct phase between the orthorhombic phase and the terminal Ru phase.

Figure 1.5 shows the proposed phase diagram compiled by Massalski [36]. This phase diagram is essentially identical to that of Hurley and Brophy except for the tetragonal (NbRu') to cubic (NbRu) transition boundary reported by Tsukamoto and the B2 + bcc two-phase region reported by Raub and Fritzsche. Massalski also labels the $NbRu_3$ phase as Ll_2 following Popova. No reference to the orthorhombic phase reported by Raub and Fritzsche and by Das *et al* is included.
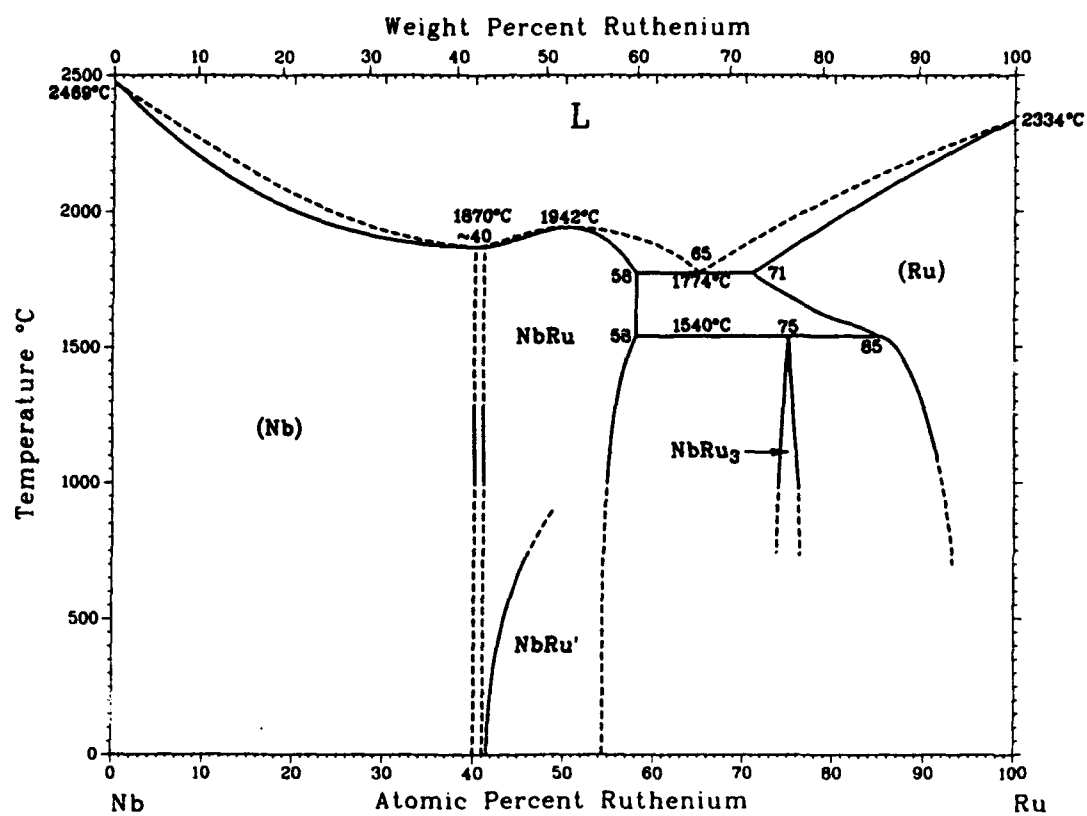
Figure 1.5. Proposed Nb-Ru phase diagram from Reference 36.

1.5 Total-energy calculations

The Hamiltonian for a system with many interacting electrons may be written

$$H = T + U + V, \qquad\qquad [1.1]$$

where T is the kinetic energy operator, U is the Coulombic electron-electron potential, and V is the external potential including the electrostatic interaction with fixed nuclei. The **Density Functional Theory (DFT)** [1] states that V is a unique functional of the electron density and that the minimum energy is reached for the correct electron density. The many-electron problem is intractable, and thus the functional may not be ascertained. Kohn and Sham [2] applied the DFT formalism to the one-electron problem by including a suitable functional for the external potential. This functional requires the calculation of the one-electron kinetic energy and an exchange-correlation energy. The **Local-Density Approximation (LDA)** is made by adopting an analytical form of the exchange-correlation functional which depends on the electron density and is exact for a homogeneous electron gas. The calculation of the one-electron band structure is then required to obtain the kinetic energy. For computational expediency linear band-structure methods are

required. Such linear techniques as FLAPW (full-potential augmented plane-wave [52]), ASW (augmented spherical wave [53]), and LMTO (linearized muffin-tin orbital [54, 20]) are well-developed and in general use. In the LMTO method, energy-independent basis functions are constructed as the solutions of the one-electron Schrödinger equation for the atomic-like muffin-tin potential. The solution method has leading error terms of second order in energy. In this study, the **Atomic-Sphere Approximation (ASA)**, which restricts the muffin-tin potentials to spherical symmetry, was included. In the ASA, only high-symmetry close-packed structures may be treated accurately.

In this study, spin-orbit interactions were included and the exchange-correlation potential of Hedin and Lunqvist [55] was used. The total energies, E^{total}, of each compound were calculated at 12 unit-cell volumes close to the equilibrium volume. The crystal structures used are represented in Figures 1.6 a, b, and c. The figures show the basal-plane projections of one or more unit cells of each of the structures in the bcc and hcp lattices. Filled and empty circles represent atoms of type a or b, respectively. The smaller circles denote atoms with positions displaced one half a unit cell vector normal to the basal plane. Half-filled circles denote alternations in the stacking sequence of atoms in the direction normal to the basal plane.
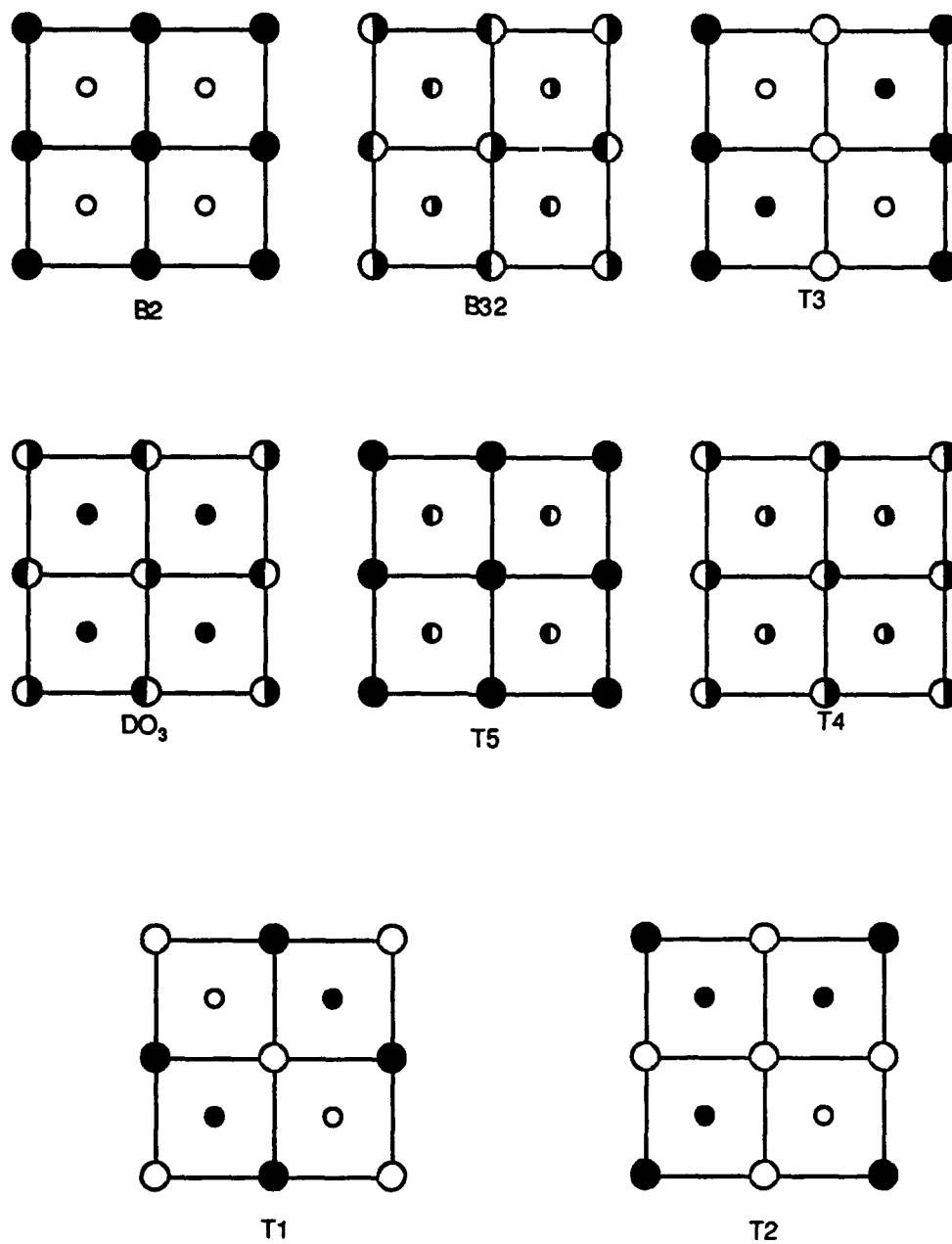
Figure 1.6 a. Basal-plane projections of bcc based ordered structures used in this study.
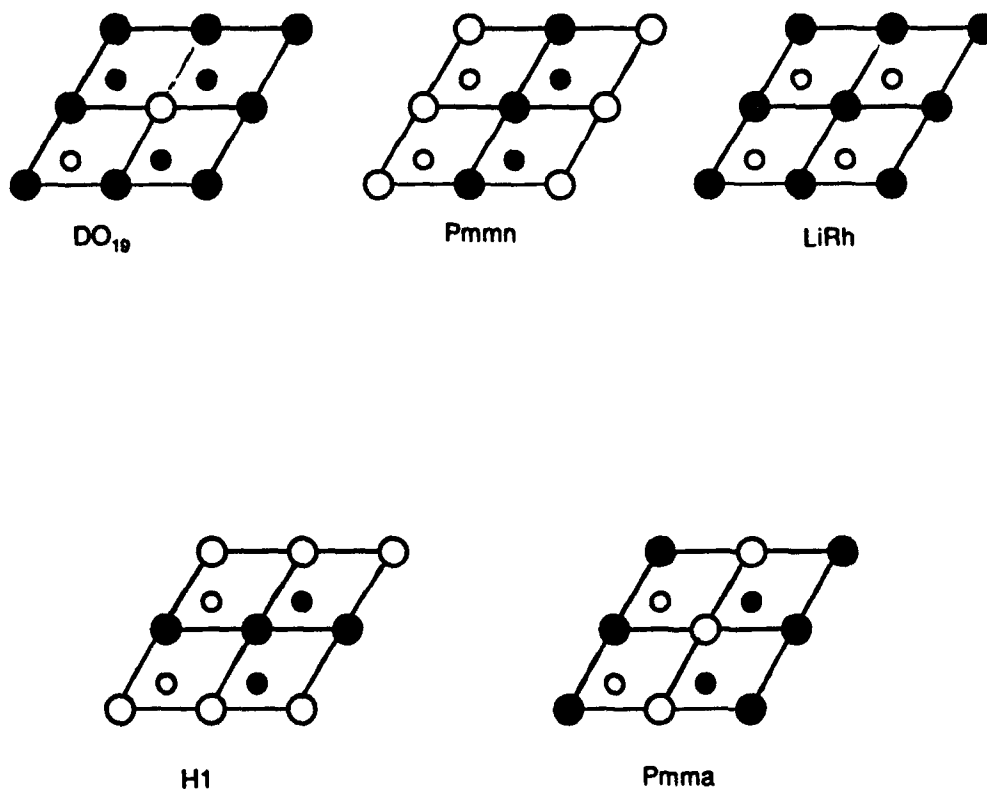
Figure 1.6 b. Basal-plane projections of hcp based crystal structures used in this study. The smaller circles indicate lattice positions c/2 above basal plane.
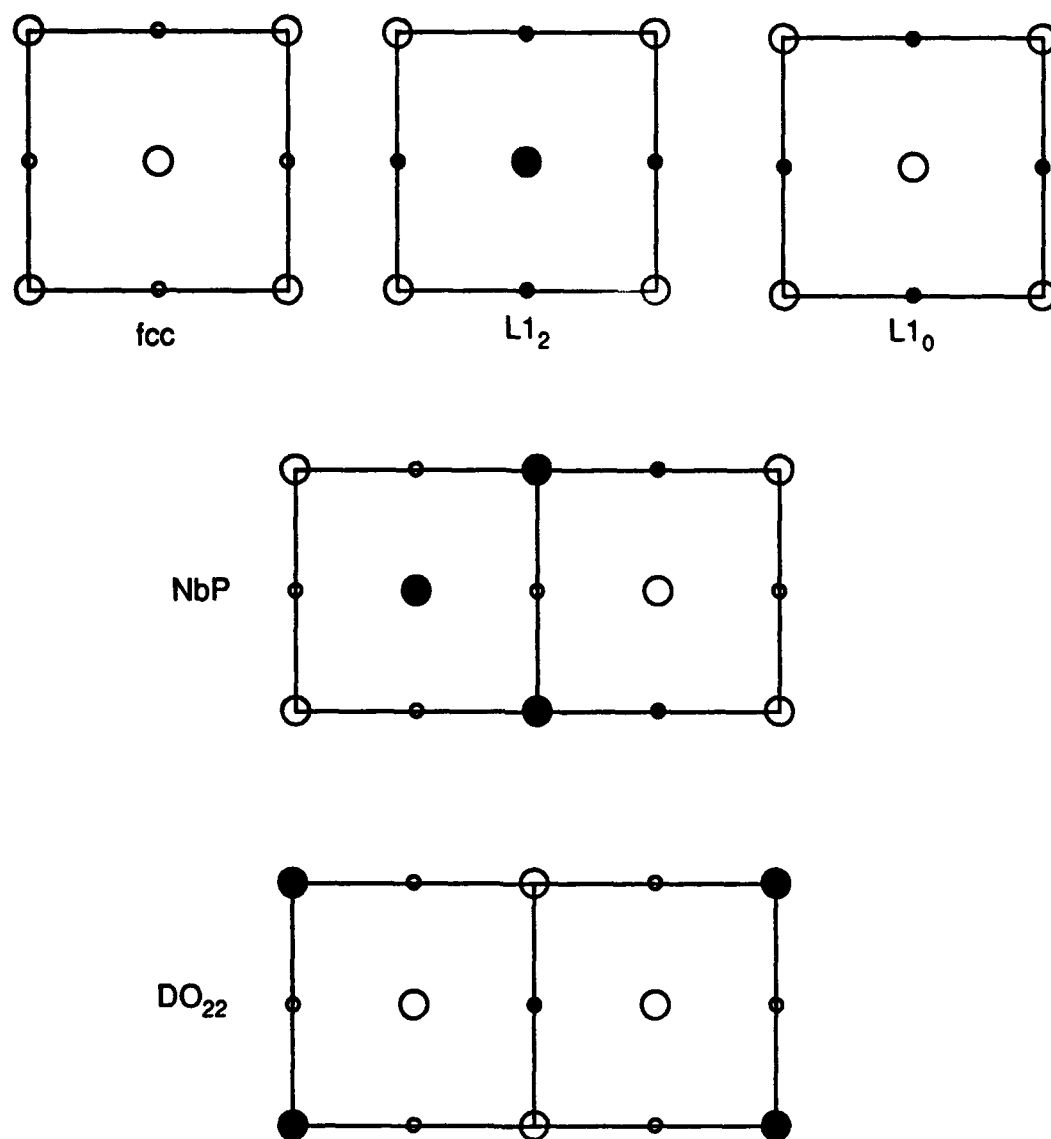
Figure 1.6 c. Basal-plane projections of ordered fcc structures used in total-energy calculations.

The **cohesive energy** per atom, E^{coh}, of each compound A_nB_m was determined at each unit cell volume from:

$$E^{coh}(A_nB_m) = \frac{E^{total}(A_nB_m) - n \cdot E_A^{atom} - m \cdot E_B^{atom}}{m + n} \qquad [1.2]$$

where E^{atom} is the energy of the free atom calculated using the Hartree method. The **formation energy**, E, is then calculated according to the definition:

$$E(A_nB_m) = E^{coh}(A_nB_m) - \frac{n \cdot E_A^{ref} + m \cdot E_B^{ref}}{m + n} \qquad [1.3]$$

where E^{ref} is the **reference energy** of each pure solid. In this study the cohesive energy of each element in its stablest configuration is used as the reference energy, i.e., $E_{Zr}^{ref} = E_{Zr}^{hcp}$, $E_{Ru}^{ref} = E_{Ru}^{hcp}$, and $E_{Nb}^{ref} = E_{Nb}^{bcc}$, unless otherwise noted. Equation 1.3 may be generalized to any configurational property $F(A_nB_m)$, thus defining an **excess configurational property**:

$$F^{xs}(A_nB_m) = F(A_nB_m) - \frac{n \cdot F_A^{ref} + m \cdot F_B^{ref}}{m + n} \qquad [1.4]$$

A Morse-type potential function of average atomic radius (Wigner-Seitz radius), r:

$$E(r) = A - 2 D \exp(-\lambda(r-r_0)) + D \exp(-2\lambda(r- r_0)) \, , \qquad [1.5]$$

was then fit to the formation energies for each compound. Note that the minimum energy is given by,

$$E = A - D \, , \qquad \text{for } r = r_0 \, . \qquad [1.6]$$

Also note that if the cohesive energy of a solid is fit with a Morse potential, the energy approaches that of the free atom(s) in the large limit of r:

$$E \rightarrow A \quad , \qquad \text{as } r \rightarrow \infty \, . \qquad [1.7]$$

Thus the parameter A should be a linear function of the composition, and there are only three degrees of freedom, r_0, λ, and D, in the fit. However, due to (i) the artificial shape of the Morse potential, (ii) the inaccuracy inherent in the solution method of the Hartree method for calculating the energy of the free atoms, and (iii) the fact that the Morse function is fit to data within a relatively narrow domain of r, the fit values of A do not agree precisely with the calculated free-atom energies (errors are typically 10-20 mRy/atom). This, however, is not a significant problem, as the fit of the potential within the domain of interest -- atomic radii between those of the constituent atoms -- has discrepancies on the order of tenths of milli-Rydbergs. Figure 1.7 shows the Morse fit to the calculated formation energies of $NbRu_3$
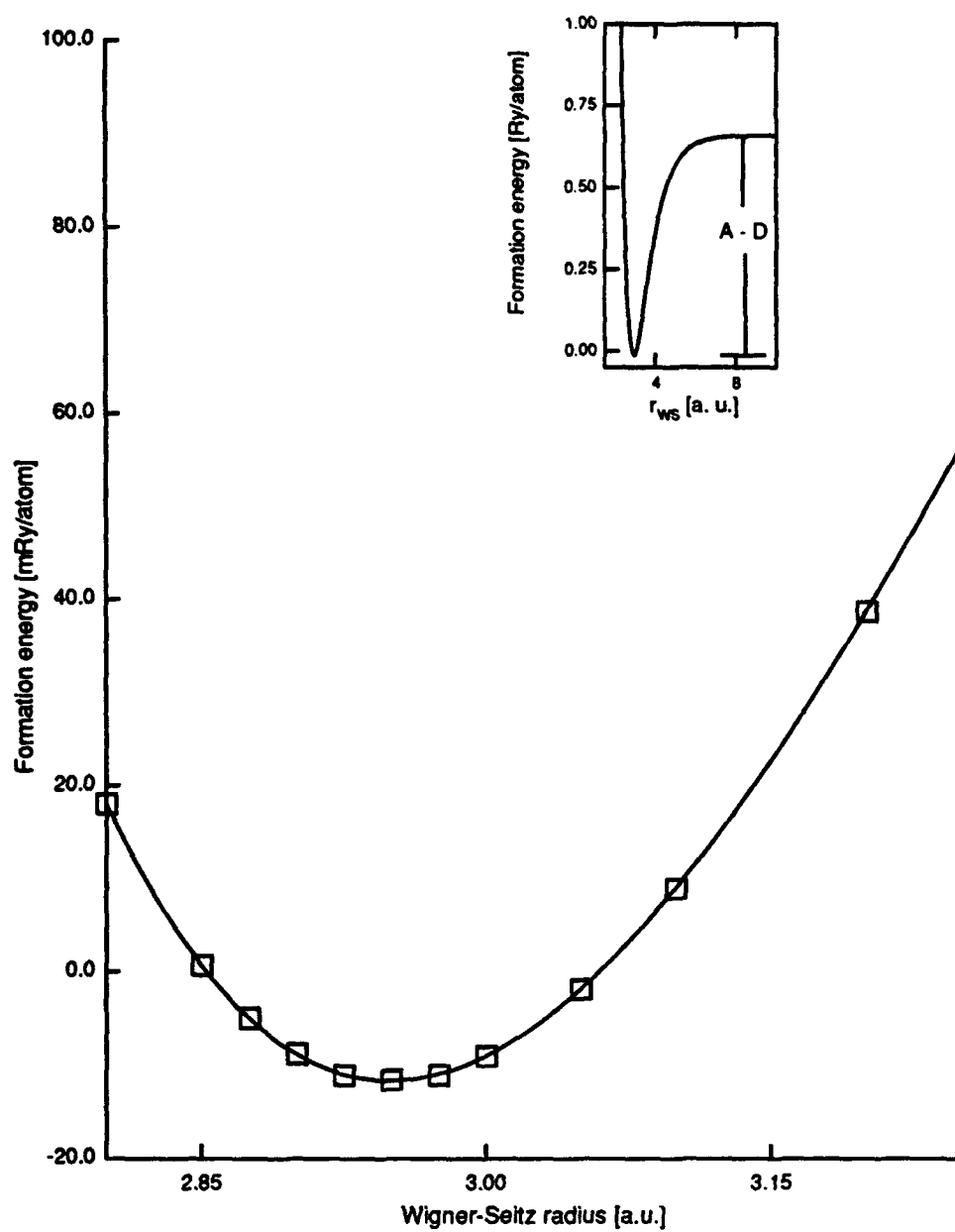
Figure 1.7. Morse fit to calculated formation energies for NbRu$_3$ - DO$_{19}$ as a function of Wigner-Seitz radius. Inset shows cohesive energy A - D.

with a DO_{19} structure. The inset figure shows the overall shape of the Morse potential and indicates the scale of the formation energy with respect to the cohesive energy.

The calculated Morse parameters and minimum energies for each compound studied are shown in Table 1.2 a-c. The average atomic volume is $\Omega_0 = \frac{4}{3}\pi r_0^3$. The experimentally determined equilibrium atomic volumes of the pure elements compare with those calculated as follows:

hcp-Zr   experimental - 157.00 a.u.^{3} calculated - 166.82 a.u.^{3}

hcp-Ru   experimental - 91.85 a.u.^{3} calculated - 99.78 a.u.^{3}

bcc-Nb   experimental - 133.18 a.u.^{3} calculated - 121.26 a.u.^{3}

Typically, LDA calculations predict lower equilibrium volumes than measurements, and this effect is seen for niobium. However the calculations for hexagonal structures were confined to lattices with ideal close-packing, i.e., $c/a = (8/3)^{1/2} \approx 1.63$, whereas the measured c/a ratios for Zr and Ru from Table 1.1 are 1.59 and 1.58 respectively. This artificially high value for c/a accounts partially for the overestimation of the atomic volume in the hexagonal structures. Due to the constraints of the ASA the total-energy calculations were generally confined to close-packed structures in this study -- though some results for distorted lattices were included and are discussed later in this section. Lu *et al* [56] used the (FLAPW) method to

Table 1.2 a. The Morse parameters fit to excess structural energy for each compound in Nb-Ru studied.

Compound/ Structure	r_0 [a.u.]	λ [a.u.$^{-1}$]	D [Ry.]	A [Ry.]	E_{min} [Ry.]
Nb/hcp	3.1878	1.0423	0.71738	0.74348	0.026101
Nb$_3$Ru/DO$_{19}$	3.1046	1.109	0.7056	0.71511	0.009519
NbRu/Pmma	3.0267	1.1887	0.69147	0.68674	-0.00473
NbRu$_3$/DO$_{19}$	2.9494	1.2793	0.67003	0.65837	-0.01166
Ru/hcp	2.8773	1.3938	0.63	0.63	0
NbRu/LiRh	3.0228	1.178	0.68868	0.68674	-0.00193
NbRu/Pmmn	3.0273	1.1825	0.68685	0.68674	-0.0001
NbRu/AB5	3.026	1.186	0.68989	0.68674	-0.00314
Nb/fcc	3.1912	1.0451	0.71835	0.74348	0.025128
Nb$_3$Ru/L1$_2$	3.1071	1.1105	0.70641	0.71511	0.008705
NbRu/L1$_0$	3.0265	1.1905	0.69351	0.68674	-0.00676
NbRu$_3$/L1$_2$	2.9492	1.2808	0.66935	0.65837	-0.01098
Ru/fcc	2.8813	1.3936	0.62399	0.63	0.006015
Nb$_3$Ru/DO$_{22}$	3.1066	1.1106	0.70559	0.71511	0.009521
NbRu$_3$/DO$_{22}$	2.9519	1.2824	0.6664	0.65837	-0.00802
NbRu/NbP	3.0263	1.1938	0.69207	0.68674	-0.00532
NbRu/T1	3.0238	1.1966	0.69455	0.68674	-0.00781
Nb/bcc	3.1678	1.0438	0.74348	0.74348	0
Nb$_3$Ru/DO$_3$	3.0887	1.1153	0.73233	0.71511	-0.01722
NbRu/B2	3.0313	1.1966	0.69953	0.68674	-0.01279
NbRu/B32	3.0261	1.1845	0.69221	0.68674	-0.00546
NbRu$_3$/DO$_3$	2.9698	1.2769	0.64682	0.65837	0.011555
Ru/bcc	2.9095	1.3885	0.58893	0.63	0.041073
NbRu/T1	3.025	1.187	0.69669	0.68674	-0.00995
NbRu/T2	3.0329	1.1987	0.69237	0.68674	-0.00563
NbRu/T3	3.0329	1.1987	0.69235	0.68674	-0.00561

Table 1.2 a continued

	r_0	λ	D	A	E_{min}
NbRu/T4	3.0334	1.1856	0.69088	0.68674	-0.00414
Nb$_3$Ru/T5	3.0968	1.1148	0.73046	0.71511	-0.01535
NbRu$_3$/T5	2.9728	1.2805	0.64568	0.65837	0.01269
Nb/bcc *	3.1725	1.0388	0.73884	0.74348	0.004647
Nb$_3$Ru/DO$_3$*	3.094	1.1209	0.72558	0.71511	-0.01047
NbRu/B2 *	3.0278	1.2062	0.70209	0.68674	-0.01534
NbRu/B32 *	3.026	1.1934	0.69026	0.68674	-0.00351
NbRu$_3$/DO$_3$*	2.9649	1.2825	0.65243	0.65837	0.005945
Ru/bcc *	2.9005	1.3878	0.60048	0.63	0.029522
NbRu/T1 *	3.0255	1.1909	0.69489	0.68674	-0.00814
NbRu/T2 *	3.0324	1.1939	0.6927	0.68674	-0.00596
NbRu/T3 *	3.0333	1.1898	0.68803	0.68674	-0.00128
NbRu/T4 *	3.0368	1.1898	0.68718	0.68674	-0.00043
Nb$_3$Ru/T5 *	3.1005	1.1197	0.72544	0.71511	-0.01032
NbRu$_3$/T5 *	2.9701	1.2814	0.64756	0.65837	0.010814

* denotes distorted bcc lattice with c/a=1.122.

Table 1.2 b. The Morse parameters fit to excess structural energy for each compound in Zr-Ru studied.

Compound/ Structure	r_0 [a.u.]	λ [a.u.$^{-1}$]	D [Ry.]	A [Ry.]	E_{min} [Ry.]
Zr/bcc	3.3994	0.84306	0.68675	0.68923	0.002483
Zr_3Ru/DO_3	3.2437	0.963	0.69483	0.67442	-0.02041
ZrRu/B2	3.1221	1.0892	0.71137	0.65962	-0.05175
ZrRu/B32	3.1117	1.0636	0.6806	0.65962	-0.02099
$ZrRu_3/DO_3$	3.014	1.1992	0.64553	0.64481	-0.00072
Ru/bcc	2.9095	1.3885	0.58893	0.63	0.041073
ZrRu/T1	3.1125	1.0593	0.67913	0.65962	-0.01951
$ZrRu_3/T2$	3.1206	1.0617	0.67744	0.65962	-0.01782
ZrRu/T3	3.1191	1.0577	0.67142	0.65962	-0.0118
ZrRu/T4	3.1203	1.0458	0.66821	0.65962	-0.0086
$Zr_3Ru/T5$	3.2536	0.94904	0.68999	0.67442	-0.01557
$ZrRu_3/T5$	3.0155	1.2101	0.64394	0.64481	0.000865
Zr/hcp	3.4154	0.85552	0.68923	0.68923	0
Zr_3Ru/DO_{19}	3.2654	0.94832	0.67978	0.67442	-0.00535
ZrRu/Pmma	3.127	1.0589	0.67989	0.65962	-0.02027
$ZrRu_3/DO_{19}$	3.004	1.1976	0.65615	0.64481	-0.01134
Ru/hcp	2.8773	1.3938	0.63	0.63	0
ZrRu/LiRh	3.1248	1.0405	0.66751	0.65962	-0.00789
ZrRu/Pmmn	3.1264	1.0475	0.66679	0.65962	-0.00718
ZrRu/H1	3.1252	1.0645	0.67235	0.65962	-0.01273

Table 1.2 c. The Morse parameters fit to excess structural energy for each compound in Zr-Nb studied.

Compound/ Structure	r_0 [a.u.]	λ [a.u.$^{-1}$]	D [Ry.]	A [Ry.]	E_{min} [Ry.]
Zr/bcc	3.399	.84306	0.68675	0.68923	0.00252
Zr$_3$Nb/DO$_3$	3.337	.8886	0.69913	0.70279	0.00366
ZrNb/B2	3.281	.9366	0.70905	0.71635	0.00730
ZrNb/B32	3.278	.9397	0.71346	0.71635	0.00289
ZrNb$_3$/DO$_3$	3.222	.9903	0.72665	0.72992	0.00326
Nb/bcc	3.168	1.0438	0.74348	0.74348	0.00000
ZrNb/T1	3.277	.9386	0.71182	0.71635	0.00453
ZrNb/T2	3.278	.9366	0.71047	0.71635	0.00588
ZrNb/T3	3.277	.9367	0.71104	0.71635	0.00532
ZrNb/T4	-	-	0.71013	0.71635	0.00622
Zr/hcp	3.415	.8554	0.68923	0.68923	0.0000
Zr$_3$Nb/DO$_{19}$	3.360	.8843	0.69120	0.70279	0.0116
ZrNb/Pmma	3.302	.9358	0.69678	0.71635	0.0196
ZrNb/Pmmn	3.302	.9418	0.69705	0.71635	0.0193
ZrNb$_3$/DO$_{19}$	3.246	.9870	0.70509	0.72992	0.0248
Nb/hcp	3.188	1.0423	0.71738	0.74348	0.0261
ZrNb/H1	3.304	.9381	0.69965	0.71635	0.0167
ZrNb/LiRh	3.303	.9438	0.69718	0.71635	0.0192

calculate total energies for hcp-Zr. They predicted an equilibrium volume of 158.92 a.u.^{3} and a c/a ratio of 1.593.

The pressure P is simply:

$$P = - \frac{\partial E}{\partial V} ,$$

[1.8]

and the bulk modulus B is:

$$B = -V \frac{\partial P}{\partial V} = V \frac{\partial^2 E}{\partial V^2} .$$

[1.9]

or, at the equilibrium volume

$$B(r_0) = \frac{D \lambda^2}{6\pi r_0} \cdot \frac{1 \text{ bar}}{6.7977 \text{ E-9 } (Ry/a.u.^3)}$$

[1.10]

The calculated bulk moduli of each compound are shown in Tables 1.3 a-c. The only measured values of bulk moduli reported for these systems are for the pure elements (see Table 1.1). The calculated bulk modulus of Niobium is 1.996 Mbar, the reported value 1.7 Mbar. For Ruthenium the calculated bulk modulus is 3.319 Mbar, the measured value, 3.21 Mbar. For Zirconium the calculated value is 1.153 Mbar, the reported value is 0.83 Mbar.

Table 1.3 a. Calculated bulk moduli for each compound in Nb-Ru studied.

Compound/ Structure	bulk modulus [Mbar]
Nb/hcp	1.908
Nb_3Ru/DO_{19}	2.181
NbRu/Pmma	2.519
$NbRu_3/DO_{19}$	2.896
Ru/hcp	3.319
NbRu/LiRh	2.467
NbRu/Pmmn	2.475
NbRu/H1	2.503
Nb/fcc	1.919
$Nb_3Ru/L1_2$	2.188
$NbRu/L1_0$	2.535
$NbRu_3/L1_2$	2.906
Ru/fcc	3.283
Nb_3Ru/DO_{22}	2.186
$NbRu_3/DO_{22}$	2.898
NbRu/NbP	2.543
Nb/bcc	1.996
Nb_3Ru/DO_3	2.301
NbRu/B2	2.579
NbRu/B32	2.505

Compound/ Structure	bulk modulus [Mbar]
$NbRu_3/DO_3$	2.771
Ru/bcc	3.046
NbRu/T1	2.532
NbRu/T2	2.560
NbRu/T3	2.560
NbRu/T4	2.499
$Nb_3Ru/T5$	2.288
$NbRu_3/T5$	2.780
Nb/bcc *	1.916
Nb_3Ru/DO_3*	2.300
NbRu/B2 *	2.633
NbRu/B32 *	2.536
$NbRu_3/DO_3$*	2.825
Ru/bcc *	3.112
NbRu/T1 *	2.542
NbRu/T2 *	2.541
NbRu/T3 *	2.506
NbRu/T4 *	2.500
$Nb_3Ru/T5$ *	2.289
$NbRu_3/T5$ *	2.794

* denotes distorted bcc lattice with c/a=1.122.

Table 1.3 b. Calculated bulk moduli for each compound in Zr-Nb studied.

Compound/ Structure	bulk modulus [Mbar]
Zr/hcp	1.153
Zr_3Nb/DO_{19}	1.282
ZrNb/Pmma	1.454
$ZrNb_3/DO_{19}$	1.660
Nb/hcp	1.908
ZrNb/LiRh	1.463
ZrNb/Pmmn	1.460
ZrNb/H1	1.454
Zr/bcc	1.120
Zr_3Nb/DO_3	1.291
ZrNb/B2	1.479
ZrNb/B32	1.500
$ZrNb_3/DO_3$	1.726
Nb/bcc	1.996
ZrNb/T1	1.493
ZrNb/T2	1.484
ZrNb/T3	1.486

Table 1.3 c. Calculated bulk moduli for each compound in Zr-Ru studied.

Compound/ Structure	bulk modulus [Mbar]
Zr/hcp	1.153
Zr_3Ru/DO_{19}	1.461
ZrRu/Pmma	1.902
$ZrRu_3/DO_{19}$	2.445
Ru/hcp	3.319
ZrRu/LiRh	1.875
ZrRu/Pmmn	1.826
ZrRu/H1	1.854
Zr/bcc	1.120
Zr_3Ru/DO_3	1.552
ZrRu/B2	2.102
ZrRu/B32	1.933
$ZrRu_3/DO_3$	2.406
Ru/bcc	3.046
ZrRu/T1	1.914
ZrRu/T2	1.912
ZrRu/T3	1.882
ZrRu/T4	1.830
$Zr_3Ru/T5$	1.492
$ZrRu_3/T5$	2.435

Zr-Ru

The formation energies of the compounds in Zr-Ru are displayed graphically in Figure 1.8. The only stable intermediate compound ZrRu has a B2 (CsCl) structure. The calculated formation enthalpy is 51.75 milli-Rydbergs per atom. The measured value is 52.29 ± 2.59 mRy/atom [57]. The ground-state line extends from the pure element points -- which by definition are zero -- through the compounds with the lowest energies at each concentration. In Figure 1.8 no compound has an energy which is lower than the linear combination of the B2 compound with one of the pure elements. Of course, only a small number (11) of total energy calculations have been performed for this system, so the question as to whether an unexamined compound might be stable looms large. This question is addressed in Chapter 2.

Pearson [58] reported the average atomic volume for ZrRu (B2) as 116.15 a.u.^{3}, the computed equilibrium volume is 127.48 a.u.^{3}. Mehl *et al* [59] calculated the total energy versus volume for ZrRu using the FLAPW method and predicted an equilibrium volume of 112.65 a.u.^{3}.

Figures 1.9 a and b show the calculated atomic volumes and bulk moduli of each compound in Zr-Ru. The **excess atomic volume** calculated according to Equation 1.4 is also shown in Figure 1.9 a, and the dashed lines indicate a linear rule of mixtures for each lattice type. The average volume obeys the linear rule with small negative
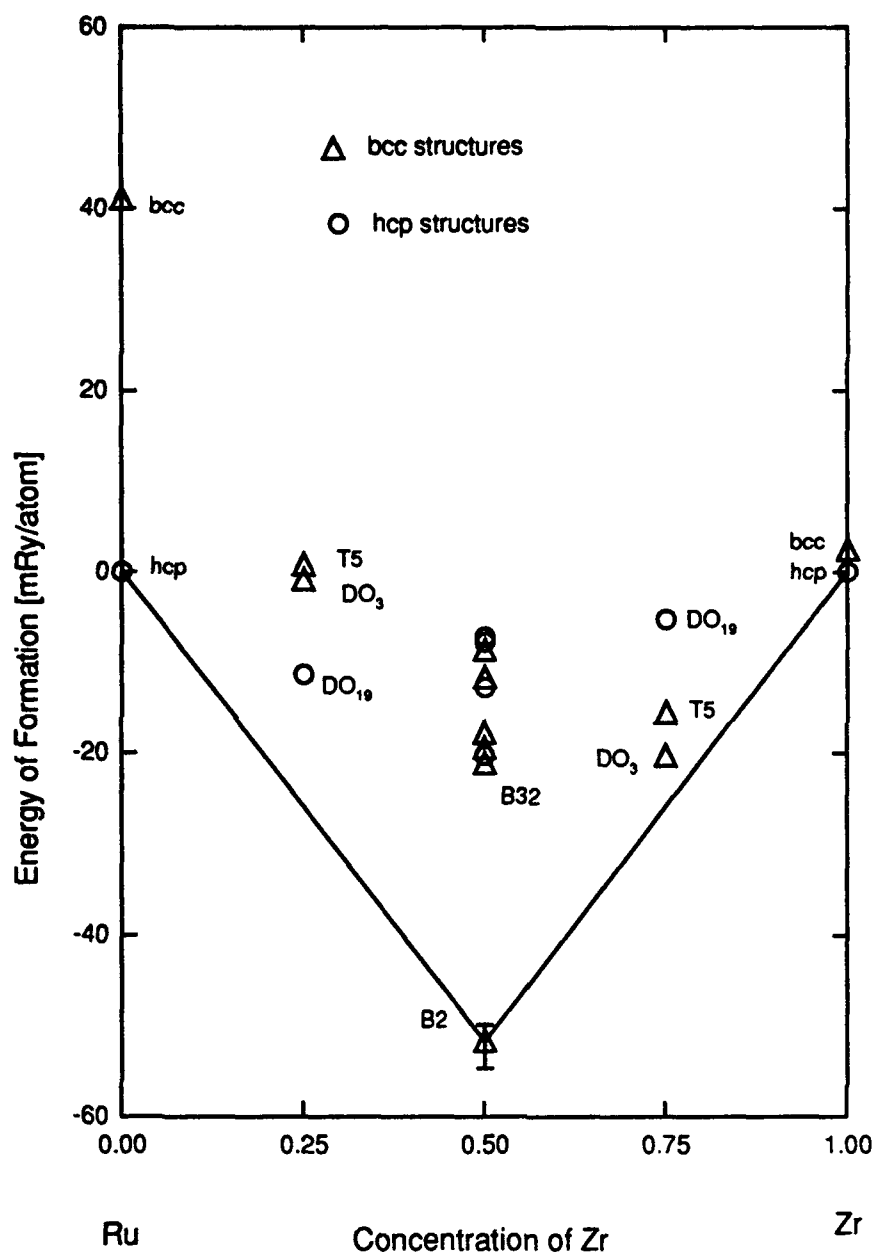
Figure 1.8. Calculated formation energies for selected compounds

in Zr-Ru. The reported value for the B2 compound, 52.29 mRy/atom

is from [57].
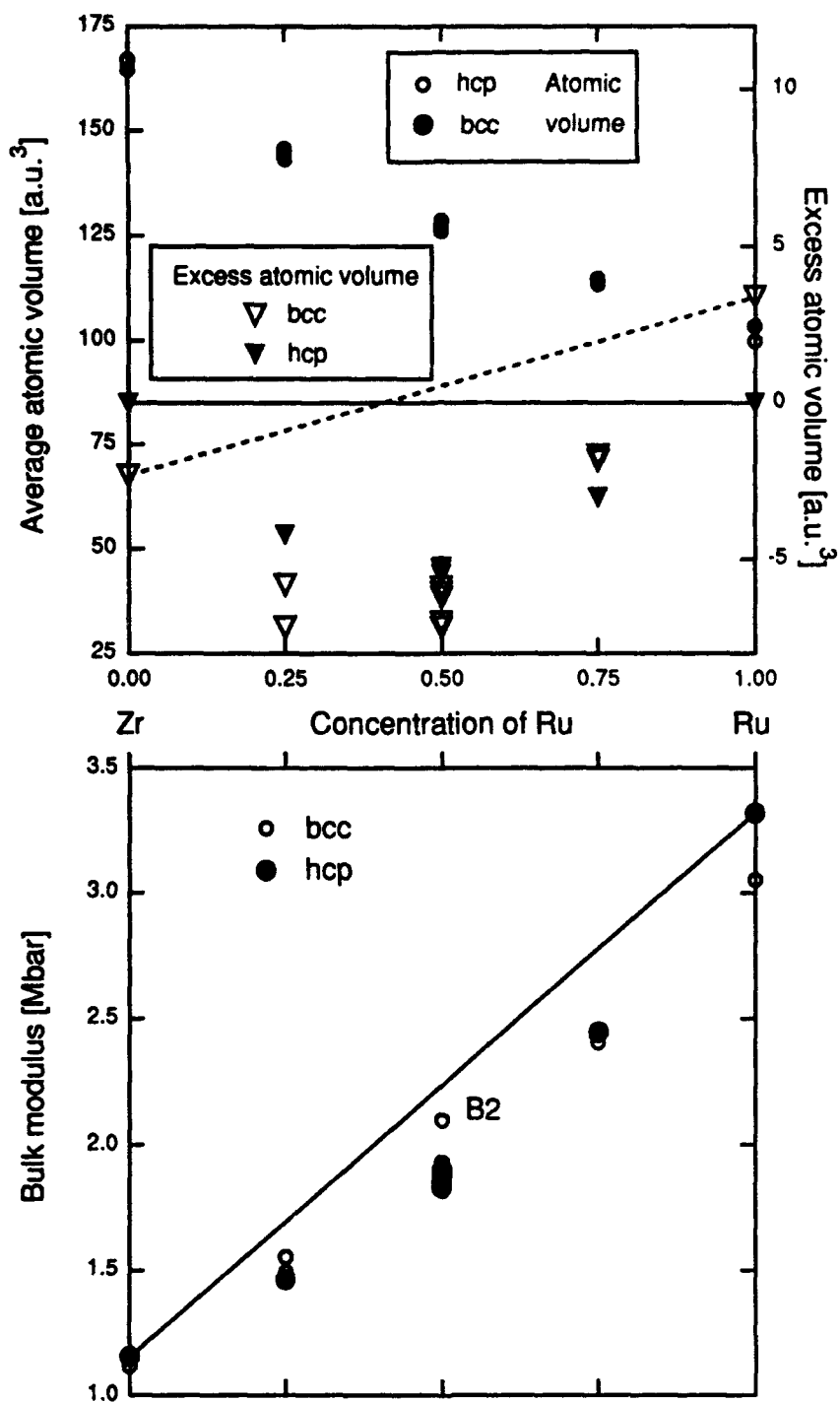
Figure 1.9. (a) Calculated atomic volumes of selected compounds in Zr-Ru. (b) Bulk moduli.

deviations (approximately 6%). The bulk moduli of the intermediate compounds deviate more drastically (18%), and, as seen from Table 1.3 c, the bulk modulus exhibits significant dependence upon the type of ordering. The calculated bulk modulus of ZrRu (B2) is 2.102 Mbar, and Mehl *et al* [59] predicted 2.25 Mbar.

Nb-Ru

The ground-state diagram for Nb-Ru is shown in Figure 1.10. The ground-state line passes through Nb_3Ru with the DO_3 structure. No such compound has been reported. Possibly due to the small scattering difference between Nb and Ru, it is difficult to discern the ordered bcc structure from diffraction measurements.

A stable $L1_0$ phase with $c/a = 1.122$ is seen in the ground-state diagram, and the average of the measured c/a and c/a ratios of the orthorhombic phase at that composition is 1.1165 [10]. This is remarkable since the LMTO-ASA typically loses accuracy with deviations from close-packing. Part of the explanation lies in the fact that at $c/a = 1$ the lattice is bcc and at $c/a = \sqrt{2} \approx 1.414$ the lattice is fcc (see Figure 1.11), thus bounding the aspect ratio of the $L1_0$ structure with close-packed lattices. Further remarks on the stabilization of the $L1_0$ phase are found in Section 2.6.
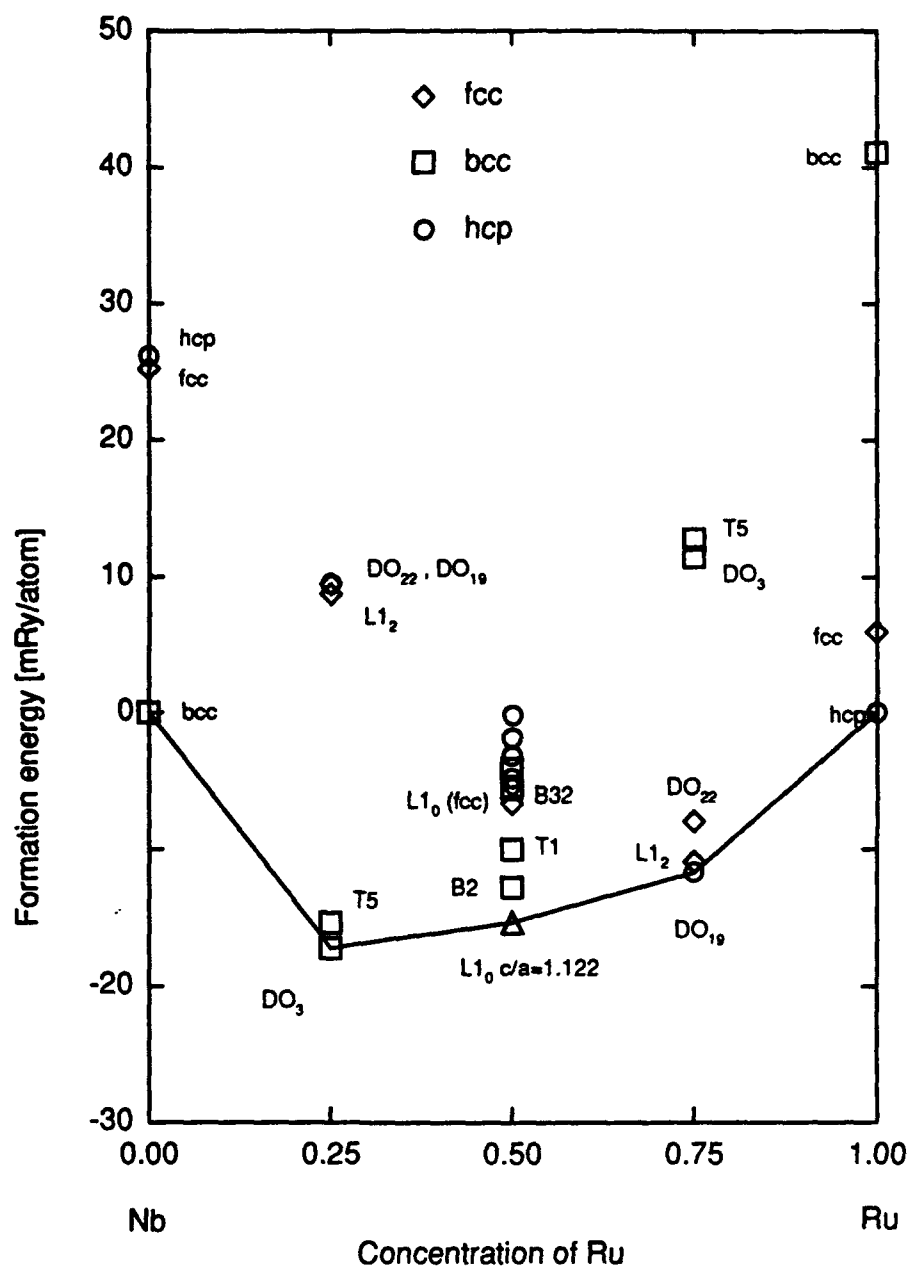
Figure 1.10. Ground-state energies of selected compounds in Nb-Ru.

B2 - bcc; $c/a=1$

$L1_0$ - tetragonal
$1 < c/a < (2)^{1/2}$

$L1_0$ - fcc; $c/a = (2)^{1/2}$
$c = a'$
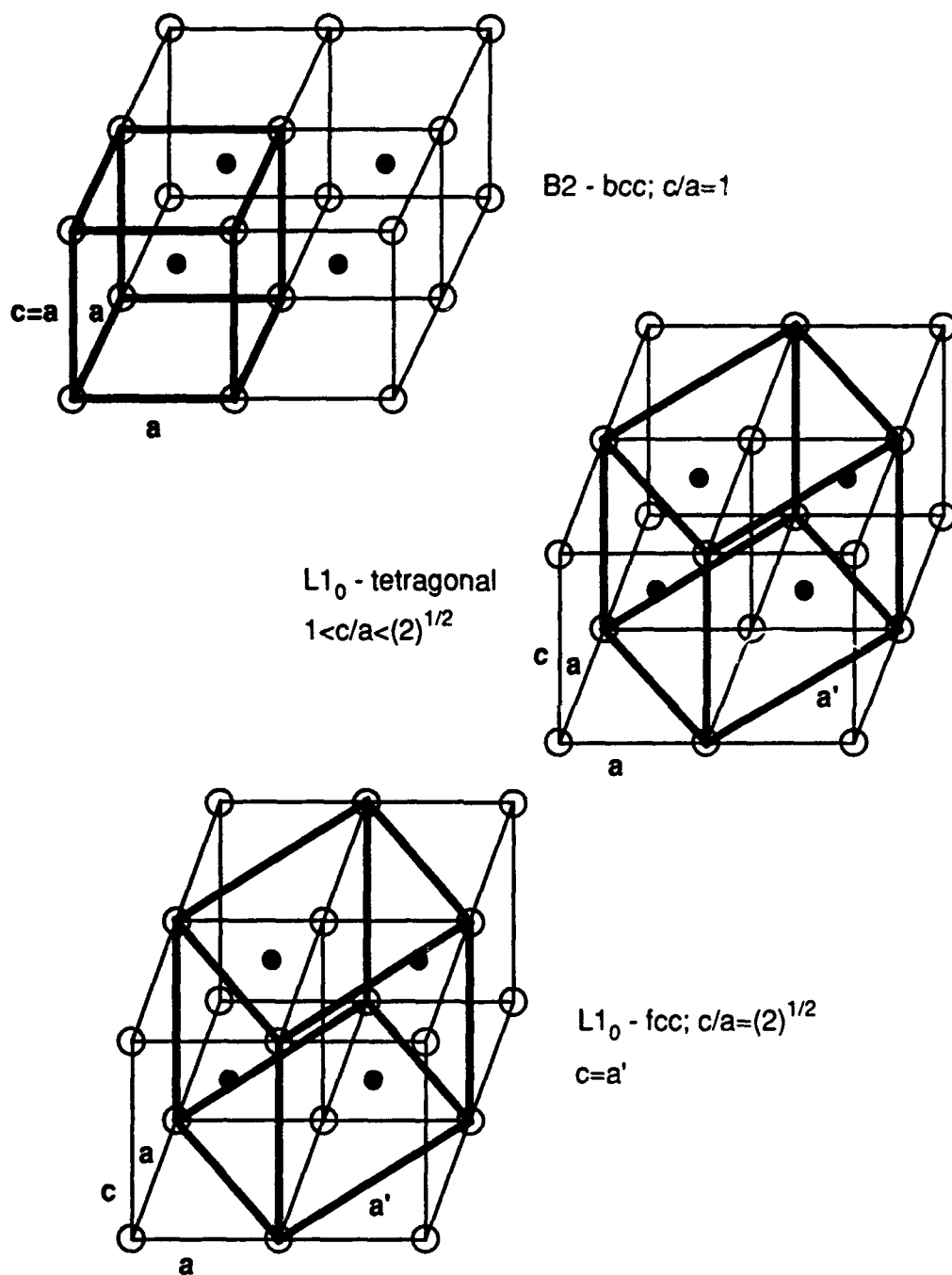
Figure 1.11. Change of crystal symmetry due to tetragonal distortions of B2 structure.

The stable structure of the $NbRu_3$ compound is not obvious from the ground-state diagram. Table 1.2 a shows the hexagonal DO_{19} structure to have a slightly lower formation energy than the $L1_2$ structure. Notably, the constraint of close-packing in the total-energy calculations yields a less negative energy than would be found upon relaxation of the c/a ratio, thus the DO_{19} structure is certainly the more stable.

The atomic volumes and bulk moduli of the fcc-, hcp-, and bcc-lattice structures in Nb-Ru are shown in Figure 1.12. As with Zr-Ru, the deviations from an ideal rule of mixtures of the atomic volumes is negative for each lattice type. That is, a straight line between the volumes of the pure elements (indicated by the dashed lines in Figure 1.12) of a single lattice type lies above the volumes of all the intermediate compounds of the same lattice type. The deviations of the volumes and of the bulk moduli from the straight line mixture rule are small (less than 3%).

Zr-Nb

The ground-state energies of the Zr-Nb system are shown in Figure 1.13. As expected from the well-documented phase diagram there are no stable intermediate compounds. Figure 1.14 shows the calculated atomic volumes and bulk moduli of each compound. As in the other two systems, the volumes and bulk moduli of the
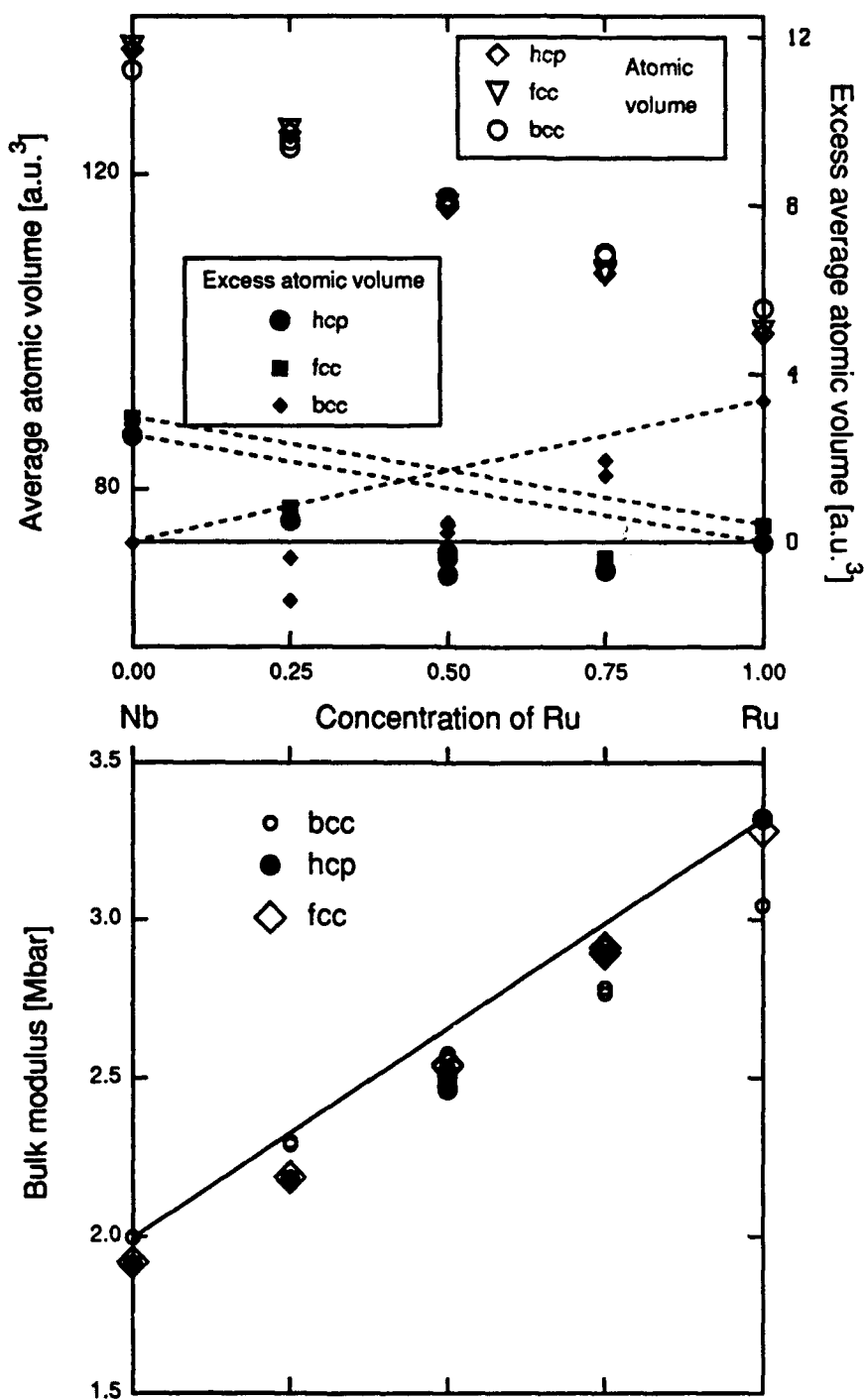
Figure 1.12. (a) Calculated atomic volumes of selected compounds in Nb-Ru. ; (b) Bulk moduli.
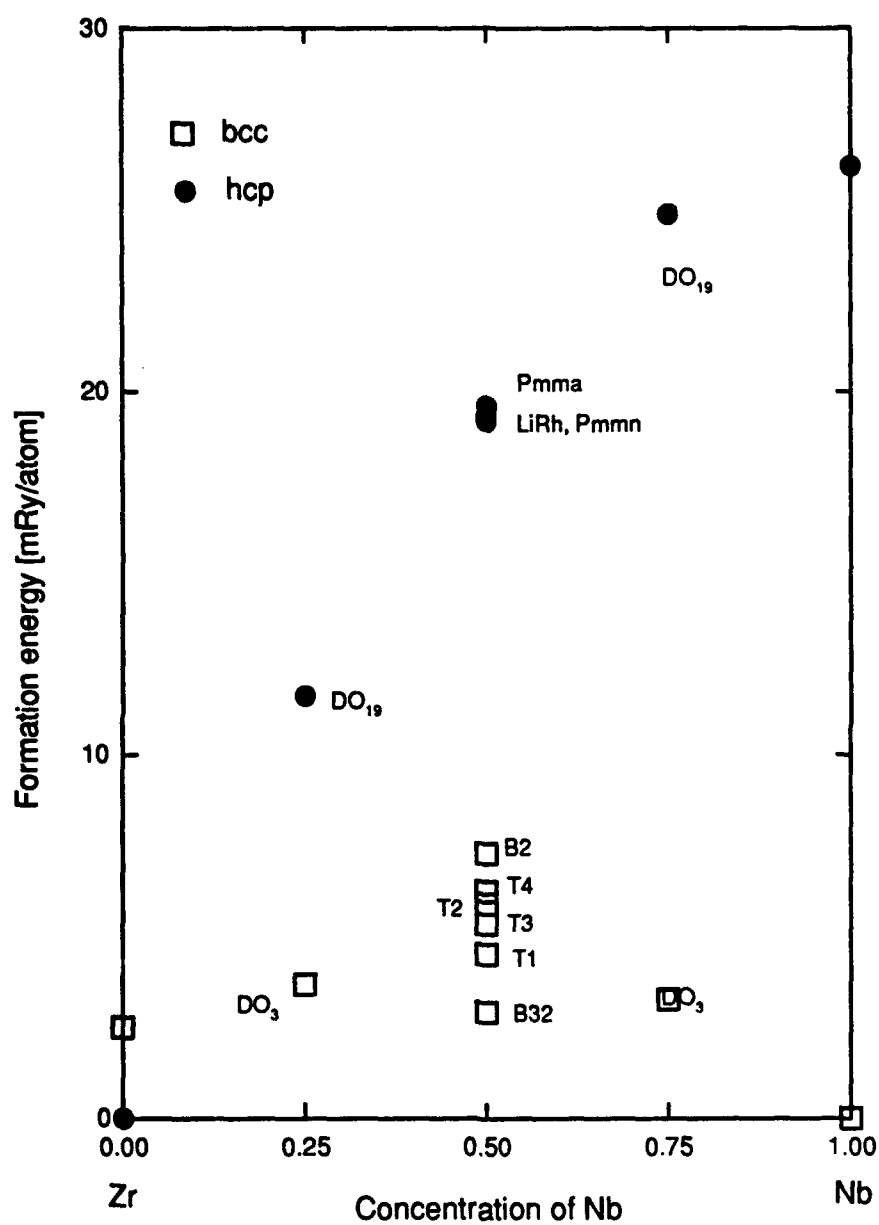
Figure 1.13. Calculated formation energies of selected compounds in Zr-Nb.
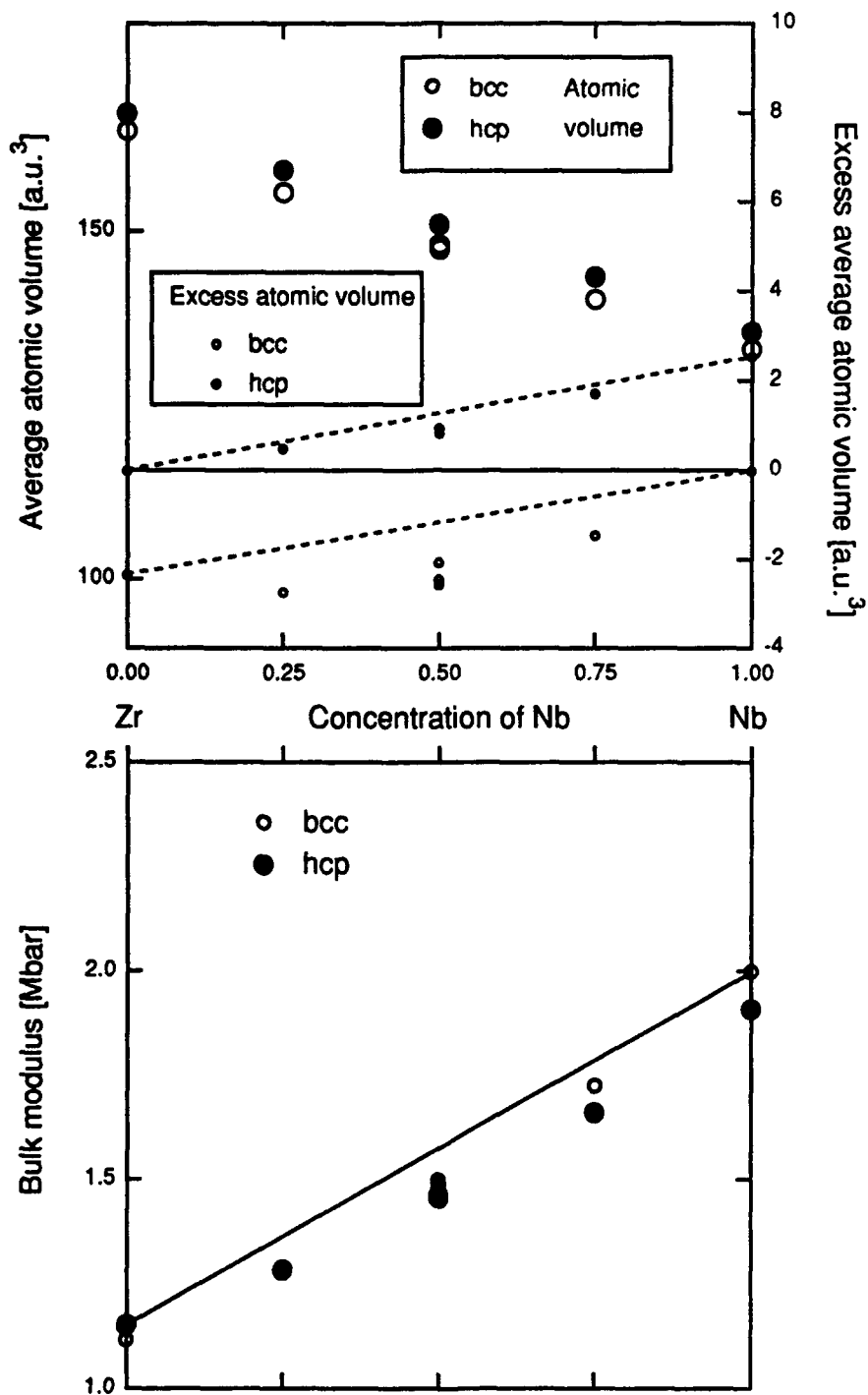
Figure 1.14. (a) Calculated atomic volumes of selected compounds in Zr-Nb. (b) Bulk moduli.

intermediate compounds have small negative deviations from linear mixture theory.

The total-energy calculations predict ground-state structures matching those reported by experimentalists with the exception of the orthorhombic phase of near equi-atomic Nb-Ru alloys which is not within the realm of the atomic sphere approximation. Additionally, the ordering of the compound $NbRu_3$ is posited to be DO_{19}, and an undetected ground-state phase Nb_3Ru with DO_3 structure is also predicted. The calculated atomic volumes of the elements fall within 9% of the measured values. The calculated atomic volume of ZrRu is within 10% of the measured value. The calculated c/a ratio of the NbRu $L1_0$ compound is within 0.5% of the measured value. The calculated bulk moduli of the Zr, Nb, and Ru are within 18% ⋅ and 39% respectively of the reported values, and the predicted valuे ⸰ ZrRu is within 7% of the calculated value of Mehl *et al* [59].

The total-energy calculations of the small number of structures of Table 1.1 are not sufficient to determine the complete ground-state of these systems. Due to the fact that LDA calculations for structures with more than eight atoms per primitive unit cell become very expensive, only a small select set of structures is practical. The cluster expansion described in Chapter 2 may be used to estimate the formation energy of any ordered structure on a bcc, fcc, or hcp lattices. This expansion is a powerful tool which lends confidence to the predicted ground-state configurations made in this chapter.

CHAPTER 2. CLUSTER EXPANSION

In the next section, highlights of the general formalism of the **cluster expansion** techniques developed by Sanchez *et al* [21, 22] are reviewed. Only binary systems will be considered here, but the theory has been generalized to multi-component systems by Sanchez *et al* [21]. The main result, that any **function of lattice configuration** (used synonymously in this chapter with **configurational property**) can be described by a cluster expansion, will be established, as will several other useful notions.

The second section details how a truncated cluster expansion can be inverted to derive the expansion coefficients **(effective interactions)** from a set of known configurational properties, e.g., the cohesive energy. Section 2.3 sets forth several schemes for including structural relaxation in the cluster expansion. A truncated cluster expansion is not unique, and the final three sections of this chapter describe the optimization methods used to insure adequate convergence of the expansion. The most important method for testing the convergence is using the cluster expansion to predict cohesive energies of various ordered structures for which the energies have been previously determined using the local density approximation (LMTO) calculations. The results of the convergence tests are discussed in Section 2.6.

47

2.1 Cluster expansion formalism

In the Ising model a binary crystal with N lattice-sites has 2^N possible configurations. To a site i occupied by an A-atom, a **spin** s_i of +1 is assigned, and for B-atoms -1. Each of the 2^N possible configurations is then described completely by the N-vector $\sigma = \{ s_1, s_2, s_3, ..., s_N \}$. A set of **orthonormal characteristic functions**, Φ, for N-dimensional discrete space spanned by σ is given by [21]:

$$\Phi_\alpha(\sigma) = \prod_{i \in \alpha} s_i = s_{i_1} s_{i_2} \cdots s_{i_n} , \qquad [2.1]$$

where $\alpha = \{ i_1, i_2, i_3, ...i_n \}$ includes every **cluster** of n sites in the crystal lattice, and where the inner product is defined as:

$$<\Phi_\alpha(\sigma) \cdot \Phi_\beta(\sigma)> = \frac{1}{2^N} \sum_\sigma \Phi_\alpha(\sigma) \, \Phi_\beta(\sigma) \qquad [2.2]$$

Hence, there is a one-to-one correspondence between the set of orthogonal functions Φ and the set of all clusters α, including the empty cluster for which, $\Phi_0(\sigma) = 1$.

As Φ forms a complete orthonormal basis, any function of configuration (**configurational property**), $F(\sigma)$, may be written as [21]:

$$F(\sigma) = \sum_{\alpha} J_{\alpha} \Phi_{\alpha}(\sigma) \ . \qquad\qquad [2.3]$$

where the sum extends over all inequivalent clusters in the crystal, and J_{α} , given by:

$$J_{\alpha} = \ < F(\sigma)\cdot \Phi_{\alpha}(\sigma) \ >$$

$$= \frac{1}{2^N} \sum_{\sigma} F(\sigma) \ \Phi_{\alpha}(\sigma) \qquad\qquad [2.4]$$

are the projections of $F(\sigma)$ on the orthogonal cluster basis, Φ -- often called the **effective interactions**. Equation 2.3 is simplified by the requirement that each J_{α} be the same for all clusters that are related by any of the space-group operations of the crystal.

The correlation functions, ξ_{α}, are defined as the expectation values of the characteristic functions:

$$\xi_{\alpha} = \ < \Phi_{\alpha}(\sigma) \ > \ ,$$

$$\qquad\qquad [2.5]$$

$$= \ < s_1 \ s_2 \cdots s_{n_{\alpha}} \ >$$

For a perfectly ordered crystal, the correlation function of a cluster type is an average of the spin product over all equivalent clusters in the crystal:

$$\xi_\alpha = \frac{1}{z_\alpha \cdot N} \sum_{(p_i)} s_{p_1} s_{p_2} \cdots s_{p_n} \qquad [2.6]$$

where α labels each type of inequivalent cluster of which there are $z_\alpha \cdot$ N in the crystal. Combining Equation 2.3 with Equation 2.5 leads to an expression for the expectation value of any configurational property $^\sigma\overline{F}$:

$$^\sigma\overline{F} = \frac{1}{N} < F(\sigma) > = \sum_{n=0}^{N} z_n J_n \xi_n \ . \qquad [2.7]$$

in terms of the configurational variables, ξ_n, and the interaction coefficients, J_n. The technique for determing the interactions is discussed in the next section.

2.2 Obtaining cluster interactions from configurational properties

Since the sum in Equation 2.6 cannot be evaluated exactly (there are on the order of 10^{23} terms), a truncated approximation must be used, and the practical application of the representation of the expectation value of a configurational function depends upon the rapid convergence of the cluster projections, J_n. The key step is choosing, *a priori*, a trial maximum cluster size and establishing the convergence of the truncated series, with the dual task of determining

the cluster interactions. The former is discussed in section 2.6. The latter is the natural first step and is accomplished using a system of equations of the form of Equation 2.6 for the value of the energy of an ordered configuration p:

$$^P E = \sum_{k=0}^{M} z_k\, ^P\xi_k\, J_k \ ,$$

[2.8]

where k denotes the cluster type and $^P\xi_k$ is the correlation function corresponding to cluster k in the ordered structure p which is evaluated directly from the geometry of the configuration. For convenience Equation 2.8 is rewritten:

$$^P E = \sum_{k=0}^{M} \Xi_{pk}\, J_k$$

[2.9]

The energy E is not an average because the correlations are not expectation values but rather geometric defined quantities. The **basis** of the expansion, defined here for clarity, consists of the **basis structures** p=1 ... m and the **basis clusters** k=1 ... M. Therefore, for a system of M equations, there exists an inverse:

$$J_k = \sum_{p} \Xi_{kp}^{-1}\, E_p \ ,$$

[2.10]

provided the matrix of coefficients Ξ_{pk} is not singular. Thus, from a finite set of values of configurational functions a set of cluster interactions may be calculated.

Using Equation 2.9, Connolly and Williams [23] calculated cluster interaction energies from the first-principles total energies of a set of ordered compounds. In the present study, such an expansion of the cohesive energies is used to examine cluster expansions for several lattice types. To this end, the excess $\Delta F(\sigma)$, of any configurational function $F(\sigma)$ is defined according to:

$$\Delta F(\sigma) \equiv F(\sigma) - (1-x) \cdot F(A) - x \cdot F(B) , \qquad [2.11]$$

where x is the compositional fraction of B for configuration σ, and $F(A)$ and $F(B)$ denote the properties of pure A and B crystals respectively. Note that the properties may have dependence on variables beside the configuration σ. For example, the cohesive energy has explicit dependence on the average atomic volume. By establishing a definition of the excess internal energy, a reference energy level for the alloy free energy is defined implicitly.

2.3 Relaxation

As mentioned above, the energy depends explicitly on the volume. Therefore, Equations 2.8 and 2.9 must be generalized to

include explicit dependence of the cluster interactions of the volume V:

$$J_k(V) = \sum_p \Xi_{kp}^{-1} E_p(V) \quad .$$

The correlations themselves depend only upon the configuration. However, there is no basis to suppose that the "true" chemical interactions can be obtained from Equation 2.11 using a single value of V. That is, the cluster interactions of the equilibrium configuration of the disordered alloy probably depend upon the configurational energies of the basis structures in a more complex sense than the above relation. If the equilibrium configuration can be determined by constraining each atom to some average volume and then minimizing the energy with respect to this global volume, then Equation 2.11 is appropriate. This approach is called **global relaxation** in this study.

If it is assumed that each type of atom "prefers" some particular volume irrespective of its environment (location in a cluster), then the interactions can be relaxed locally -- at the expense of excluding non-local effects. This **total relaxation** is achieved by rewriting Equation 2.11 as:

$$J_k = \sum_p \Xi_{pk}^{-1} E_p(V_p) \quad , \quad$$

[2.13]

where V_p is, for example, the equilibrium volume of configuration p at absolute zero temperature. In section 2.6 it will be shown that generally cluster expansions converge more rapidly with global relaxation than with total relaxation.

Ferreira *et al* [6, 10] "split" the cohesive energy into chemical (ε) and elastic parts (G). By assuming that the equilibrium volume of an alloy of fixed concentration is independent of the chemical order they proposed the so-called ε-G representation:

$$E(\sigma, V) = \varepsilon(\sigma) + G(x) \quad . \qquad [2.14]$$

The elastic energy G has explicit dependence on the concentration x through a functional in which the equilibrium volume and bulk modulus of an alloy are considered independent of the state of order σ. The chemical energy ε is independent of volume. This approach led to satisfactory cluster expansions for semiconductor alloys [4], but the underlying assumptions -- particularly, that the elastic constants are independent of the state of order -- are questionable for intermetallics.

Sluiter *et al* [13] proposed a simpler scheme that does not require the elastic energy be independent of the chemical order. The approach consists of three steps.

1) All the atoms (A and B) in the alloy are compressed (or expanded) to the alloy volume V'. Associated with this compression is

an elastic energy called in this study the volume deformation energy E^{VD}:

$$E^{VD} = \frac{(1-x)(V_A - V')^2 B_A}{V_A} + \frac{x(V_B - V')^2 B_B}{V_B} \qquad [2.15]$$

where V_A, B_A, V_B, and B_B are the equilibrium volumes and bulk moduli of elements A and B. Note, E^{VD} is positive.

2)   The atoms are mixed isochorically at volume V' to the equilibrium state of order.

3)   A relaxation energy is approximated:

$$E^{relax} = QW^2 , \qquad [2.16]$$

where W is the difference between the alloy volume V' and the ideal alloy volume:

$$W = V' - (1-c) V_A - cV_B , \qquad [2.17]$$

and Q is concentration-dependent effective elastic constant. This relaxation energy is then added to the configurational energy. The global relaxation method used in this study is equivalent to steps 1 and 2 outlined above.

Both the techniques of Sluiter *et al* and Ferreira *et al* described above are restricted to volume relaxation (as is the method

used in this study), i.e., the atoms are confined to the ideal positions on lattice points. This treatment ignores the often significant energy associated with relaxation of atoms from their ideal positions. Zunger *et al* [24] include two structural relaxation modes in addition to the volume deformation described above: cell-internal and cell-external relaxations. The cell-external relaxation lowers the energy by relaxing the unit-cell vectors, e.g., the tetragonal distortion of CuAu or deviation of the c/a ration in hexagonal structures. Cell-internal relaxations preserve the unit-cell vector lengths but allow relaxation of atomic positions not constrained by the crystal symmetry, e.g., interplanar distances in CuPt-type structures. Note, this relaxation is non-existent in certain structures such as $L1_0$, $L1_2$, and DO_{22}. These two relaxation modes often capture dominant effects which elude analyses that include only hydrostatic relaxations. For example, in this study cell-external relaxations lead to a change in lattice type of the equilibrium structure of $NbRu_3$ and of NbRu. Lu *et al* [24] reported large shifts in the computed electronic density of states caused by relaxation which produce better agreement with measurements. Due to the inapplicability of the LMTO-ASA to low-symmetry crystal structures, cell-internal and cell-external relaxations were not used extensively in this study.

Finally, Zunger *et al* [24] show that the effects of relaxation -- in particular, cell-internal relaxation -- are critical in superlattices with 3 or more repeat periods. Further, the standard form of the cluster expansion, Equation 2.8, fails completely to determine the cell-

internal relaxation that produces the strain energy in the long-period superstructures.

To overcome this deficiency Zunger, *et al* [24] used a reciprocal-space formulation for the cluster expansion. The real-space interactions J_i are replaced with a single reciprocal-space function $J(\mathbf{k})$. This expansion leads to a rapidly convergent cluster expansion which predicts accurately the results of valence force field model of long-period superlattice.

2.4 Configuration Space

The method of extracting cluster interaction energies from the configurational energies of a set of ordered structures has been presented. As mentioned in the preceding section a trial maximum cluster size is chosen, and the convergence of the series in Equation 2.8 must be established. The studies cited previously [1.1-13] used cluster expansions including interactions up to fifth nearest neighbors. Figures 2.1 a and b show clusters used in a typical expansion for hcp- and bcc-based structures. The number of clusters chosen determines the order of the system of Equation 2.8.

The characteristic functions of Equation 2.3 form a complete orthogonal basis of configuration space (discrete N-space) [21]. The correlation functions form a dual orthogonal basis.
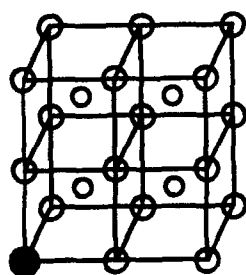
Cluster #2
point
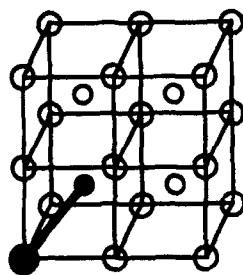
Cluster #3
nearest-neighbor pair
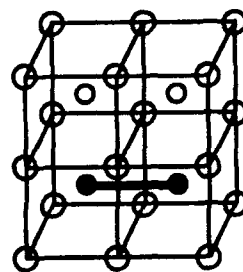
Cluster #4
2nd nearest-neighbor
pair
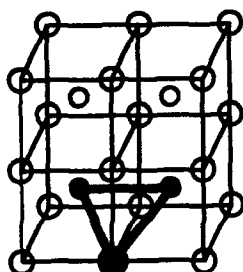
Cluster #5
triangle
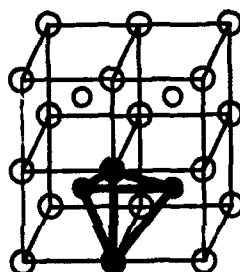
Cluster #6
tetrahedron
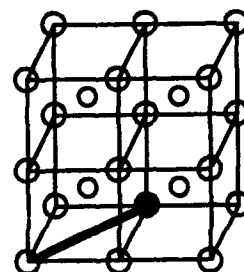
Cluster #7
3rd nearest-neighbor
pair
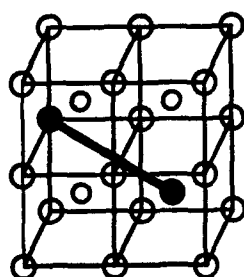
Cluster #8
4th nearest-neighbor
pair
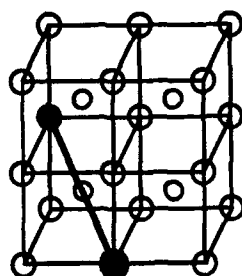
Cluster #9
5th nearest-neighbor
pair
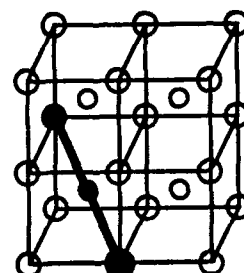
Cluster #10
linear triplet

Figure 2.1 a. Typical choices for clusters on the bcc lattice.
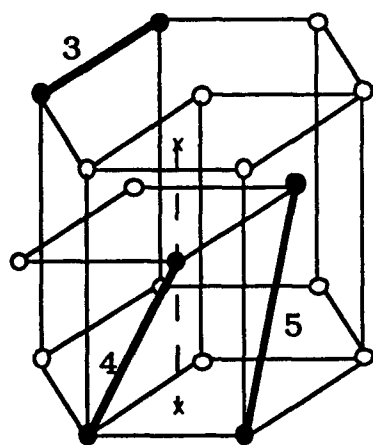
3 - nearest-neighbors pair
(in-plane)

4 - nearest-neighbors pair
(out-of-plane)

5 - 2nd nearest-neighbors pair

7 - "filled" triangle

8 - out-of-plane

triangle
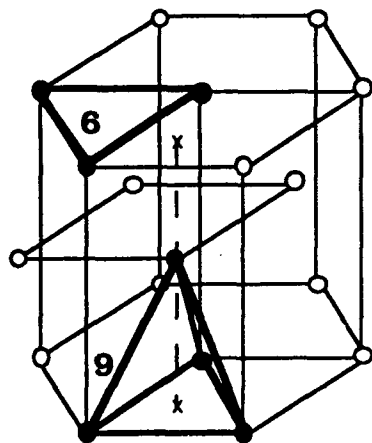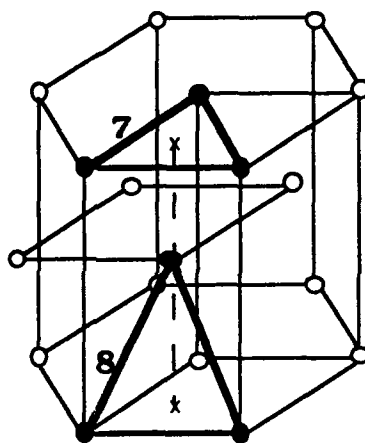
6 - "empty" triangle

9 - tetrahedron

Figure 2.1 b. Typical clusters and their designated

numbers for the hcp lattice.

The probability $x_n(\sigma)$ of finding a type-n cluster with configuration $s_n = \{i, j, ..., k\}$ (e.g., $\{+1, -1, -1, ..., +1\}$) is:

$$x_n(\sigma) = \frac{N_{\sigma_n}}{N_n}$$

[2.18]

$$= \frac{\text{No. of n-type clusters with configuration } \sigma_n}{\text{Total no. of n-type clusters}}$$

The occupation operator $\Gamma_i(p)$ is defined as [22]:

$$\Gamma_i(p) = \frac{1}{2}[1 + i s_p]$$

[2.19]

$$= 1 \quad \text{if site p is occupied by i-type atom, and}$$

$$= 0 \quad \text{if not.}$$

Using the occupation operator, the n-type cluster probability may be rewritten as [22]:

$$x_n(\sigma) = \frac{1}{N_n} \sum_{\{p_i\}} \Gamma_i(p_1)\Gamma_j(p_2)\cdots\Gamma_k(p_n) \quad .$$

[2.20]

summing over all n-type clusters. Combining Equations 2.5 and 2.19 and expanding leads to an expression relating the cluster correlation functions with the cluster probabilities [22]:

$$x_n(\sigma) = \frac{1}{2^n}[1 + \sum_\beta A_{n\beta}(\sigma) \xi_\beta] \quad ,$$

[2.21]

where the components $A_{n\beta}$ are sums of products of the cluster spins i,j,...k. The requirement that all cluster probabilities have positive values, $0 \leq x_\beta \leq 1$, leads to a set of constraints on the correlations, ξ_β [60]:

$$1 + \sum_{\beta > 0} A_\beta(\sigma) \, \xi_\beta \geq 0 \quad . \tag{2.22}$$

not summing on the empty cluster. Thus, for any choice of the maximum cluster size, the configuration space (sub-space) is limited to a convex polyhedron. The correlation vectors which form the K vertices of the configurational polyhedron, $\xi^{(m)}$, form the orthogonal basis of the sub-space. Using barycentric coordinates, any possible configuration, ξ, may be expressed as:

$$\xi = \sum_{m=1}^{K} \rho_m \, \xi^{(m)} \tag{2.23}$$

where the ρ_m are non-negative coordinates. Combining Equation 2.23 with Equation 2.7 leads to the configurational description of the energy using clusters p=1...K and structures m=1...K:

$$E = \sum_{p=1}^{K} J_p \xi_p = \sum_{m=1}^{K} \rho_m E^{(m)} \tag{2.24}$$

where

$$E^{(k)} = \sum_{p=1}^{K} J_p \xi_p^{(k)} \qquad [2.25]$$

is the energy of the state corresponding to vertex k. With this representation, Sanchez and de Fontaine [60] have shown that all possible ground-state configurations must correspond to a vertex or to a linear combination of at most two configurations each corresponding to a vertex [60]. The lattice configurations corresponding to the correlation vectors then seem the natural choice for the **basis set** of the expansion of Equation 2.8. Indeed, this choice will be shown to be optimum (though sometimes elusive) in the next section.

The enumeration of the vertices of the configurational polyhedron is a difficult problem in linear programming and has been accomplishe only a limited number of cluster expansions. The range of clus nteraction energies for which different configurations are the ground states have been delineated for hcp structures with up to second nearest-neighbor interactions [61], and fcc and bcc structures including up to fourth nearest neighbors [62, 63]. These studies, however, did not include many-body interactions and relied on the assumption that nearest- and next nearest-neighbor interactions were dominant. Sanchez and de Fontaine [22] performed a full ground-state search for the fcc lattice including 10 sub-clusters of the joint cluster formed by the regular tetrahedron (T), composed of nearest neighbors, and the regular octahedron (O) which includes first

and second nearest neighbors. The results of the ground-state search using the T-O approximation yielded 17 possible ordered configurations whereas the first and second nearest neighbor approximation used by Kanamori [62] yielded only 10 of those structures. Wei et al [24] showed that fourth-neighbor interactions are comparable in magnitude to nearest-neighbor interactions for fcc-based semiconductors. They performed a ground-state search of fcc structures including the many-body interactions while limiting the maximum unit cell size to fifteen atoms. This search, in contrast to the vertex enumeration studies, calculates the correlation vectors of all possible independent structures and then, using the cluster expansion equation, the cohesive energies. Such a method is employed in this study, in a limited manner, and is discussed in Section 2.6.

2.5 How to choose a basis set

For the alloy systems in this study (as well as most other studies) interaction ranges longer than nearest neighbors are required. Without knowing the vertices of the configurational polyhedron, a means of estimating the optimum choice of basis structures for a given maximum cluster size is required. Three techniques are considered -- yielding different conclusions:

(i)   Random alloy convergence.

(ii)   Minimum eigenvalue norm.

(iii)   Maximum determinant method.

The expectation value of the point cluster, ξ_1, depends only upon the alloy concentration c:

$$\xi_1 = 2c - 1 \quad . \tag{2.26}$$

In a random alloy each lattice site is equivalent, thus each site in a cluster has the same value of ξ_1, and the correlation function of a cluster with k sites ξ_k:

$$\xi_k^{random} = (2c - 1)^k \quad . \tag{2.27}$$

Notably, at c = 0.5 , all terms vanish except at the k = 0 term, i.e., the empty cluster:

$$\overline{F}^{random}(c = 0.5) = J_0 \quad . \tag{2.28}$$

If the value of $\overline{F}^{random}$ can be calculated directly, using such techniques as the CPA-GPM, then Equation 2.21 can be used to evaluate the accuracy of the expansion.

Combining Equations 2.8 and 2.9:

$$^\sigma\overline{F} = \sum_{k,p} \, ^\sigma\eta_k \, \Xi_{kp}^{-1} \, F_p \quad . \tag{2.29}$$

$$= \sum_{p} {}^{\sigma}Q_p \, F_p$$

where,

$$^{\sigma}Q_p = \sum_{k} {}^{\sigma}\eta_k \, \Xi_{kp}^{-1} \, . \qquad\qquad [2.30]$$

Thus, the cluster expanded configurational property of a random alloy is:

$$\xi_k^{\text{rand.}} = \sum_{p} Q_p^{\text{rand.}} \, F_p \quad , \qquad\qquad [2.31]$$

where,

$$Q_p^{\text{rand.}} = \sum_{k} (2c - 1)^{k} \, \Xi_{kp}^{-1} \quad . \qquad\qquad [2.32]$$

The sensitivity of the random alloy property is:

$$\frac{\partial \overline{F}^{\text{rand.}}}{\partial F_p} = Q_p^{\text{rand.}} \qquad\qquad [2.33]$$

Ferreira *et al* [12] use this result to determine the stability of the expansion of the excess cohesive energy. They integrate the norm of $Q_p^{\text{rand.}}$ over all concentrations:

$$y(k,p) = \sum_{p} \int_{0}^{1} Q_p^{\text{rand.}} Q_p^{\text{rand.}} \, dc \qquad\qquad [2.34]$$

giving:

$$y(k,p) = \sum_{k,l} \sum_{p} \Xi_{kp}^{-1} \, \Xi_{pl}^{-1} \times \frac{1 - (-1)^{k+l+1}}{2(k + l + 1)} \quad .$$

[2.35]

The set of basis structures, k=1,....n, that yields the minimum value of y corresponds to the expansion least sensitive to errors in the cohesive energy for the choice of clusters, p=1, ... n.

The second and third methods also use estimates of the sensitivity of the interactions to errors in the excess cohesive energies. From Equation 2.9, the sensitivity of J_k is:

$$\delta J = \Xi^{-1} \, \delta F \quad .$$

[2.36]

Using a standard result of numerical analysis (see Wilkinson [64]), Equation 2.35 may be refined to:

$$\frac{|\delta J|}{|J|} = C(\Xi^{-1}) \frac{|\delta F|}{|F|} \quad .$$

[2.37]

where C(A) is the condition number of A, defined by:

$$C(A) = |A| \, |A^{-1}| \quad ,$$

[2.38]

and $|A|$ denotes some type of matrix norm. The norm used in this study is:

$$|A| = (\text{max. eigenvalue of } A^T A)^{1/2} \quad .$$

[2.39]

The choice of Ξ which minimizes $C(\Xi^{-1})$ is deemed the optimum basis structure.

Finally, noting that:

$$\delta J_k = \sum_p \left| \Xi^{-1}_{k\,p} \right| \left| \delta F_p \right| \quad ,$$

[2.40]

the uncertainty in each potential δJ_k depends upon the sum of the absolute values of each element in the corresponding row of $\Xi^{-1}_{k\,p}$. By Kramer's rule:

$$\left| \Xi^{-1}_{k\,p} \right| = \frac{\left| \text{Det } (\Xi_{i\,j}) \right|}{\left| \text{Det } (\Xi) \right|} \quad i \neq k, j \neq p \quad ,$$

[2.41]

it is clear that the condition number of Equation 2.36 is minimized for the choice of Ξ for which the determinant is a maximum and the determinant of each minor is minimum. Thus, the simple norm, the determinant of the correlation matrix, Ξ is adopted.

Figures 1.6 a and b show the bcc- and hcp-based structures considered as candidates for use as basis structures. They are chosen due to their small unit-cell sizes, a necessity for the LDA

Table 2.1 a. Correlation functions for selected bcc structures of Figure 1.1 a.

Structure	No.	◯	●	(pair)	(pair)	(triangle)	(diamond)
bcc (A)	1	1	1	1	1	1	1
DO$_3$ (A$_3$B)	2	1	1/2	0	0	-1/2	-1
B2 (AB)	3	1	0	-1	1	0	1
B32 (AB)	4	1	0	0	-1	0	1
DO$_3$ (AB$_3$)	5	1	-1/2	0	0	1/2	-1
bcc (B)	6	1	-1	1	1	-1	1
T1 (AB)	7	1	0	0	-1/3	0	-1/3
T2 (AB)	8	1	0	-1/4	1/3	0	0
T3 (AB)	9	1	0	0	0	0	-1/3
T4 (AB)	10	1	0	0	1/3	0	-1/3
T5 (A$_3$B)	11	1	1/2	0	2/3	1/6	1/3
T5 (AB$_3$)	12	1	-1/2	0	2/3	-1/6	1/3
Degeneracy		1	1	4	3	12	6

Table 2.1 b. Correlation functions for selected hcp structures of

Figure 1.1 b.
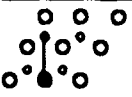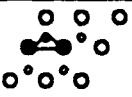
Structure	#	○	●						
hcp (A)	1	1	1	1	1	1	1	1	
DO_{19} (A_3B)	2	1	1/2	0	0	1	-1/2	-1/2	-
Pmma (AB)	3	1	0	-1/3	-1/3	1	0	0	
Pmmn (AB)	4	1	0	1/3	-1/3	-1	0	0	
DO_{19} (AB_3)	5	1	-1/2	0	0	1	1/2	1/2	1
hcp (B)	6	1	-1	1	1	1	-1	-1	
LiRh (AB)	7	1	0	-1	1	-1	0	0	
H1 (AB)	8	1	0	0	-1/3	0	0	0	
Degeneracy		1	1	3	3	3	6	1	

Table 2.1 c.   Correlation functions for selected
hcp structures. Isotropic   interactions are
assumed.

Structure	No.	○	●				
hcp (A)	1	1	1	1	1	1	1
DO_{19} (A_3B)	2	1	1/2	0	1	-1/2	-1
Pmma (AB)	3	1	0	-1/3	1	0	1
Pmmn (AB)	4	1	0	0	-1	0	-1
DO_{19} (AB_3)	5	1	-1/2	0	1	1/2	-1
hcp (B)	6	1	-1	1	-1	-1	1
LiRh (AB)	7	1	0	0	-1	0	-1
H1 (AB)	8	1	0	-1/6	0	0	0
Degeneracy		1	1	6	3	8	2

calculations. The correlation functions of clusters of up to fifth nearest neighbors are given for each of these structures in Tables 2.1 a, b, and c. The first column is the crystal structure, and the second column is the structure number provided for convenience. The rest of the columns are the correlation functions for each of the cluster types represented by the column heading. The final row is the cluster degeneracy.

Table 2.2 lists the best choices for a basis set according to criteria (i) maximum determinant, (ii) smallest eigenvalue, and (iii) random alloy parameter for each of three different sets of basis clusters A, B, and C. For cluster set A, the basis-structure set 1-6 is the optimum choice for each of the criteria. This is not surprising since the correlation vectors of these structures are the vertices of the associated configuration polyhedron. For cluster set B, the three basis sets [1-6] + (7, 9, or 10) yield the same determinant. This degeneracy is removed by criteria (ii) and (iii). Notably, criterion (iii) predicts an optimum basis set which excludes structure 3 (CsCl structure) for both cluster bases B and C whereas criterion (i) is optimized by basis sets which include the structure. These convergence criteria for the expansion basis are used in the next section for numerical evaluation of the convergence of the cluster expansion for the three different systems.

Table 2.2. Optimum choices of basis sets for bcc structures for each of the three criteria described in section 2.5. Note: the structure numbers in the basis sets are given in Table 2.1 a.

Basis clusters*	Optimization criterion		
number of sub-clusters	determinant	eigenvalues	random alloy
A 6	[1-6]	[1-6]	[1-6]
B 7	[1-6] + 9 [1-6] + 7 [1-6] + 10	[1-6] + 9 [1-6] + 7	1 2 4 5 6 7 8 1 2 4 5 6 8 9
C 8	[1-7] + 10 [1-7] + 8	1 2 4 5 6 8 9 10 1 2 4 5 6 7 8 9	1 2 4 5 6 7 8 10 1 2 4 5 6 7 10 12

*   Cluster set A consists of clusters # 1, 2, 3, 4, 5, and 6 [see Figure 2.1a].

"   "   B "   "   "   "   "   "   "   1, 2, 3, 4, 5, 6, and 7.

"   "   C "   "   "   "   "   "   "   1, 2, 3, 4, 5, 6, 7, and 9.

2.6 Convergence of the cluster expansion

Recall that Equation 2.8 allows an estimate of any configurational property for a given choice of a basis set of structures and maximum cluster size. The obvious method of gauging convergence of the cluster expansion is to evaluate the expansion coefficients, i.e., the cluster interactions. The interactions should vanish with interaction distance and with cluster complexity. The value of each type of interaction should also converge to a stable value as the size of the basis set grows. Thus, any configurational property, for example, the cohesive energy calculated using Equation 2.8, should converge to a value in a stable manner; note though, this is not necessarily uniform convergence. This second observation leads to a direct method for evaluating the accuracy of the cluster expansion: comparing the value of a configurational property evaluated directly with the cluster-expanded value. In this section, the convergence of a cluster expansion is judged by estimating the cohesive energy of an ordered compound using Equation 2.8 and comparing the value with the LDA value from Table 1.2. These assessments are performed for bcc- and hcp-based lattice structures in Zr-Nb, Nb-Ru, and Zr-Ru. The success with which the cohesive energies of the ordered compounds are predicted lends confidence to the predictions for disordered alloys.

Zr-Nb

Figure 2.2 shows the ground-state excess cohesive energies of selected hcp- and bcc-based compounds in the Zr-Nb system. Clearly there are no stable intermediate compounds -- as expected in system with a predominant miscibility gap. Using the different basis sets advocated by each of the three optimization techniques shown in Table 2.2, the excess cohesive energies of extra structures were calculated using the cluster expansion with both global and total volume relaxation. The resultant errors for each expansion are summarized in Table 2.3 using different error norms. The expansion using clusters up to second nearest neighbors converges quickly for the globally relaxed case, but at least third nearest neighbors are needed for the totally relaxed expansion. Omitting the B2 structure from the basis set for expansions of up to fifth nearest neighbors yields predictions with a larger error norm than the second neighbor expansion. This effect is due, in part, to the strong dependence of the B2 energy on the nearest neighbor interaction. Figure 2.3 shows the unstable description of this interaction for expansions that omit the B2 structure from the basis(curves #3, 4, and 5) and the very stable result of basis sets of varying size that include B2 (curves #1-3).

Figure 2.4 shows the derived interactions for the "best" expansions with seven (up to third nearest neighbors) and eight cluster interactions (up to fifth nearest neighbors). For each of the expansions the nearest neighbor interactions are nearly identical.
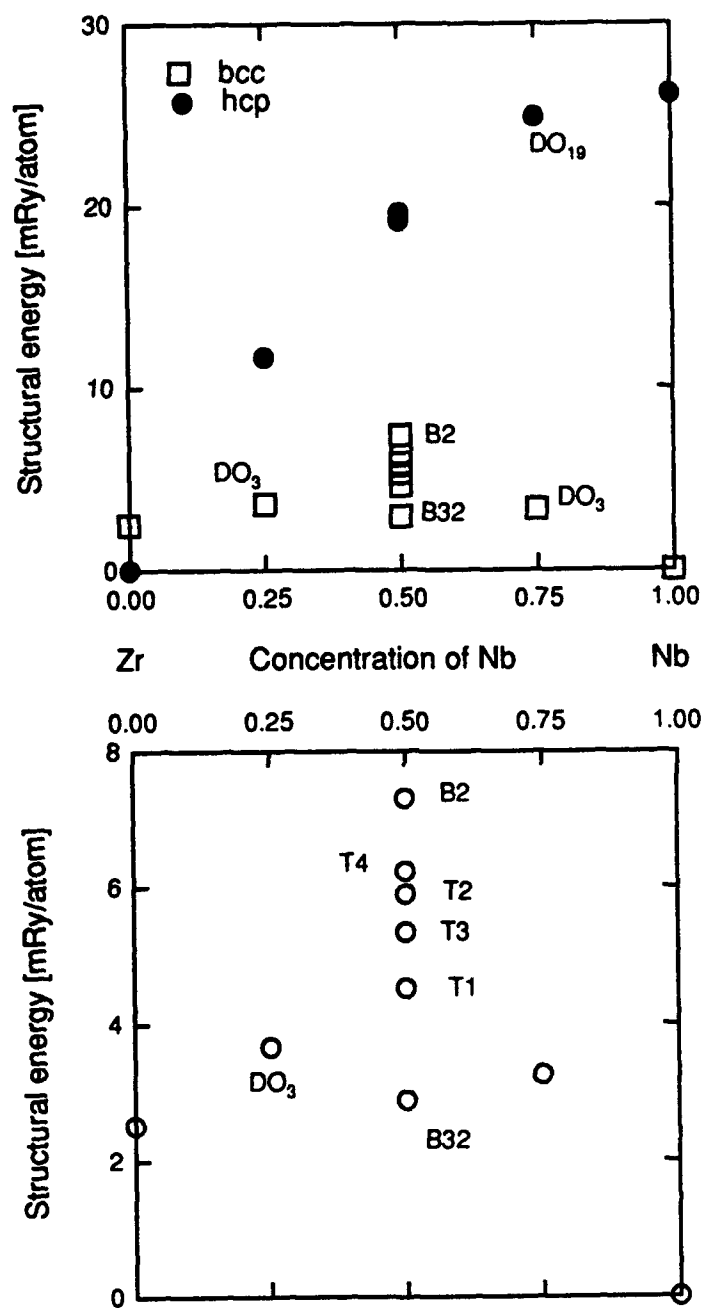
Figure 2.2. Calculated formation energies for selected compounds in Zr-Nb. The lower figure shows only the bcc structures.

Table 2.3. Errors of cluster expanded excess structural energy of "extra" bcc structures (i.e., those not included in basis set) in Zr-Nb. Values are given for globally relaxed potentials and (totally relaxed).

cluster basis, number	basis	max |error| [mRy.]	$\frac{1}{n}[\sum_n \|error\|^2]^{1/2}$ [mRy.]	$\frac{1}{n}[\sum_n \frac{\|error\|^2}{\|\Delta E\|^2}]^{1/2}$ [percent]
A 6	1-6	.59 (2.52)	.19 (.91)	4.0 (21.0)
B 7	1-7	.49 (1.23)	.20 (.35)	4.1 (7.4)
B 7	1-6 + 9	.32 (.69)	.13 (.22)	3.0 (5.4)
B 7	1 2 4 5 6 7 8	.89 (1.22)	.32 (.41)	5.5 (7.7)
B 7	1 2 4 5 6 8 9	.64 (.69)	.23 (.22)	4.1 (5.4)
C 8	1-8	.13 (.42)	.08 (.11)	1.9 (2.3)
C 8	1 2 4 5 6 7 8 9	.53 (.52)	.27 (.14)	4.6 (2.3)
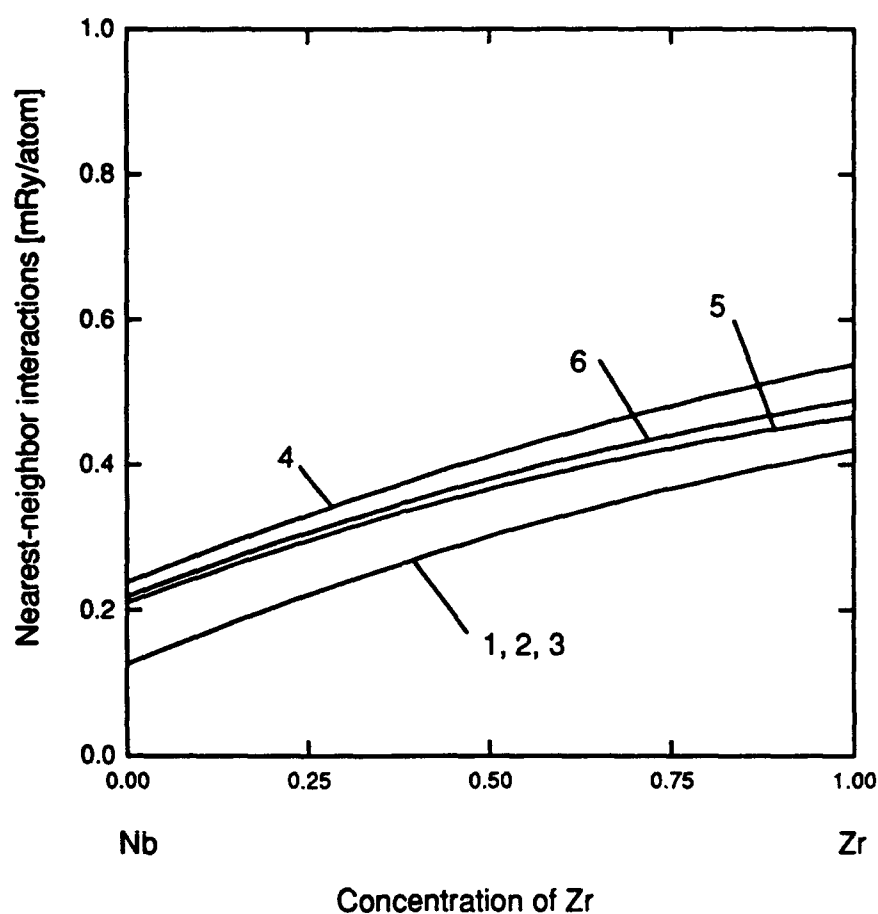
Figure 2.3 Nearest neighbor interactions calculated using cluster expansions with different bases and global relaxation.

1 - 1 2 3 4 5 6
2 - 1 2 3 4 5 6 9
3 - 1 2 3 4 5 6 7 8
4 - 1 2 4 5 6 7 8 9
5 - 1 2 4 5 6 8 9
6 - 1 2 4 5 6 7 8

The second nearest-neighbor interactions are identical for the expansions including second nearest and third nearest neighbors, but the inclusion of fifth nearest neighbors causes a shift in the interaction. The third- and fifth-neighbor interactions are small (approximately 0.05 mRy./atom) and nearly constant over the entire concentration range. The magnitudes of the pair interactions are closely related to the relative stabilities of alloys of equi-atomic concentrations. At a concentration of 50%, the second nearest-neighbor interaction is approximately 2.5 times as large as the nearest-neighbor interaction. The correlation functions of the two pair clusters for the B2 and B32 structures are $\xi_{1st}^{B2} = -1$, $\xi_{2nd}^{B2} = 1$, $\xi_{1st}^{B32} = 0$, $\xi_{2nd}^{B32} = -1$ (see Table 2.1). Thus, the contribution to the B2 formation energy of the second nearest neighbor interaction is positive (ferromagnetic) and destabilizing. However, the B32 structure is stabilized by the relatively large negative (-2.8 mRy/atom) second neighbor-interaction, and the B32 compound is much more stable than the B2. Why is the the B32 structure not stable? The answer lies in the empty cluster interaction which can be associated with the random alloy formation energy . The random formation energies (both globally and totally relaxed) as a function of concentration with those of the bcc-based compounds are shown in Figure 2.5. Recall from Equation 2.26 that the formation energy for a random alloy with 50% concentration is equal to the value of the effective interaction J_0, for the empty cluster. As seen in Figure 2.5 the value of J_0 is approximately 4.1 mRy/atom. This interaction is the dominant and

destabilizing contribution to the formation energies of the compounds near equi-atomic concentrations. The metastable, intermediate bcc-based compounds 2, 4, 5, 7, and 9 are stable with respect to the random alloy, which suggests short-range ordering. The difference between the formation energy of a compound and the random formation energy at that concentration is the ordering energy. Thus, the unstable B32 compound has a negative ordering energy of 2.5 mRy/atom.

A metastable hexagonal ω phase varying from $P6/mmm$ space group to $P3m1$ with increasing Nb content may be retained by quenching [65]. The hexagonal phases 1-6 are unstable with respect to the random bcc alloy, however, so no connection is made between the results of this study and those of [65].

The cluster expansion on the hexagonal lattice requires tracing the effects of clusters that lie completely within the basal plane or have out-of-plane vertices. As seen in Table 2.1 b, the correlation functions depend upon the orientation of otherwise identical clusters. If isotropic interactions are assumed, then the first neighbor and first-neighbor triangles can be combined, yielding effective correlation functions (see Table 2.1 c). Such an assumption renders the correlation vectors for structures 4 (Pmmn) and 7 (LiRh) identical up to (and including) second nearest neighbors. This
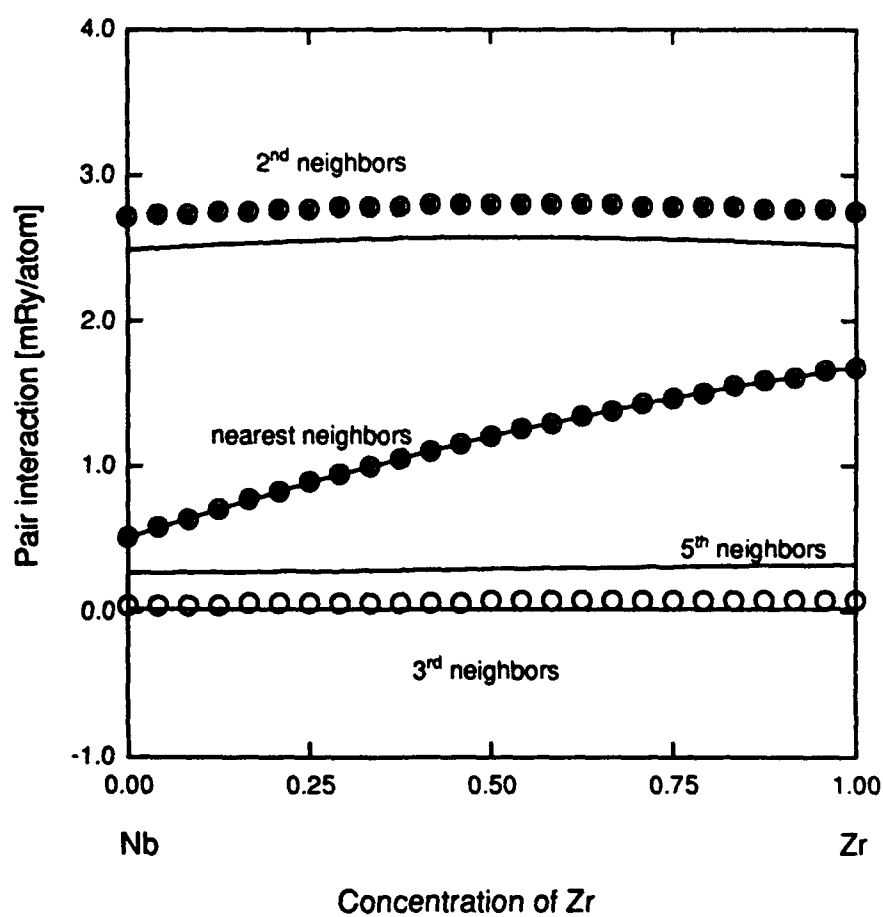
Figure 2.4. Pair interactions in Zr-Nb derived from cluster expansions of different range. The size of the basis set is indicated by the symbol type:

- Nearest neighbors only. Basis = 1 2 3 4 5 6
- O 3rd nearest neighbors included. Basis = 1 2 3 4 5 6 7
- —— 5th nearest neighbors included. Basis = 1 2 3 4 5 6 7 8
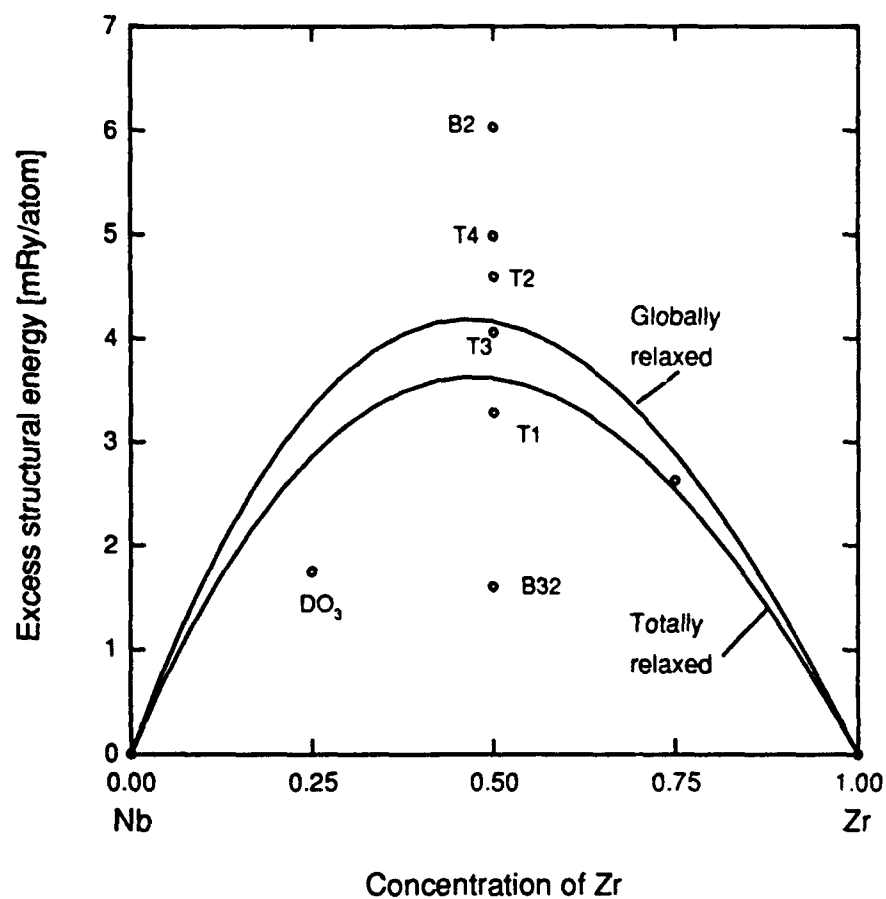
Figure 2.5. Random energy for bcc alloys in Zr-Nb calculated using both globally and totally relaxed cluster expansions. Superimposed are the excess structural energies of bcc compounds from Figure 2.4 using Zr-bcc and Nb-bcc as reference energies.

observation suggests an obvious check for the isotropy assumption: if the formation energies for compounds with crystal structures 4 and 7 are approximately equal, then the assumption of isotropic short-range interactions is valid. This is the case for the Zr-Nb system. Table 1.6 b and Figure 2.6 show the cohesive energies of the two compounds (curves #2 and #3) as a function of average atomic volume which are nearly identical (ΔE=0.1 mRy./atom). Curve #1 is the projected cohesive energy for both compounds using a cluster expansion of up to nearest neighbors and assuming isotropy. Clearly, the error, 1.5 mRy./atom, indicates an unconverged expansion. If second nearest neighbors are included in the expansion, and structure 4 is included in the basis, then curve #2 is the projected energy for structure #7. Thus, for Zr-Nb the hexagonal cluster interactions are reasonably converged using the isotropy assumption and including clusters of up to second nearest neighbors.

The excess volumes and bulk moduli of the hcp-, and bcc-based compounds were cluster expanded using the total relaxation. The effective interactions are shown in Table 2.4 for each type of cluster used in the expansion. The bcc expansion includes 2nd nearest neighbors. The hcp expansion includes nearest-neighbor pair interactions and includes the full isotropy assumptions made in the energy expansion. The convergence of the bulk modulus effective interactions B_i is rapid. The four-body interaction is four to five orders of magnitude below 1 Mbar, the nominal size of the bulk
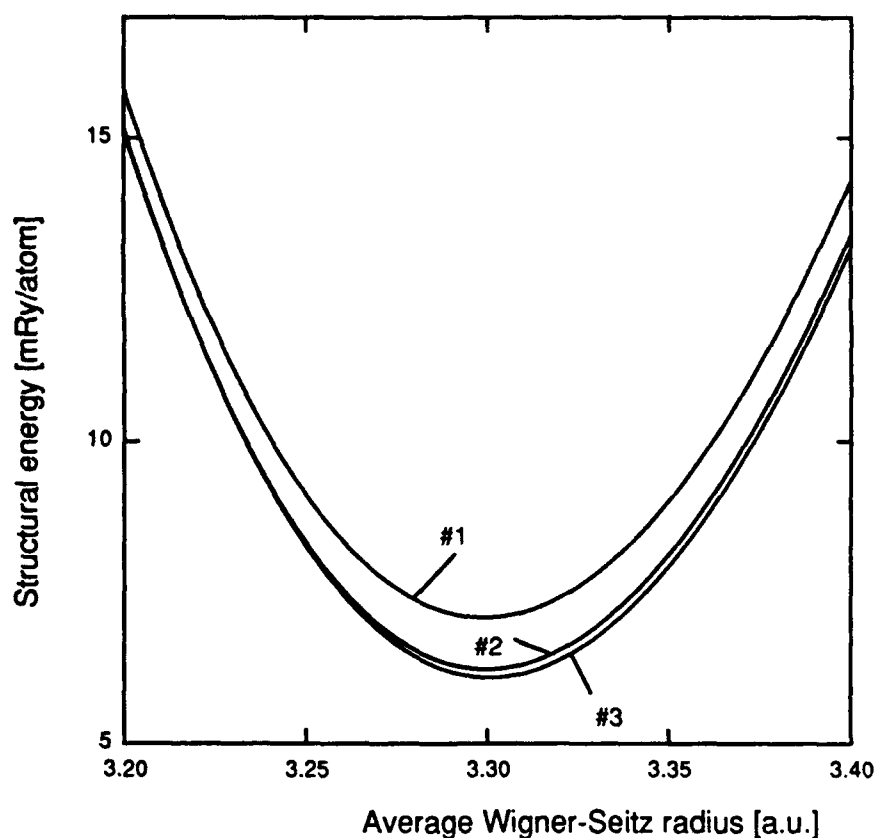
Figure 2.6. Excess structural energies of ZrNb with Pmmn and LiRh structures from fitted Morse potentials and cluster expansion. The cluster expansion includes only nearest neighbors and uses isotropy assumption and is indicated by curve #1. Curve #3 is the Morse fit for the LiRh structure. Curve #2 is the the fit for the Pmmn structure. When second nearest neighbors are included in the expansion, and Pmmn is included in the basis set, curve #2 becomes the projected energy for the LiRh structure since the correlation vectors for LiRh and Pmmn are identical when isotropic interactions are assumed.

moduli in this sytem. The convergence of the volume expansion is rapid for the bcc-based structures, and sufficient in the hcp alloys.

Table 2.4. The interaction coefficients for cluster expansion of bulk modulus and the volume of (a) bcc structures and (b) hcp structures in Zr-Nb. The cluster labels are from Figure 2.1.

(a)

Cluster	Effective interactions	
(label)	B_i [Mbar]	V_i [a.u.^{3}]
Empty (1)	-0.049120	-0.937820
Point (2)	0.001500	-0.069780
Pair (3)	0.009875	0.114747
2nd pair (4)	0.003083	0.144064
Triangle (5)	-0.000120	0.005817
Tetrahedron (6)	0.000062	0.007776

(b)

Cluster	Effective interactions	
(label)	B_i [Mbar]	V_i [a.u.^{3}]
Empty (1)	-0.058440	-0.297440
Point (2)	-0.000250	0.024432
Pair (3 4)	0.009563	0.061917
Triangle (6 7 8)	0.000031	-0.003060
Tetrahedron (9)	0.000531	-0.037020

Nb-Ru

The ground-state energies of selected compounds in the Nb-Ru system are shown in Figure 2.7. The stable-equilibrium structure of the $NbRu_3$ compound is predicted to be DO_{19}, but the margin of stability with respect to the $L1_2$ structure (0.1 mRy./atom) is on the order of the precision of the total energy calculations. This delicate balance provokes the question of whether a different fcc or hexagonal structure might have an even more negative (stable) formation energy.

To resolve this question the cohesive energies of several candidate structures were predicted using the cluster expansion. For the fcc and hexagonal cluster expansions, interactions of up to second nearest neighbors were included. The correlation functions of all fcc- and hcp-based structures with stoichiometry AB_3 and up to 16 atoms per unit cell were calculated. The unit cells were restricted to those occupying a supercell obtained by doubling the standard unit cell size in each principal direction.

The cluster interactions were obtained with a globally relaxed expansion using the basis set deemed optimum by the maximum determinant technique. The assumption of isotropy in the cluster expansion of hexagonal lattice structures is invalid as shown in Figure 2.8 a, since the cohesive energies of the compounds with structures 4 and 7 have a significant difference (1.8 mRy/atom). The projected
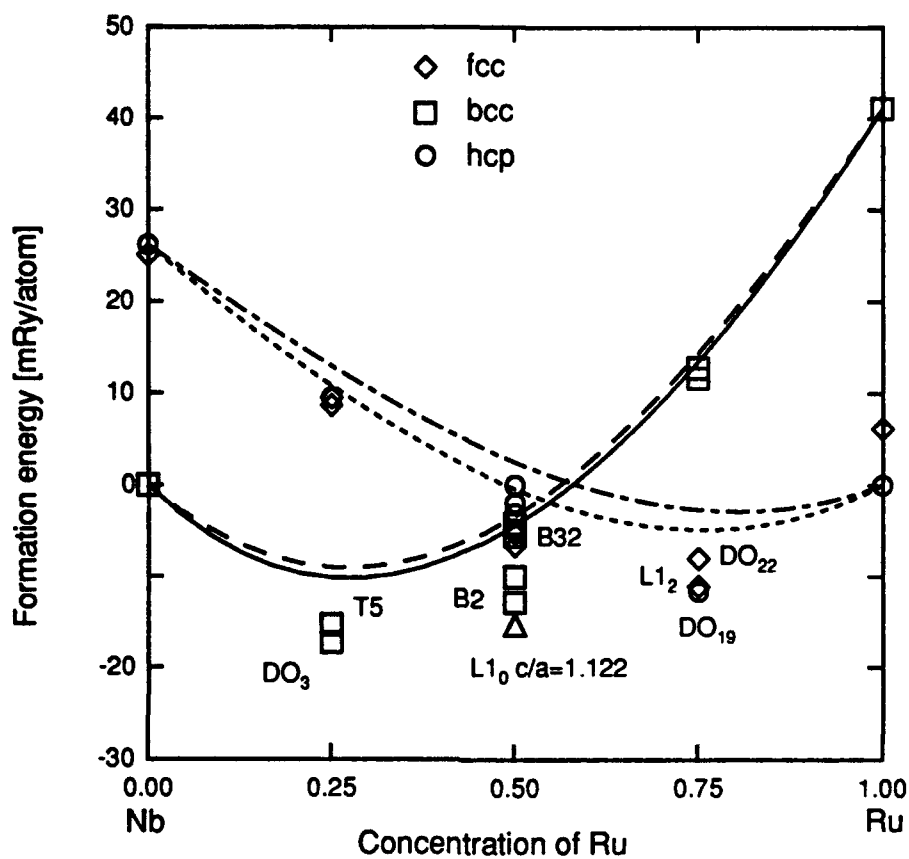
Figure 2.7. Ground-state energies of selected compounds in Nb-Ru, and random energies of hcp and bcc alloys.

——— Bcc random alloy (Totally relaxed)

— —   "   "   "   (Globally relaxed)

- - - - Hcp random alloy (Totally relaxed)

—·— "   "   "   (Globally relaxed)
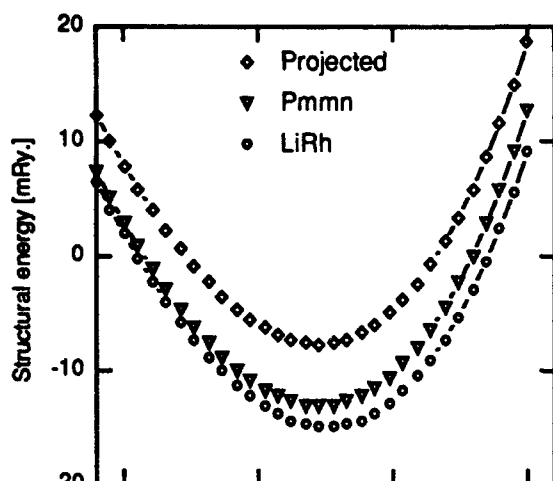
Figure 2.8 a. Projected and calculated structural energies for NbRu Pmmn- and LiRh structures. Expansion includes nearest neighbors, and isotropic pair interactions are assumed. Note: projected energy for LiRh and Pmmn structures are identical for this expansion.
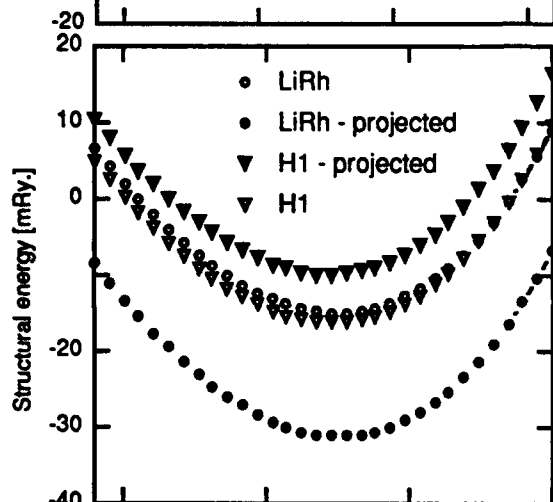
Figure 2.8 b. Projected and calculated structural energies for NbRu Pmmn, LiRh, and H1 structures. Expansion includes nearest neighbors, and anisotropic pair interactions are assumed.
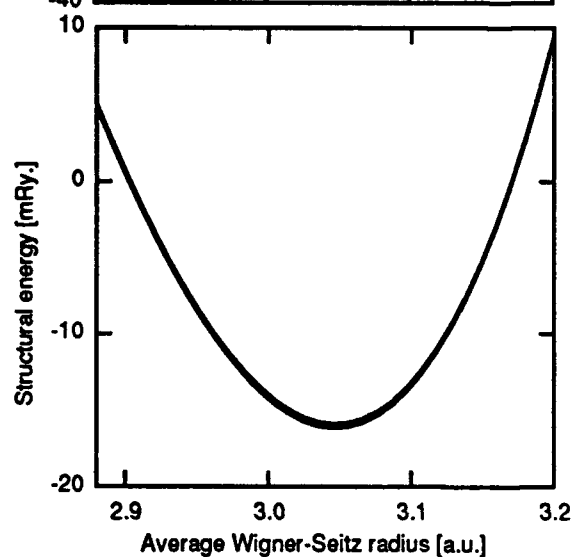
Figure 2.8 c. Projected and calculated structural energies for NbRu with H1 structure. Expansion includes second nearest neighbors with anisotropic pair interactions.

energy for the two structures using a nearest-neighbors expansion and isotropic interactions is also shown in Figure 2.8 a with an obviously large error (~ 5 mRy./atom). Figure 2.8 b shows the projected energies for structures 7 and 8 in a nearest-neighbors expansion with anisotropic pair interactions. The discrepancies are as large as 15 mRy./atom. Including second nearest neighbors improves the expansion significantly. The projected energy for structure 8 using this expansion is shown in Figure 2.8 c. The pair interactions of this well converged expansion are shown Figure 2.9.

No hexagonal or cubic structures were found with projected formation energies more negative than that of the DO_{19}. However, it must be noted that the LMTO-ASA approximation loses validity for hexagonal structures varying significantly from ideal close packing. Thus, an improved energy analysis will require full-potential total-energy calculations.

The Nb-rich DO_3 is also a predicted ground state, however no observation of such a phase has been reported. A ground-state search similar to the one for $NbRu_3$ was performed yielding no compound more stable than DO_3.

Table 2.4 shows the results of a convergence study of the bcc expansion. The last column, the percent error norm, is of comparable magnitude to the Zr-Nb bcc cluster expansion. Figure 2.10 shows the cohesive energy of the random bcc alloys calculated using global relaxation and different basis sets. The random energy appears to be well converged using the basis set {1 2 3 4 5 6 7}. The
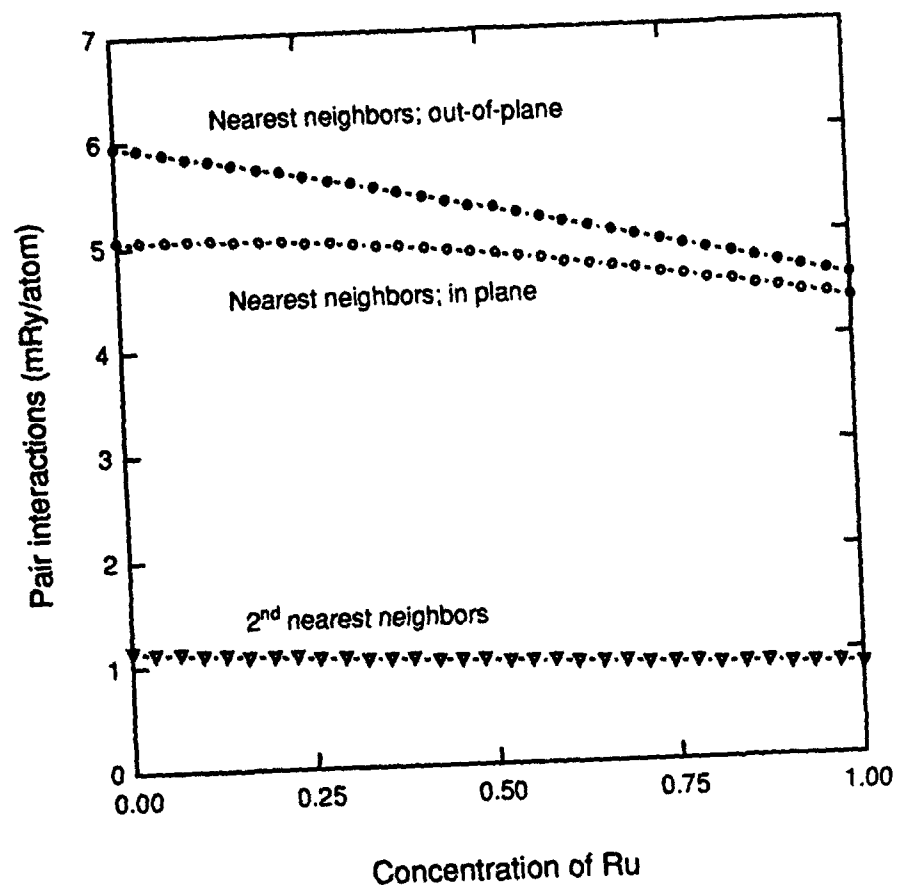
Figure 2.9. Pair interactions derived from cluster expansion of Nb-Ru hcp structural energies.

Table 2.5. Errors of cluster expanded excess structural energy of "extra" bcc structures (i.e., those not included in basis set) in Nb-Ru.

cluster basis, *number*	basis	max |error| [mRy.]	$\frac{1}{n} [\sum_n \|error\|^2]^{1/2}$ [mRy.]	$\frac{1}{n} [\sum_n \frac{\|error\|^2}{\|\Delta E\|^2}]^{1/2}$ [percent]
A 6	1-6	8.5 (5.8)	2.8 (1.5)	10.9 (5.5)
B 7	1-7	4.2 (3.5)	1.0 (1.2)	4.1 (5.2)
B 7	1 2 4 5 6 7 8	6.6 (10.4)	1.8 (2.4)	6.4 (7.9)
B 7	1-6 + 9	4.6 (3.6)	1.0 (.98)	4.0 (3.7)
B 7	1 2 4 5 6 8 9	5.0 (4.6)	1.7 (1.3)	6.1 (4.8)
C 8	1 2 4 5 6 7 8 10	8.5 (8.5)	2.6 (2.6)	8.9 (8.7)
C 8	1-7 + 10	4.0 (3.6)	1.2 (1.1)	4.8 (4.6)
C 8	1 2 4 5 6 8 9 10	5.6 (5.6)	2.1 (2.0)	7.2 (6.9)
C 8	1 2 4 5 6 7 8 9	5.9 (5.7)	1.8 (1.8)	7.0 (6.7)
C 8	1-7 + 8	5.9 (5.7)	1.6 (1.8)	7.5 (7.2)
C 8	1 2 4 5 6 7 10 12	5.0 (4.7)	1.7 (1.7)	6.0 (6.1)
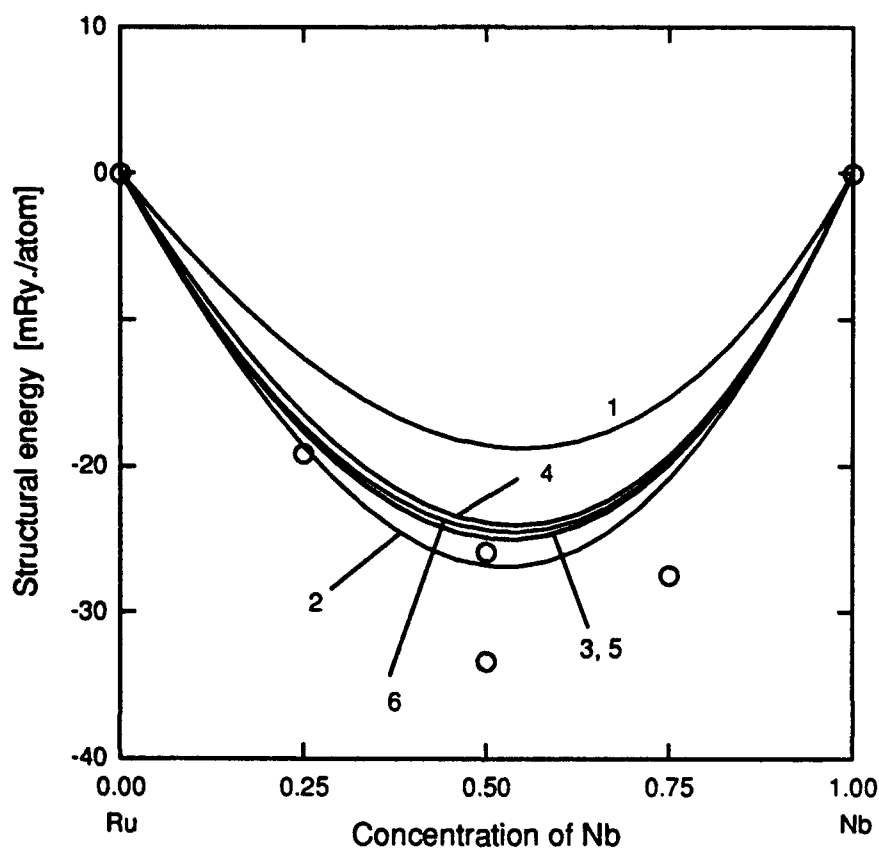
Figure 2.10. Excess structural energy of random bcc alloys in Nb-Ru derived from globally relaxed cluster expansions of different approximations. Symbols denote formation energies of selected bcc compounds. The different cluster expansions are:

1 - 2nd neighbors, basis = 1 2 3 4 5 6   A

2 - 3rd neighbors, basis = 1 2 4 5 6 7 8   B

3 - " "   "   = 1 2 3 4 5 6 7   B

4 - 3rd neighbors (B)+ linear triplet, basis = 1 2 3 4 5 6 9 12

5 - 5th neighbors, basis = 1 2 3 4 5 6 7 10   C

6 - "   "   "   = 1 2 4 5 6 7 8 10   C

cluster interactions obtained from the expansion with a basis set {1 2 3 4 5 6 7 8} and interactions of up to fifth nearest neighbors are shown in Figure 2.11.

A NbRu compound with the $L1_0$ structure is predicted to be stable as expected. Figure 2.12 shows the strong dependence of the cohesive energy on the tetragonality of the phase. The calculated c/a ratio is 1.122, which is identical to the measured value reported by Hurley and Brophy [49]. Das *et al* [38] observed a tetragonal to orthorhombic transition at 46 % Ru (see Figure 1.7), and the average of the orthorhombic a/c and b/c ratios measured at a concentration of 51% Ru is 1.126. An explanation of the stabilization of the NbRu phase by a tetragonal distortion lies in an analysis of the pair interactions. Figure 2.13 displays the interactions derived from a globally relaxed cluster expansion at the optimum atomic volumes for each of three c/a ratios -- corresponding to a B2 phase, $L1_0$ phase with c/a=1.122, and a cubic $L1_0$ phase. The $L1_0$ phase is stabilized by a change in sign of the third nearest neighbor interaction in conjunction with a slight increase in the nearest neighbor interaction. Further tetragonal distortion is destabilized by the "mixing" of what were the first and second nearest neighbors of a bcc lattice to nearest neighbors in an fcc lattice, i.e., the cubic $L1_0$ has a correlation function of zero for the nearest neighbor cluster.
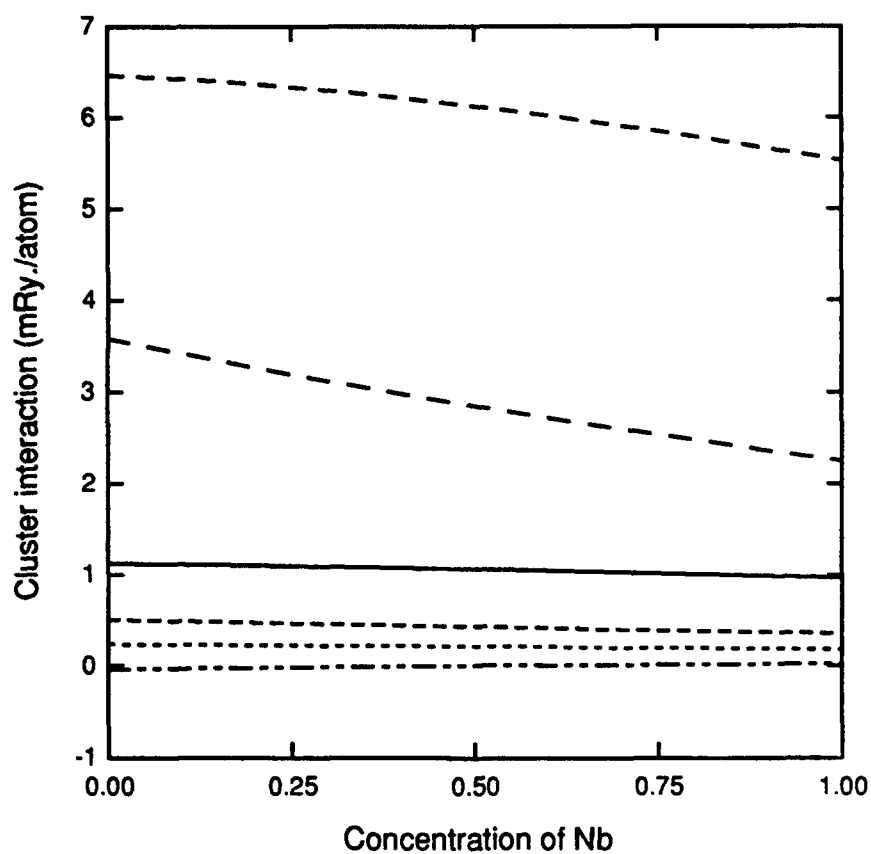
Figure 2.11. Cluster interactions of bcc alloys in Nb-Ru including 5th nearest neighbor interactions and global relaxation.

—----5th nearest neighbors

----- Tetrahedron

----Triangle

——3rd nearest neighbors

— — 2nd nearest neighbors

— — -Nearest neighbors
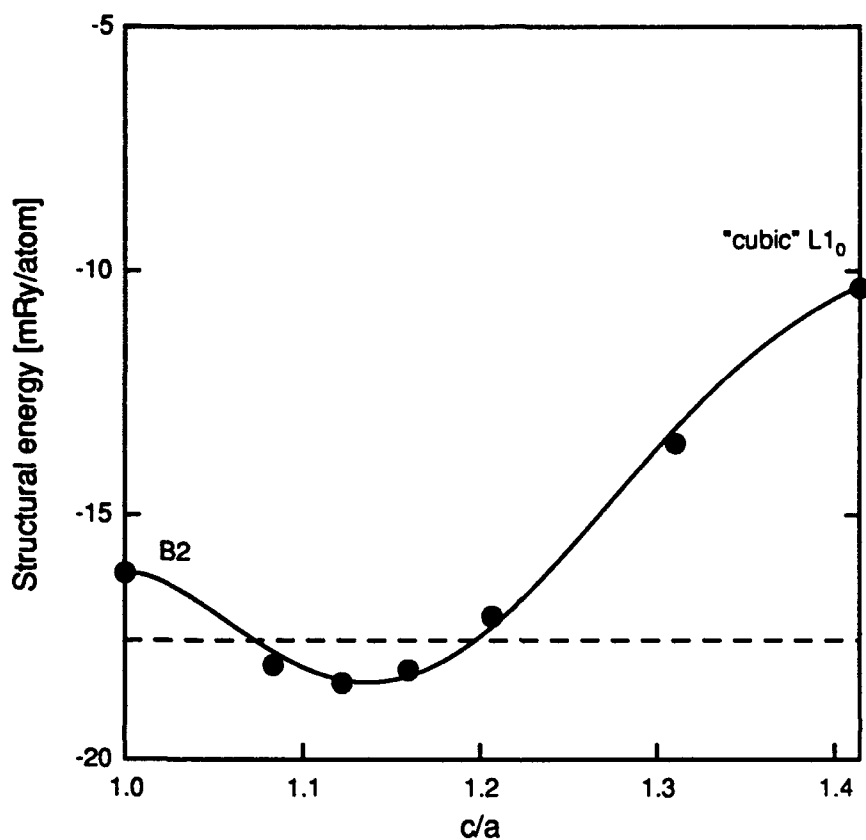
Figure 2.12. Structural energy of $NbRu$-$L1_0$ as a function of the c/a ratio. At c/a=1 the structure is equivalent to B2, and at c/a = 1.414 the structure is a cubic $L1_0$. The dashed line indicates the energy corresponding to the line of stability between Nb_3Ru-DO_3 and $NbRu_3$-DO_{19}.
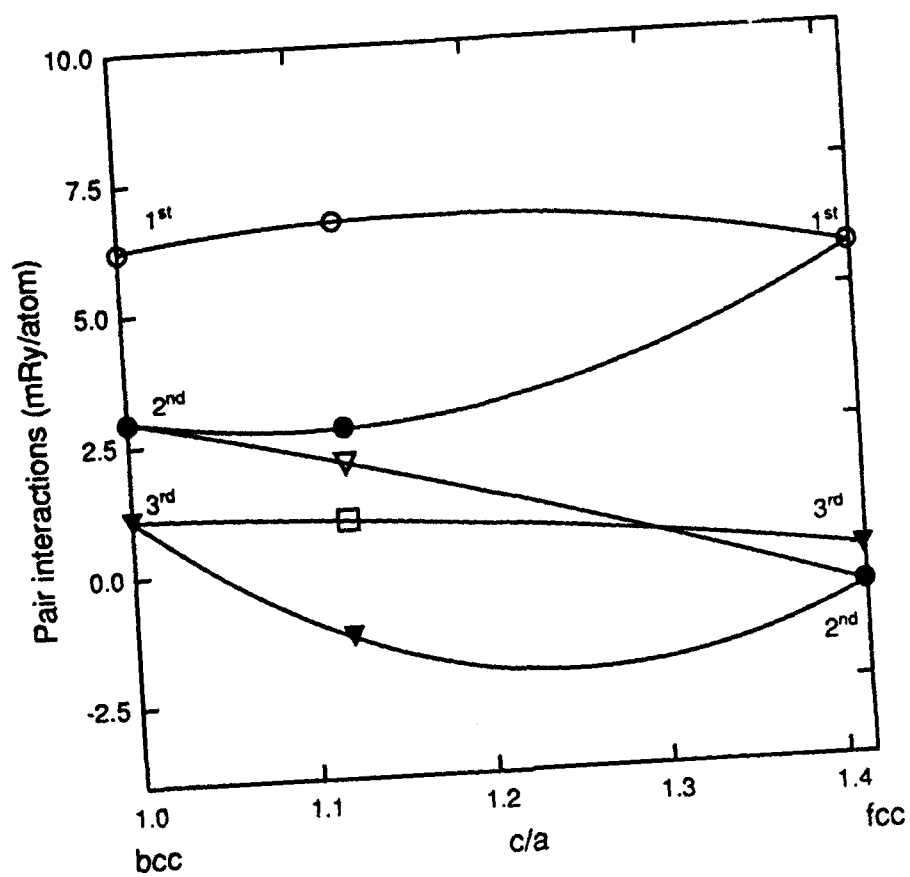
Figure 2.13. Pair interactions as a function of the c/a ratio. Note that the 3rd nearest neighbor interactions for the fcc lattice are forced to zero.

Table 2.6 shows the interaction coefficients from a cluster expansion of the excess bulk moduli and volumes of bcc-, hcp-, and fcc-based structures in Nb-Ru. The convergence of the bulk modulus expansion appears to be more rapid than for the volume expansion. The tetrahedron interaction for the hcp volume expansion is relatively large (one order of magnitude less than the pair interaction) as is the case with Zr-Nb.

Table 2.6. The interaction coefficients for cluster expansion of bulk modulus and the volume of (a) bcc structures (b) hcp structures, and (c) fcc structures in Nb-Ru. The cluster labels are from Figure 2.1.

(a)

Cluster (label)	Effective interactions	
	B_i [mbar]	V_i [a.u.^{3}]
Empty (1)	0.010750	-1.502580
Point (2)	0.027500	-0.640950
Pair (3)	-0.007250	0.185959
2nd pair (4)	0.007500	0.223879
Triangle (5)	-0.002290	0.053412
Tetrahedron (6)	-0.000710	0.014518

(b)

Cluster (label)	Effective interactions	
	B_i [mbar]	V_i [a.u.^{3}]
Empty (1)	-0.072940	-1.262280
Point (2)	-0.004750	-0.041540
Pair (3 4)	0.011813	0.199157
Triangle (6 7 8)	0.000594	0.005192
Tetrahedron (9)	0.001031	0.033671

(c)

Cluster	Effective interactions	
	B_i [mbar]	V_i [a.u.^{3}]
Empty	-0.039790	-1.607730
Point	-0.018030	0.116430
Pair	0.008256	0.255239
2nd pair	0.002253	-0.014550
Triangle	0.001128	0.020825
Tetrahedron	-0.004000	0.011547

Zr-Ru

Table 2.7 shows the error norms for bcc cluster expansions using the basis sets optimized according to criterion 1. The expansion seems to converge rapidly with the inclusion of 3rd nearest neighbors, but including 5th nearest neighbors does not improve the expansion. Figure 2.14 shows the random alloy formation energies for hcp and bcc alloys in Zr-Ru. The energies were calculated using both total and global relaxation. The difference between these two extreme methods of volume, approximately 7 mRy/atom for both lattice types, is significant, indicating the large effect relaxation has in this system. The ordering energy of ZrRu with the B2 structure is 38 mRy/atom. Based on the total-energy calculations reported by Lu *et al* [24] the ordering energies for NiAl (B2) and Ni$_3$Al are 50 mRy/atom and 13.5 mRy/atom respectively.

Table 2.7. Errors of cluster expanded excess structural energy of "extra" bcc structures (i.e., those not included in basis set) in Zr-Ru. Values are given for globally relaxed potentials and (totally relaxed).

cluster basis. *number*	basis	max |error| [mRy.]	$\frac{1}{n} [\sum_n \|error\|^2]^{1/2}$ [mRy.]	$\frac{1}{n} [\sum_n \frac{\|error\|^2}{\|\Delta E\|^2}]^{1/2}$ [percent]
A *6*	1-6	12.3 (6.5)	3.37 (1.7)	9.7 (5.3)
B *7*	1-6+9	2.8 (6.4)	0.95 (2.0)	2.8 (6.0)
C *8*	1-7+8	3.4 (5.0)	1.46 (1.7)	4.5 (5.6)
D *8*	1-7+10	6.8 (6.8)	1.74 (1.8)	5.7 (6.0)
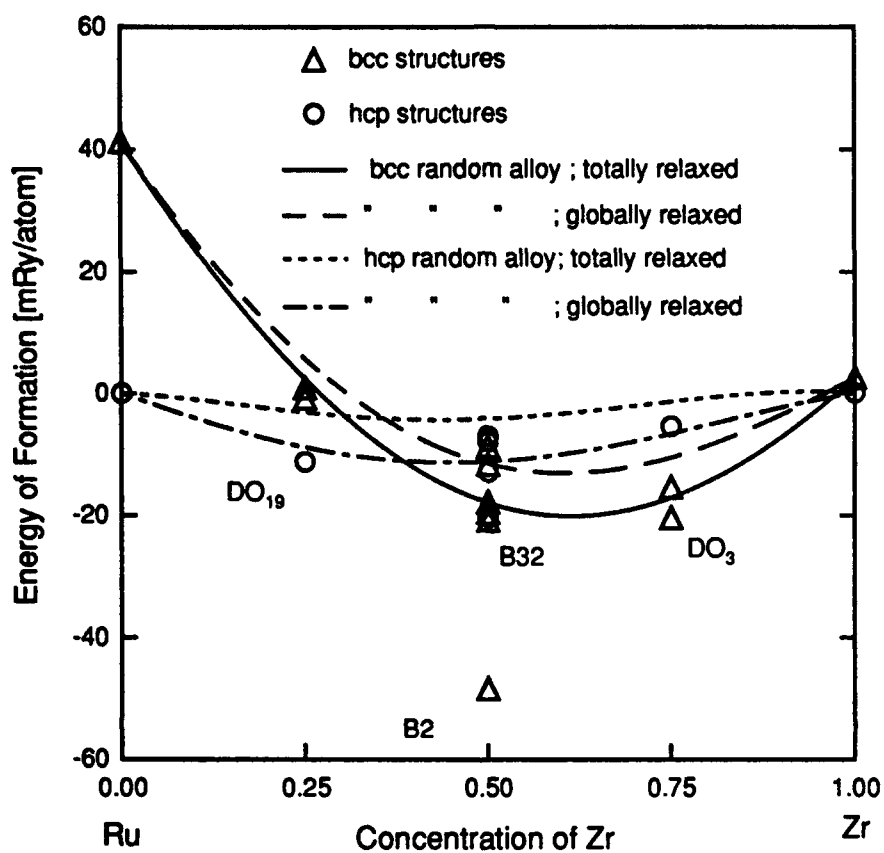
Figure 2.14 Calculated formation energies for selected compounds and random bcc and hcp alloys in Zr-Ru.

The cluster expansion coefficients of the excess volume and bulk moduli in Zr-Ru are shown in Table 2.8. The interactions converge rapidly beyond pair clusters as with Zr-Nb and Nb-Ru. The value of the empty cluster interaction for the bulk modulus, -0.087 Mbar is the excess bulk modulus of the random alloy with an equi-atomic concentration. Thus, for a given lattice type it appears that the effect of order on the bulk modulus is small, but the relaxed L10 structure has a bulk modulus of 2.633 Mbar, 0.2 Mbar higher than the random bcc alloy modulus -- a significant difference.

Table 2.8. The interaction coefficients for cluster expansion of bulk modulus and the volume of (a) bcc- and (b) hcp-based structures in Zr-Ru. The cluster labels are from Figure 2.1.

(a)

Cluster	Effective interactions	
(label)	B_i [mbar]	V_i [a.u.^{3}]
Empty (1)	-0.087120	-5.228230
Point (2)	0.054500	-1.210090
Pair (3)	-0.002370	0.797773
2nd pair (4)	0.026583	0.743473
Triangle (5)	-0.004540	0.100842
Tetrahedron (6)	0.002812	-0.032210

(b)

Cluster	Effective interactions	
(label)	B_i [mbar]	V_i [a.u.^{3}]
Empty (1)	-0.266750	-3.786960
Point (2)	0.049500	-0.627460
Pair (3 4)	0.041750	0.656809
Triangle (6 7 8)	-0.006190	0.078431
Tetrahedron (9)	0.008125	-0.076950

As seen from this section the effective interactions extracted from the Morse-type equations of state via Equation 2.8 provide an adequate description of the alloy energy. Clearly, a more comprehensive treatment of relaxation is required to advance the accuracy of the cluster expansion to complete reliability. Additionally the use of a full-potential LDA total-energy calculation is needed in the cases where structural relaxation is significant; especially for hexagonal metals. The optimization criteria for selecting the expansion basis was indispensable. For even these small sets of structures most combinations of basis sets produced inadequate expansions. There remains no rigorous selection method for the basis structures or clusters. Yet, combining the simple criterion of the maximum determinant of the correlation matrix in combination with expanding the size of the basis by selecting clusters in an, as yet, non-rigorous heirarchy of increasing cluster range and complexity does produce sufficiently accurate expansion for phase stability calculations.

CHAPTER 3. FINITE TEMPERATURE CALCULATIONS

The solution to the Ising model of the alloy free energy is accomplished using the CVM. Section 3.1 outlines the assumptions used to incorporate vibrational free energy into the CVM. The expression for configurational entropy is developed in Section 3.2. The solution technique is outlined in Section 3.3, and calculated phase equilibrium diagram for Zr-Nb is compared with reported measurements.

3.1 Vibrational free energy

In the Debye approximation, the velocity of sound is constant for each polarization as in the case of a classical elastic medium. The resulting linear dispersion relation leads to the well-known result (see, for example, Kittel [40]):

$$\omega_D = (6\pi^2 N/V)^{1/3} v \ , \tag{3.1}$$

for a crystal with N primitive cells of volume V, and ω_D is the characteristic cut-off frequency. Further, if the velocity is assumed to be independent of the polarization, the characteristic frequency is

104

related to a single characteristic temperature, the **Debye temperature**, by:

$$\hbar \, \omega_D = k \, \Theta_D .$$ [3.2]

where $\hbar$ is Planck's constant, h, divided by 2π, and k is Boltzmann's constant. Using the the velocity of sound in an elastic isotropic continuum:

$$v = [\, B/ \, \rho \,]^{1/2} ,$$ [3.3]

where B is the bulk modulus and ρ the density leads to:

$$\Theta_D = (6\pi^2)^{1/3} \frac{\hbar}{k} \left(\frac{4\pi}{3}\right)^{1/6} \left(\frac{rB}{M}\right)^{1/2}$$ [3.4 a]

$$= 67.48 \left(\frac{rB}{M}\right)^{1/2} ,$$ [3.4 b]

for the Wigner-Seitz radius r in atomic units, the atomic mass, M in kg, and the bulk modulus in kbar, the coefficient 67.48 has units of Kelvins - seconds. Equation 3.4 b leads to estimates of Debye temperatures much larger than experimentally determined values. The discrepancy arises from the treatment of the velocity of sound.

Anderson [66] writes an average velocity of sound as:

$$v = \left[\frac{1}{3}\left[\frac{2}{v_t^3} + \frac{1}{v_l^3} \right] \right]^{-1/3} \quad . \qquad\qquad [3.5\ a]$$

where,

$$v_t = \sqrt{S/\rho}, \qquad\qquad [3.5\ b]$$

and

$$v_l = \sqrt{L/\rho}, \qquad\qquad [3.5\ c]$$

for longitudinal and shear moduli, L and S. Moruzzi *et al* [35] combine Equations 3.5 a-c with the observation of Anderson that for the non-magnetic cubic elements:

$$L \approx 1.42\ B \quad , \qquad\qquad [3.6\ a]$$

which is equivalent to the assumption that Poisson's ratio is approximately 1/3. Figure 3.1 a shows longitudinal and bulk moduli for several cubic transition metals along with the functional result of Equation 3.6. Anderson's data also imply:

$$S \approx 0.30\ B \ , \qquad\qquad [3.6\ b]$$

(see Figure 3.1 b). From these two assumptions an average velocity of sound is:

$$v = 0.617 \left[\frac{B}{\rho}\right]^{1/2} \quad , \qquad\qquad [3.7]$$

which leads upon substitution into Equation 3.4 to:

$$\Theta_D = 41.63 \left(\frac{rB}{M}\right)^{1/2} \quad . \qquad\qquad [3.8]$$

Figure 3.2 compares the values predicted by Equation 3.8 with experimentally determined Debye temperature for the cubic non-magnetic elemental metals. Notably, a least-squares fit through the measured values yields an effective coefficient of 46.23 K-sec.

The anharmonicity of the binding energy curve leads to volume-dependent effects in the vibration spectrum that can be described simply by the Grüneisen relation:

$$\gamma = - \frac{\partial \ln \Theta_D}{\partial \ln V} , \qquad\qquad \text{or} \qquad\qquad [3.10\text{ a}]$$

$$\Theta_D = (\Theta_D)_0 \left[\frac{V_0}{V}\right]^{\gamma} \quad . \qquad\qquad [3.10\text{ b}]$$
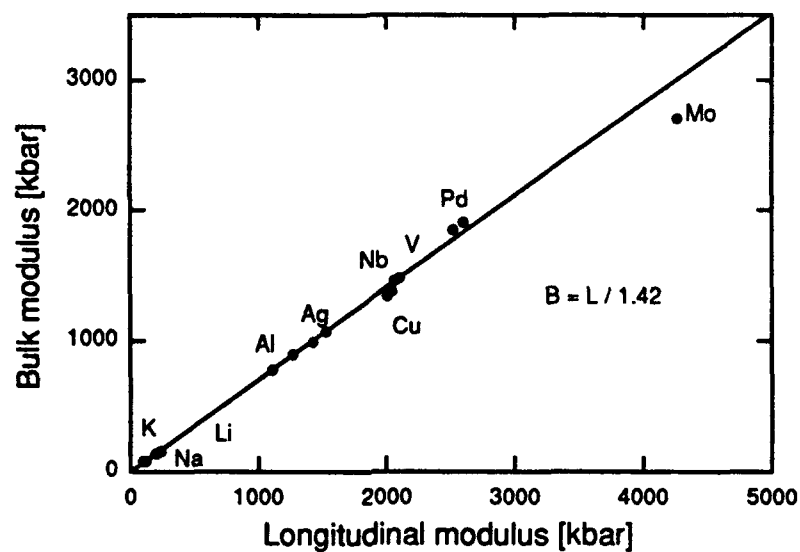
Figure 3.1 a. Longitudinal versus bulk modulus for non-magnetic cubic metals demonstrating the validity of Equation 3.6 a. (From Refence 35).
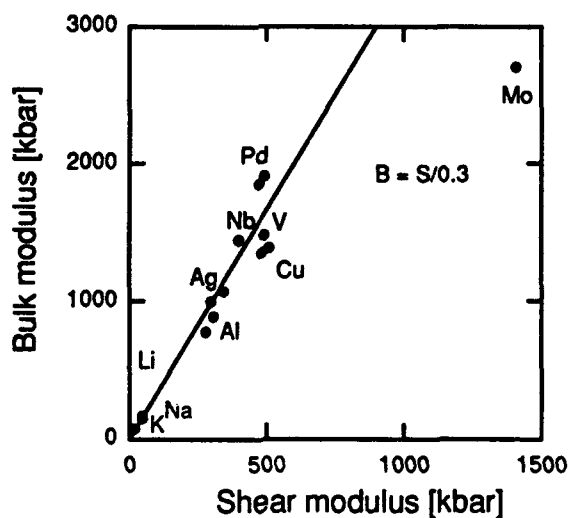
Figure 3.1 b. Shear versus bulk modulus for non-magnetic cubic metals compared with relation of Equation 3.6 b. (From Reference 35).
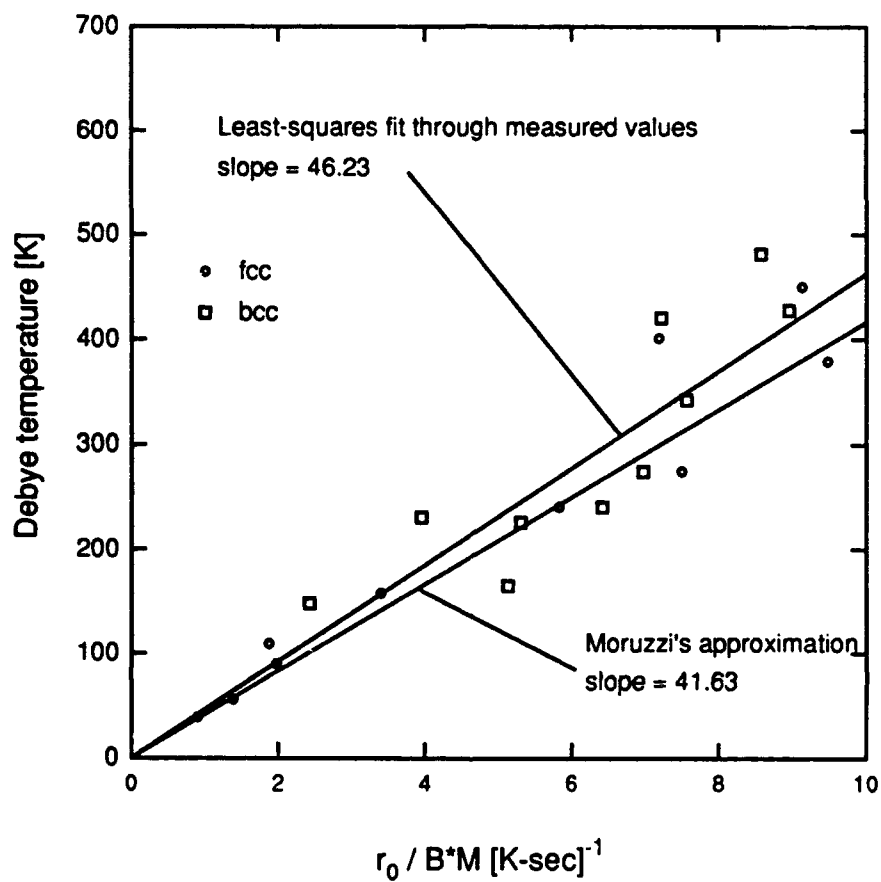
Figure 3.2. Comparison of the measured values of Debye temperatures with those predicted by Equation 3.8 for the cubic non-magnetic transition metals.

If a constant (volume-independent) Poisson's ratio is assumed, then:

$$\gamma = -\frac{1}{6} - \frac{1}{2}\frac{\partial \ln B}{\partial \ln V} \cdot \qquad [3.11\ a]$$

or:

$$\gamma = -\frac{2}{3} - \frac{V}{2}\frac{\partial^2 P/\partial V^2}{\partial P/\partial V} \cdot \qquad [3.11\ b]$$

The validity of this relation rests upon the assumption that all vibrational modes are equally excited which is, effectively, a high-temperature average. Moruzzi *et al* use a low-temperature average of the Grüneisen constant on the grounds that most thermal expansion occurs at low temperatures. Accordingly, they refer to the result of Barron [67], that by defining appropriate high- and low-temperature averages of the Grüneisen constant, γ_{HT} and γ_{LT}:

$$\gamma_{HT} - \gamma_{LT} \approx \frac{1}{3} \cdot \qquad [3.12]$$

Combining Equation 3.12 with Equation 3.11 b:

$$\gamma = \gamma_{LT} = -1 - \frac{V}{2}\frac{\partial^2 P/\partial V^2}{\partial P/\partial V} \cdot \qquad [3,13]$$

On the same grounds as Moruzzi *et al*, Equation 3.13 is used in this study. The calculated Debye temperature for Nb is 343 K, and the Grüneisen parameter is 1.65 The experimentally determined values are 241 K and 1.74.

The volume dependence of the Debye temperature allows incorporation of thermal expansion into the vibrational free energy (see for example, Kittel [40]):

$$F_{vib} = \frac{9}{8}k\Theta_D - kT\left[3\left(\frac{T}{\Theta_D}\right)^3 \int_0^{x_D} \frac{x^3}{e^x - 1}dx - 3\ln\left(1 - e^{-\Theta_D/T}\right)\right] . \quad [3.14]$$

where $x_D = \Theta_D/T$.

Combining Equation 3.14 with the Morse potential allows computation of equilibrium volumes at finite temperatures and, therefore, coefficients of thermal expansion. Figure 3.3 shows the calculated thermal expansion coefficients of Nb as a function of temperature along with measured values. Also shown are coefficients calculated by Moruzzi *et al.*
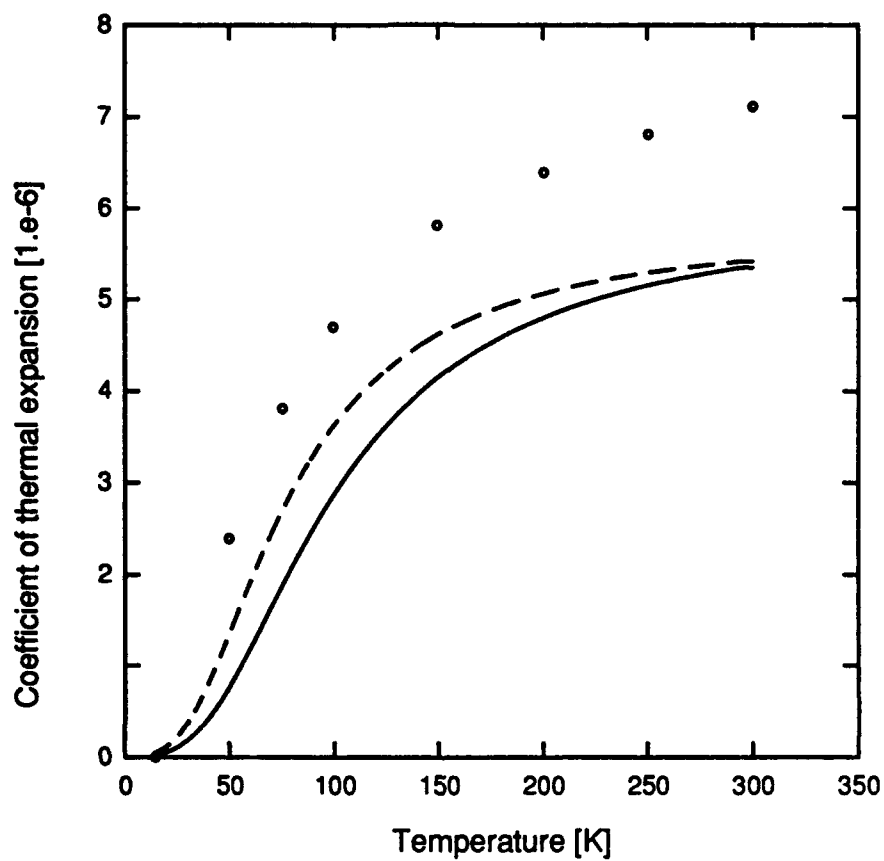
Figure 3.3. Calculated coefficients of thermal expansion for bcc Nb.
The solid line uses the total energy results of this study, and the dashed
line uses those of Reference 35. The measured values are from
Reference 68.

The development of Equation 3.8 is justified only for cubic metals. As yet, no comparably simple treatment for hexagonal metals is reported. Figure 3.4 shows experimentally determined Debye temperatures versus $\left(\frac{rB}{M}\right)^{1/2}$ for the hexagonal transition metals. A least-squares fit yields an effective coefficient of 57.54 K-sec.

An *ad hoc* treatment of vibrational modes similar to Equation 3.8 for hexagonal alloys is used in this study. Using Equations 3.8 and 3.14 the transition of pure zirconium from hcp to bcc at 866°C is reproduced by introducing an effective coefficient of 45.67 K-sec. The induced transition temperature is quite sensitive to the choice of the coefficient as is shown in Figure 3.5. This coefficient is adopted in this study for simplicity, pending a more fundamental analysis. The calculated thermal expansion of hcp zirconium is shown in Figure 3.6. The calculated Debye temperatures and Gruneisen parameters for each compound are shown in Table 3.1 a-c. Tsukamoto [50] determined the Debye temperature of the partially ordered $L1_0$ compound $Nb_{54}Ru_{46}$. The measured value is 370 K, and the value computed for NbRu $L1_0$ in the present study is 370.42 K (see Table 3.1 a).
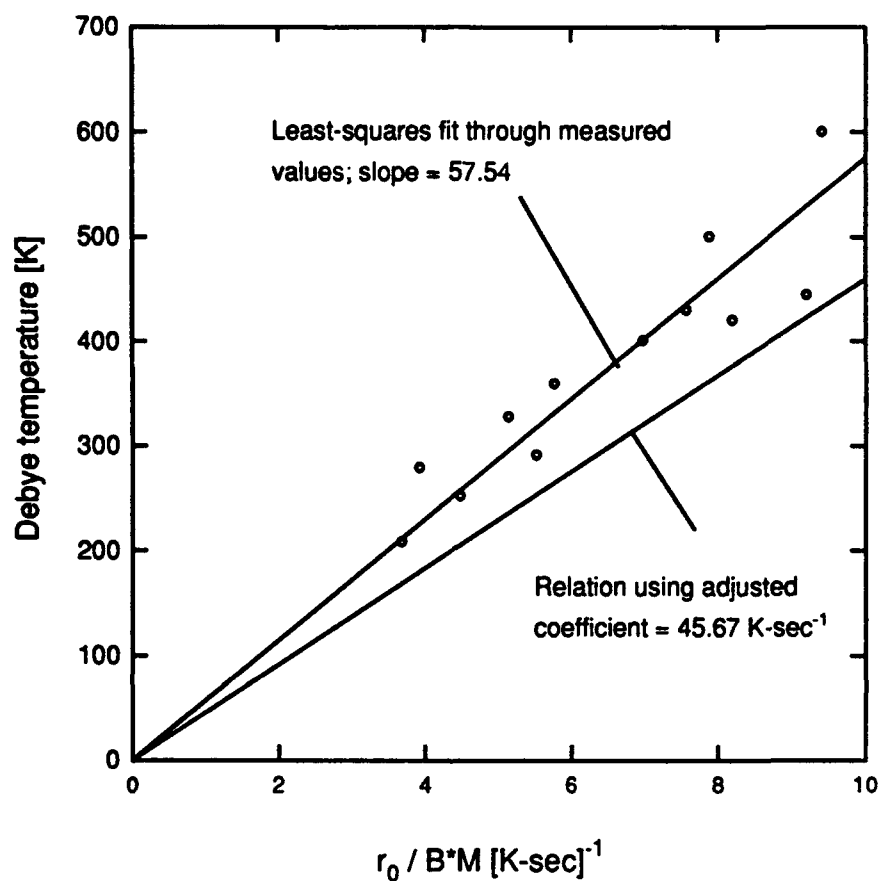
Figure 3.4. Comparison of the measured values of Debye temperatures of the hexagonal transition metals with the values obtained by adjusting the coefficient in Equation 3.8 to reproduce. a transition temperature of 866°C.

Debye temperature (Kelvin) of Zr - hcp
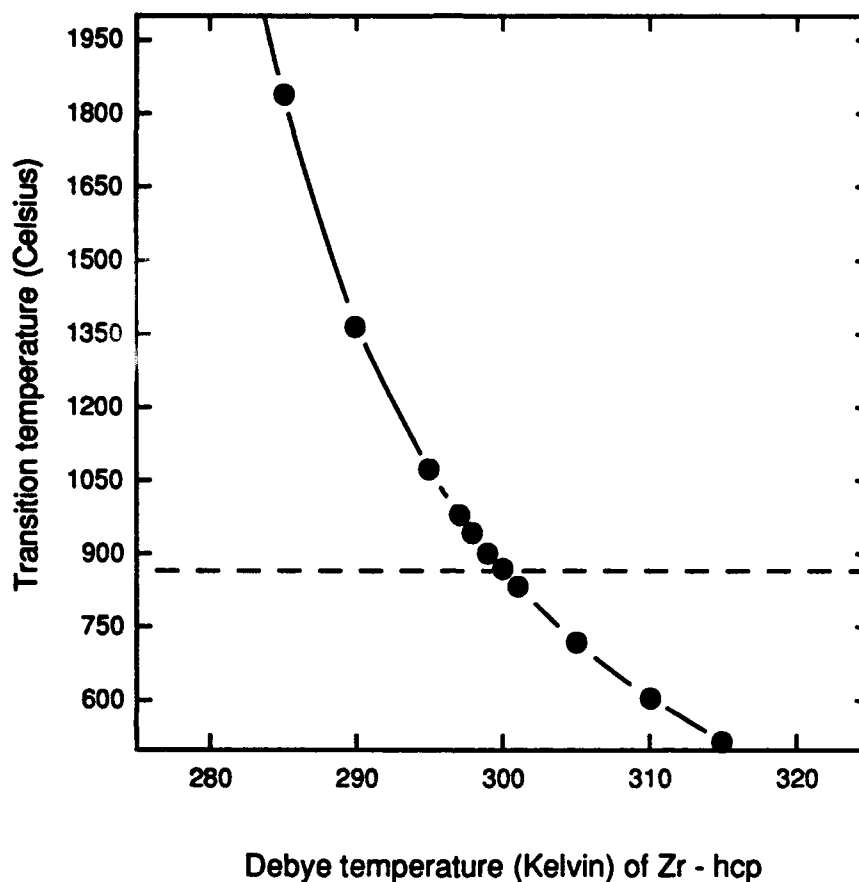
Figure 3.5. Zr hcp-bcc transition temperature as a function of the Debye temperature (Θ_0) of the hcp phase with Θ_0 of the bcc phase = 268.93 K. [The dotted line indicates the measured transition temperature, 866°C].
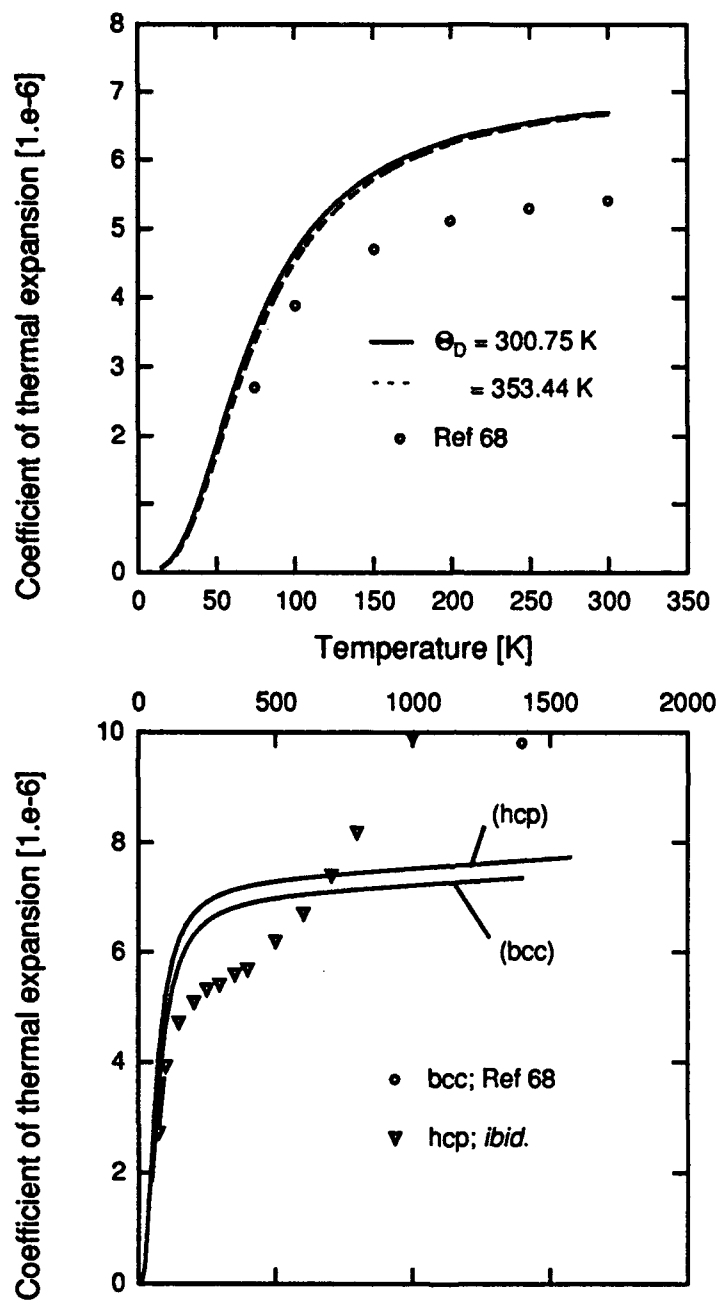
Figure 3.6. Calculated coefficients of thermal expansion of pure Zr. The top graph is for the hcp phase. The bottom graph shows the behavior of both the hcp and bcc phases.

Table 3.1 a. Calculated Debye temperatures and Grüneisen parameters for each compound in Nb-Ru studied.

Compound/ Structure	Debye temperature [K]	Grüneisen parameter
Nb/hcp	369.52	1.66
Nb_3Ru/DO_{19}	385.86	1.72
NbRu/Pmma	405.10	1.80
$NbRu_3/DO_{19}$	424.29	1.89
Ru/hcp	443.94	2.01
NbRu/LiRh	400.64	1.78
NbRu/Pmmn	401.59	1.79
NbRu/H1	403.77	1.79
Nb/fcc	337.98	1.67
$Nb_3Ru/L1_2$	352.38	1.73
$NbRu/L1_0$	370.42	1.80
$NbRu_3/L1_2$	387.40	1.89
Ru/fcc	402.74	2.01
Nb_3Ru/DO_{22}	352.19	1.73
$NbRu_3/DO_{22}$	387.05	1.90
NbRu/NbP	371.00	1.81

Table 3.1 a continued.

Compound/ Structure	Debye temperature [K]	Grüneisen parameter
Nb/bcc	343.43	1.65
Nb_3Ru/DO_3	360.29	1.72
NbRu/B2	373.92	1.81
NbRu/B32	368.20	1.79
$NbRu_3/DO_3$	379.62	1.90
Ru/bcc	389.82	2.02
NbRu/T1	370.11	1.80
NbRu/T2	372.64	1.82
NbRu/T3	372.64	1.82
NbRu/T4	368.20	1.80
$Nb_3Ru/T5$	359.74	1.73
$NbRu_3/T5$	380.43	1.90

Table 3.1 b. Calculated Debye temperatures and Grüneisen parameters for each compound in Zr-Ru studied.

Compound/ Structure	Debye temperature [K]	Grüneisen parameter
Zr/hcp	300.07	1.46
Zr_3Ru/DO_{19}	326.08	1.55
ZrRu/Pmma	359.44	1.66
$ZrRu_3/DO_{19}$	394.35	1.80
Ru/hcp	443.94	2.01
ZrRu/LiRh	356.76	1.63
ZrRu/Pmmn	352.16	1.64
ZrRu/H1	354.78	1.66
Zr/bcc	268.95	1.43
Zr_3Ru/DO_3	305.32	1.56
ZrRu/B2	344.17	1.70
ZrRu/B32	329.49	1.65
$ZrRu_3/DO_3$	357.18	1.81
Ru/bcc	389.82	2.02
ZrRu/T1	327.91	1.65
ZrRu/T2	328.16	1.66
ZrRu/T3	325.50	1.65
ZrRu/T4	321.03	1.63
$Zr_3Ru/T5$	299.82	1.54
$ZrRu_3/T5$	359.41	1.82

Table 3.1 c. Calculated Debye temperatures and Gruneisen parameters for selected structures in Zr-Nb.

Compound/ Structure	Debye temperature [K]	Grüneisen parameter
Zr/hcp	301.07	1.46
Zr_3Nb/DO_{19}	313.12	1.49
ZrNb/Pmma	329.82	1.55
$ZrNb_3/DO_{19}$	351.60	1.55
Nb/hcp	372.88	1.60
ZrNb/LiRh	325.07	1.66
ZrNb/Pmmn	330.55	1.56
Zr/bcc	268.93	1.43
Zr_3Nb/DO_3	285.43	1.48
ZrNb/B2	302.24	1.54
ZrNb/B32	304.24	1.54
$ZrNb_3/DO_3$	322.82	1.60
Nb/bcc	343.44	1.65
ZrNb/T1	303.48	1.54
ZrNb/T2	302.61	1.54
ZrNb/T3	302.77	1.53

3.2 Configurational entropy

In this study the configurational entropy is calculated using the cluster variation method (CVM). The CVM is based on the fact that for a given probability distribution $X(\sigma)$, the exact configurational entropy is given by [69]:

$$S= -k_B \sum_{\sigma} X(\sigma)\ln X(\sigma) \, , \qquad [3.15]$$

where the sum is over all 2^N configurations of the crystal. A sequence of cluster entropies defined by:

$$S_\alpha= -k_B \sum_{\sigma} X_\alpha(\sigma_\alpha)\ln X_\alpha(\sigma_\alpha), \qquad [3.16]$$

clearly converges to the exact configurational entropy as the cluster size α approaches N. Sanchez and de Fontaine [69] used a Möbius transformation to write the cluster entropies, S_α, in terms of a set of irreducible cluster contributions, $\underline{S}_\beta$:

$$S_\alpha= \sum_{\beta\subseteq\alpha} \underline{S}_\beta \, . \qquad [3.17]$$

where the sum extends over all subclusters of α, including α but excluding the empty cluster. As in all cluster expansions the key approximation of the CVM is to neglect the contributions $\underline{S}_\alpha$ for clusters larger than a maximum cluster. Due to the symmetry of the space group of the crystal, Equation 3.15 can be written as:

$$S = \sum_{n=1}^{m} z_n \, \underline{S}_n \, . \tag{3.18}$$

where m labels the maximum cluster, and z_n is the number of n-type clusters per lattice site. This equation, in turn, may be rewritten in terms of cluster entropies:

$$S = N \sum_{n=1}^{m} z_n \, a_n \, S_n = -N k_B \sum_{n=1}^{m} z_n \, a_n \sum_{\sigma_n} X_n(\sigma_n) \ln X_n(\sigma_n). \tag{3.19}$$

where the coefficients a_n are determined using:

$$\sum_{\beta \subseteq \alpha} a_\beta = 1 \, . \tag{3.20}$$

which is valid for each subcluster α of the maximum cluster. In Equation 3.20 the sum extends over all subclusters β of the maximum clusters that contain α.

3.3 CVM solution method

Combining Equations 2.5, 3.14, and 3.19 into an expression for the alloy free energy functional [14]:

$$
F^{total} = \sum_{n=0}^{m} z_n J_n(V,T) \, \xi_n \\
+ kT \sum_{n=1}^{m} z_n \, a_n \sum_{\sigma_n} X_n(\sigma_n) \ln X_n(\sigma_n) \quad .
$$

[3.21]

where the cluster interactions J_n are obtained from a cluster expansion of the excess structural energy and the excess vibrational free energy. The alloy free energy expression depends explicitly only upon the volume V, the temperature, and the correlations ξ_n, where the cluster probabilities X_n may be determined by Equation 2.9:

$$
X_n(\sigma) = \frac{1}{2^n} \left[1 + \sum_{\beta=1}^{m} A_{n\beta}(\sigma) \, \xi_n \right] .
$$

[3.22]

Then, for a given temperature and concentration, the equilibrium free energy is obtained by minimizing the free energy functional with

respect to the volume and the correlations. Recall that the point correlation,

$$\xi_1 = 2x_1 - 1 = x_1 - x_2 \qquad\qquad [2.22]$$

is fixed for a given concentration x_1 (= c).

Calculation of phase boundaries is accomplished efficiently using the grand potential scheme proposed by Kikuchi [70]. The grand potential is obtained by the Legendre transformation of the free energy:

$$\Omega(\mu, T, \{\xi\}, V) = F(T, \{\xi\}, V) + \mu\xi_1 \quad, \qquad\qquad [3.23]$$

where $\{\xi\}$ is the set of all correlations, and μ is the effective chemical potential:

$$\mu = -\frac{\partial F}{\partial \xi_1} \quad, \qquad\qquad [3.24]$$

since by definition:

$$F = \mu_1 x_1 + \mu_2 x_2 \quad, \qquad\qquad [3.25]$$

and,

$$\frac{\partial F}{\partial \xi_1} = \frac{\partial F}{\partial x_1} \frac{\partial x_1}{\partial \xi_1} + \frac{\partial F}{\partial x_2} \frac{\partial x_2}{\partial \xi_1}$$

$$= \frac{1}{2} (\mu_1 - \mu_1) = \mu \quad . \tag{3.26}$$

Similarly,

$$\Omega = F - \mu(x_1 - x_2)$$

$$= \frac{1}{2} (\mu_1 + \mu_2) \quad . \tag{3.27}$$

Therefore the conditions for equilibrium between phases α and β is that:

$$\Omega^\alpha = \Omega^\beta \quad , \tag{3.28}$$

and

$$\mu^\alpha = \mu^\beta \quad . \tag{3.29}$$

The solution procedure used most often for determining phase boundaries in this study is to fix temperature and effective chemical potential μ, then using a Newton- Raphson iterative algorithm to determine the equilibrium variables V and { ξ}. This

algorithm includes an inner loop in which Ω^α and Ω^β each are minimized using a joint minimization scheme. That is, for each phase the minimization:

$$\frac{\partial \Omega}{\partial \{V, \xi\}} = 0 \quad ,$$

[3.30]

is achieved using the Newton-Raphson correction:

$$\{V, \xi\}^{new} = \{V, \xi\}^{old} - H^{-1} \times \frac{\partial \Omega}{\partial \{V, \xi\}} \quad ,$$

[3.31]

where the Hessian H is:

$$H = \begin{bmatrix} \dfrac{\partial^2 \Omega}{\partial \xi_i\, \partial \xi_j} & \dfrac{\partial^2 \Omega}{\partial \xi_j\, \partial V} \\[2ex] \dfrac{\partial^2 \Omega}{\partial \xi_i\, \partial V} & \dfrac{\partial^2 \Omega}{\partial V^2} \end{bmatrix} \quad .$$

[3.14]

The outer loop iterates on μ until Equations 3.28 and 3.29 are satisfied self-consistently.

The bcc miscibility gap in Zr-Nb was calculated using an Ising Hamiltonian varying in maximum interaction range from second nearest neighbors to fifth nearest neighbors and the CVM approximation with maximum cluster size ranging from the tetrahedron to the joint 9 point-6 point cluster. The results, shown in

Figure 3.7 indicate rapid convergence with the interaction range. Curves 1 through 4 are calculated using global relaxation. Curve 1 denotes the lowest order approximation of both the Hamiltonian and the statistical range -- 2nd nearest neighbors, i. e., cluster set A as defined in Table 2.2. If the statistical range is increased to include the joint 9 point - 6 point cluster, but the Hamiltonian is confined to the same basis set as Curve 1, there is very little change -- as seen by comparing curves 1 and 2. If the Hamiltonian range is increased to include third nearest neighbors (basis set B in Table 2.2), there is a large decrease in the critical temperature of the miscibility gap, curve 4. Inclusion of fifth nearest-neighbor interactions (basis set C Table 2.2) produces little change (curve 3) in the calculated miscibility gap. Thus, the CVM calculation of the miscibility gap is deemed converged at 3rd nearest neighbors. Using the same interaction range the miscibility gap was calculated using totally relaxed interactions. The result, curve 5, is significantly different from the well converged globally relaxed curve 4. A more physically representative relaxation method should lie somewhere between the total and global relaxation methods, but it should be reiterated that the globally relaxed cluster expansion reproduced total energies very precisely.

The equilibrium of the hexagonal phase was calculated using the joint tetrahedron- octahedron cluster with second nearest neighbor interactions included. As discussed in Section 3.1 the Debye temperatures of hexagonal alloys have been determined using a coefficient in Equation 3.8 which reproduces the measured transition

temperature of pure Zr. This treatment yielded the phase diagram shown in Figure 3.8. Also shown are several experimental data. Global relaxation is assumed in the calculation. The computed critical temperature of the miscibility gap is 975 °C at 62% Nb compared with the reported values of 988 °C and 61% Nb [7]. The computed monotectoid equilibrium temperature is 855 °C compared with the experimental 893 °C.
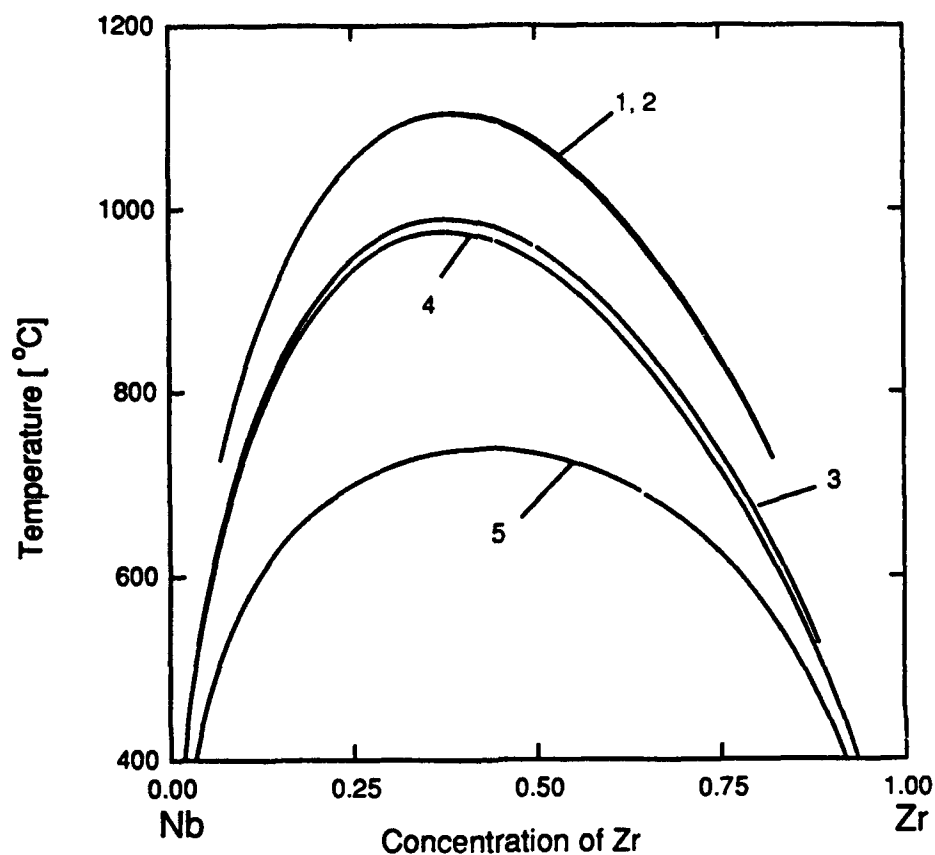
Figure 3.7. Zr-Nb miscibility gap calculated using different approximations of the CVM:

1 - 2nd nearest neighbors; tetrahedron

2 - 2nd nearest neighbors; 9 point- 6 point

3 - 5th nearest neighbors; 9 point - 6 point

4 - 3rd nearest neighbors; 9 point - 6 point

5 - 3rd nearest neighbors; 9 point - 6 point; totally relaxed
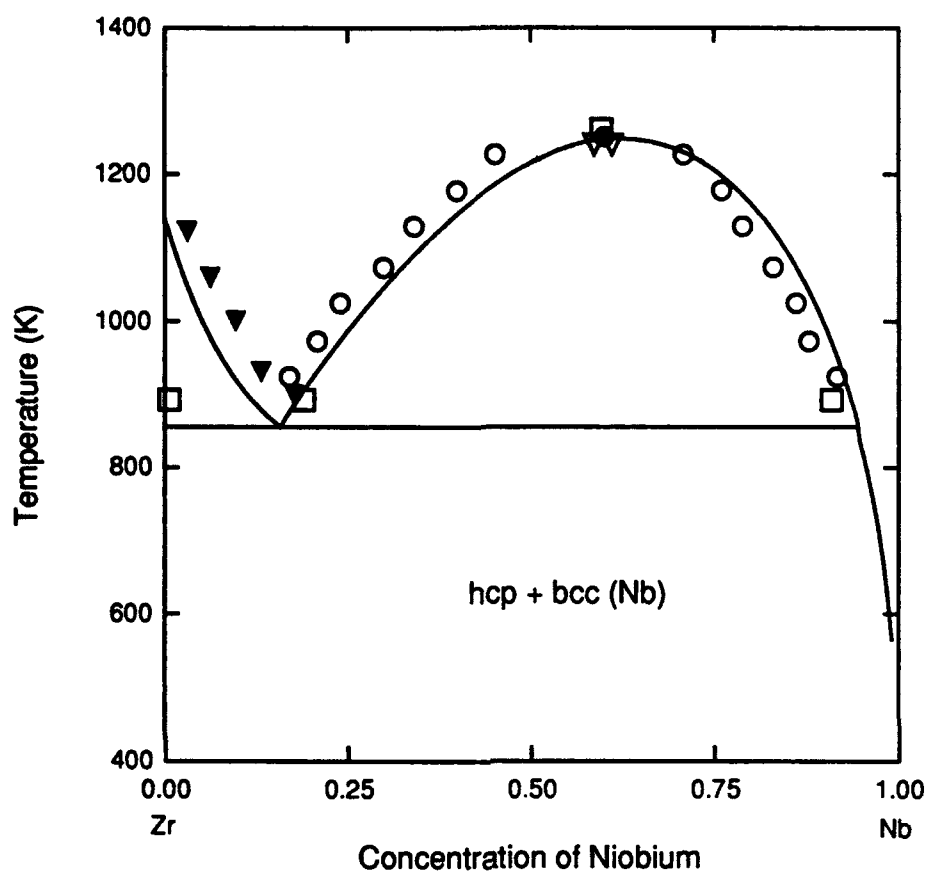
Figure 3.8. Calculated phase diagram for Zr-Nb along with data from References 41 and 42. The calculations include third nearest neighbors in the cluster expansion and globally relaxed interactions.

CONCLUSIONS

The phase stability of alloys in each of the three systems Zr-Nb, Nb-Ru, and Ru-Zr was examined using the cluster expansion technique described in Chapter 2. The equation of state (Equation 1.5) for each of several perfectly ordered structures in each system was computed using the local-density approximation [2] to density-functional theory [1]. The relatively short-range effective chemical interactions were determined using the inversion of the cluster expansion (Equation 2.9) of a set of total energies which, in general, may depend upon very long-range interactions. The convergence of the expansion and the sensitivity of the inversion to errors are coupled problems of selecting optimum basis sets of clusters and structures and are discussed in Sections 2.3-2.6. An efficient scheme for obtaining a sufficiently converged expansion was developed and applied to the three alloy systems. The method consists of an arbitrary initial choice for the maximum interaction range for a given Bravais lattice. For this maximum range there is a unique maximum cluster (or set of joint clusters) from which a set of sub-clusters are chosen to form the cluster basis. An optimum choice of the set of basis structures is then determined using the maximum determinant method, and the total energies are calculated using the local density approximation. For example, in the case of structures with the hcp

131

parent lattice a maximum range of nearest neighbors was first chosen, for which, the associated largest cluster is a regular tetrahedron. The eight different sub-clusters of this tetrahedron were reduced to five by assuming the isotropy (or equivalence) of the interactions among all three types of triangles and between the two types of pairs. Since the vertices of the configurational polyhedron for this choice of cluster set is known, the choice of basis structures was obvious: the structures corresponding to those vertices. However, for Zr-Nb the interactions derived using this representation were insufficient to reproduce the formation energy of the test structure so the cluster basis was expanded to include second-nearest neighbors with the regular tetrahedron retained as the largest cluster size. The corresponding structure set was determined using the maximum determinant method (Section 2.5), and the resulting cluster expansion was deemed adequate by the convergence criterion (Section 2.6).

In this study, the initial choices for and subsequent augmentations of the basis cluster sets were made by somewhat *ad hoc* methods. A fully rigorous implementation would consist of exhaustive searches of each combination of sub-clusters for a given interaction range and the use of large-scale vertex enumeration studies neither of which are within the scope of this study. The three criteria for choosing the basis structures yielded nearly identically converged expansions. As the determinant method is the simplest of the three, it was used as the criterion in this study. The results presented in Section 2. 6 indicate the precision of the cluster

expansions for these alloy systems as better than 5% of the formation energy.

Using the converged cluster expansions, limited ground-state searches were performed by calculating the formation energy of every possible ordered structure for an *a priori* choice of maximum unit cell size. Using this method, the ground states of each of the three systems were determined. Notably, the ground-state structure of $NbRu_3$ was predicted to be the DO_{19} structure. The calculated total energies of the DO_{19} and $L1_2$ structures are very close, and since no relaxation of the c/a parameter of the hexagonal structure is allowed within the atomic-sphere approximation, a full-potential total energy calculation is necessary for calculation of the margin of stability between the cubic and hexagonal structures.

An additional stable ground-state phase, Nb_3Ru with the DO_3 crystal structure, is predicted using the cluster expansion. There is no experimental evidence of an ordered phase at this composition, but this may due to the very similar scattering factors of Nb and Ru -- which makes experimental determination of the ordering of the other phases, NbRu ($B2$ and $L1_0$) and $NbRu_3$ difficult as well.

The cluster variation method is outlined in Sections 3.2 and 3.3 for calculation of the configurational free energy at finite temperatures. Figure 3.7 indicates the rapid convergence of the configurational entropy with the tetrahedron-octahedron or the nine point-six point approximations for the hexagonal and bcc phases respectively.

The contribution of the vibrational entropy to the excess free energy is usually insignificant for alloys of the same lattice type. However, for phase transformations in which the lattice type changes, the vibrational free energy may be significant. This is the case for pure Zr, which undergoes a transition from hcp to bcc at 866°C. In this study, vibrational free energy is calculated using the Debye-Grüneisen approximation, and Debye temperatures calculated from an effective speed of sound following Moruzzi et al [35]. This treatment allows the calculation of coefficients of thermal expansion which for niobium compare very well with measurements (Figure 3.3). The utility of this approach rests upon incorporating an effective speed of sound for the phase. Moruzzi et al obtained the relation (Equation 3.7) for cubic metals from data from Anderson [66]. For hexagonal phases this treatment is not applicable so, in this study, an ad hoc treatment was adopted which requires a single adjustable parameter. For simplicity, the parameter was adjusted to reproduce the actual transition temperature of Zr.

The incorporation of vibrational free energy allows the calculation of the full Zr-Nb phase diagram (Figure 3.8). The Ising Hamiltonian for this system is well converged for both hcp and bcc alloys as is the statistical approximation. The computed equilibria are in excellent agreement with reported data: the critical point of the miscibility gap is 975°C at 62% niobium, the measured values 988°C and 61%, respectively.

BIBLIOGRAPHY

[1] P. Hohenberg and W. Kohn, *Physical Review* **136** B864 (1964).

[2] W. Kohn and L. J. Sham, *ibid.*, **140** A1133 (1965).

[3] K. Terakura, T. Oguchi, T. Mohri, and K. Watanabe, Physical Review B, **35** 2169 (1987).

[4] S. -H. Wei, A. A. Mbaye, L.G. Ferreira, and A. Zunger, *ibid.*, **36** 4163 (1987).

[5] J. M. Sanchez, J. P. Stark, and V. L Moruzzi, *ibid.*, **44** 5411 (1991).

[6] A. A. Mbaye, L.G. Ferreira, A. Zunger, Physical Review Letters, **58** 49 (1987); G.P. Srivastava, J.L. Martins, and A. Zunger, *Physical Review B*, **31** 2561 (1985).

[7] G. Ceder, M. Asta, W. C. Carter, M. Kraitchman, D. de Fontaine, M. E. Mann, and M. Sluiter, *ibid.*, **41** 8698 (1990); L. Szunyogh and P. Weinberger, *ibid.*, **43**, 3768 (1991); P. A. Sterne and L. T. Wille, *Physica C* **162-164**, 223 (1989).

[8] A. E. Carlsson and J.M. Sanchez, *Solid State Communications*, **65** 527 (1988).

[9] T. Mohri, K. Terakura, T. Oguchi, and K. Watanabe, *Acta Metallurgica*, **36** 547 (1988).

135

[10]   A. Zunger, S.-H. Wei, A.A. Mbaye, and L.G. Ferreira, *ibid.*, 2239 (1988); L.G. Ferreira, A.A. Mbaye, and A. Zunger, *Physical Review B*, **35** 6475 (1987).

[11]   S. Takizawa, K. Terakura, and T. Mohri, *ibid.*, **39** 5792 (1989).

[12]   L.G. Ferreira, S.-H. Wei, and A. Zunger, *ibid.*, **40** 3197 (1989); *ibid.*, **41** 8240 (1990).

[13]   M. Sluiter, D. de Fontaine, X.Q. Guo, R. Podloucky, and A.J. Freeman, *ibid.*, **42** 10460 (1990).

[14]   J.D. Becker, J.M. Sanchez, and J.K. Tien, *High-Temperature Ordered Intermetallic Alloys IV*, edited by L.A. Johnson, D.P. Pope, and J.D. Stiegler, MRS Symposia Proceedings No. 213 (Materials Research Society, Pittsburgh, 1991), p. 113.

[15]   P. E. A. Turchi, M. Sluiter, F. J. Pinski, D. D. Johnson, D. M. Nicholson, G. M. Stocks, and J. B. Staunton, *Physical Review Letters*, **67** 1779 (1991).

[16]   M. Asta, D. de Fontaine, M. von Schilfgaarde, M. Sluiter, M. Methfessel, *Physical Review B* **46** 5055 (1992).

[17]   J. D. Becker and J. M. Sanchez, *Materials Science and Engineering*, [in press].

[18]   D. M. Wood and A. Zunger, *Physical Review Letters*, **61** 1501 (1988).

[19]   H. Dreysse, L. T. Wille, and D. de Fontaine, *Physical Review B* **47** 62 (1993).

[20]   H.L. Skriver, "The LMTO Method", Springer Berlin 1984.

[21]   J.M. Sanchez, F. Ducastelle, and D. Gratias, *Physica* **128A** 334 (1984).

[22]   J. M. Sanchez and D. de Fontaine, in *Structure and Bonding in Crystals*, edited by M. O. O'Keefe and A. Navrotsky, Academic, New York, 1981, Vol. 2, 117.

[23]   J. W. Connolly and A. R. Williams, *Physical Review B*, **27** 5169 (1983).

[24]   A. Zunger, *Proceedings of the NATO ASI on "Statics and Dynamics of Alloy Phase Transformations,"* Plenum Press (1993); S. -H. Wei, L. G. Ferreira, and A. Zunger, *Physical Review B*, **45** 2533 (1992); Z. W. Lu, S. -H. Wei, and A. Zunger, *ibid.*, 10314 (1992); D. B. Laks, S. Froyen, L. G. Ferreira, and A. Zunger, *ibid.*, **46** 12587 (1992).

[25]   K. Binder, Physical Review Letters **45** 811 (1980); K. Binder, J. L. Lebowitz, M. K. Phani, and M. A. Kalos, *Acta Metallurgica* **29** 1655 (1981).

[26]   H. T. Diep, A Ghazali, B. Berge, and P. Lallemand, *Europhysics Letters*, **2** 603 (1986)

[27]   R. A. Bond and D. K. Ross, *Journal of Physics F* **12** 597 (1982).

[28]   J.M. Sanchez, W. Teitler, and D. de Fontaine, *Physical Review B* **26** 1465 (1982).

[29]   R. Kikuchi, *Physical Review* **81** 988 (1951).

[30]   J. A. Barker, *Proceedings of the Royal Society of London* **A216** 45 (1953).

[31]   T. Morita, *Journal of Mathematical Physics*, **13** 115 (1972); *Journal of the Physical Society of Japan*, **12** 753 (1957).

[32]   J.M. Sanchez and D. de Fontaine, *Physical Review B* **17** 2926 (1978); *ibid.*, **21** 211 (1980); *ibid.*, **25** 1759 (1982).

[33]   A. E. Carlsson, *ibid.*, 35 4858 (1987).

[34]   D. Vanderbilt, S.G. Louie, and M.L. Cohen, *Physical Review Letters* **53** 1477 (1984).

[35]   V.L. Moruzzi, J.F. Janak, and K. Schwarz, *Physical Review B* **37** 790 (1988).

[36]   *Binary Alloy Phase Diagrams*, editor-in-chief, T.B. Massalski, 2nd edition, Materials Park, OH, ASM International, 1990.

[37]   V. E. Raub and W. Fritzsche, *Z Metallkde* **54** 317 (1963).

[38]   B. K. Das, M. A. Schmerling, and D. S. Lieberman, *Materials Science and Engineering* **6** 248 (1970).

[39]   Y. Chen, C.-L. Fu, K.-M Ho, B. N. Harmon, and P.-A. Lindgård, *Physical Review* Brief Report **31** 6775 (1985).

[40]   C. Kittel, "Introduction to Solid State Physics," J. Wiley, New York 1986.

[41]   A. F. Gullermet, *Z. Metallkde* **82** 479 (1991).

[42]   J. P. Abriata and J. C. Bolcich, *Bulletin of Alloy Phase Diagrams* **3** 34 (1982).

[43]   V. E. Raub and E. Röschel, *Z Metallkde* **54** 455 (1963).

[44] F. M. Jaeger and E. Rosenbloom, *Konikl. Akad. Wentensch. Amsterdam Proceedings* **34** 808 (1931).

[45] E. O. Hall and J. Crangle, *Acta Crystallographica* **10** 240 (1957) Short Communications.

[46] L. A. Panteleemenov, O. P. Nesterova, Z. A. Gutz, K. G. Akhmetzyanov, and I. G. Sokolova, *Vestnik Mosckovskovo Universite* **6** 57 (1965) in Russian.

[47] P. Greenfield and P. A. Beck, *Journal of Metals* 265 (February 1965).

[48] A. E. Dwight, *Transactions of AIME*, **215** 283 (1959).

[49] G. F. Hurley and J. H. Brophy, *Journal of Less Common Metals* **7** 269 (1964).

[50] T. Tsukamoto, K. Koyama, A. Oota, and S. Noguchi, *Journal of the Japanese Institute of Metals* **53** 253 (1989), in Japanese with English abstract and captions.

[51] S. V. Popova, *10th International Congress of Crystallography, Amsterdam, 7 August 1975*, S99 (International Union of Crystallography).

[52] H. F. Jansen and A. J. Freeman, *Physical Review B*, **30** 561 (1984).

[53] C. D. Gelatt, A. R. Williams, and V. L. Moruzzi, *ibid.*, **27** 2005 (1983).

[54] O. K. Andersen, O. Jepsen, and D. Glötzel, "Highlights of Condensed Matter Theory," *Proceedings of the Enrico Fermi*

International School of Physics, North-Holland, Amsterdam, 1985.

[55]   L. Hedin and B. I. Lundqvist, *Journal of Physics C* **4** 2064 (1971).

[56]   Z. -W. Lu, D. Singh, and H. Krakauer, *Physical Review B*, **36** 7335 (1987).

[57]   L. Topor and O.J. Kleppe, *Metallurgical Transactions A* **19A** 1061 (1988).

[58]   W. B. Pearson, *A Handbook of Lattice Spacings and Structures of Metals and Alloys*, Pegammon, Oxford, 1967, Vol. 2.

[59]   M. J. Mehl, J. E. Osborn, D. A. Papaconstantopoulos, and B. M. Klein, *Physical Review B*, **41** 10311 (1990).

[60]   J. M. Sanchez and D. de Fontaine, in *Bonding and Crystals Volume II*, Academic Press, 1976.

[61]   T. Kudo and S. Katsura, *Progress in Theoretical Physics*, **56** 435 (1976).

[62]   J. Kanamori and Y. Kakehashi, *Journal of Physics (Paris) Colloq.* **38** C7-274 (1977); J. Kanamori, in *Modulated Structures 1979*, edited by J. M. Cowley, J. B. Cohen, M. B. Salamon, and B. J. Wuensch (AIP, New York, 1979).

[63]   A. Finel and F. Ducastelle, in *Phase Transformations in Solids*, edited by T. Tsakalakos, MRS Symposia Proceedings No. 21 (Materials Research Society, Pittsburgh, 1984).

[64]   J.H. Wilkinson, "The Algebraic Eigenvalue Problem" (Clarendon Press, Oxford 1965).

[65]   H.E. Cook, *Acta Metallurgica* **23** 1041 (1975).

[66]   O.L. Anderson, "Physical Acoustics," ed. W.P. Mason Academic, New York, 1965, Vol III-B.

[67]   T.H.K. Barron, *Philosophical Magazine* **46** 720 (1955).

[68]   T. Furukawa, T.B. Douglas, and N. Pearlman in "American Institute of Physics Handbook," McGraw-Hill, New York, 1957, Section 4e.

[69]   J.M. Sanchez and D. de Fontaine, *Physical Review B* **17** 2926 (1978); *ibid.* **21** 211 (1980); *ibid.* **25** 1759 (1982)

[70]   R. Kikuchi, *Journal of Physical Chemistry* **60** 1071 (1974); *Acta Metallurgica* **25** 195 (1977).